March 2016

Mammalian Egg Activation: The Roles of TRPV3 Channels and PLCZ1

Hoi Chang Lee

MAMMALIAN EGG ACTIVATION: THE ROLES OF TRPV3 CHANNELS AND PLCZ1

A Dissertation Presented

by

HOI CHANG LEE

Submitted to the Graduation School of the

University of Massachusetts Amherst

DOCTOR OF PHILOSOPHY

February 2016

Animal Biotechnology & Biomedical Sciences

MAMMALIAN EGG ACTIVATION: THE ROLES OF TRPV3 CHANNELS AND PLCZ1

A Dissertation Presented

by

HOI CHANG LEE

Approved as to style and content by:

Rafael A. Fissore, Chair

Dominic L. Poccia, Member

Pablo E. Visconti, Member

Rafael A. Fissore, Department Head
Department of Veterinary &Animal Science

ACKNOWLEDGMENTS

I would like to thank my advisor, Dr. Rafael A Fissore, for his many years of patient guidance and support. I also thank my committee members Dr. Dominic L. Poccia, Dr. Pablo E. Visconti, and all of my colleagues in Dr. Fissore's lab for their support.

ABSTRACT

MAMMALIAN EGG ACTIVATION: THE ROLES OF TRPV3 CHANNELS AND PLCZ1

FEBRUARY 2016

HOI CHANG LEE, B.S., CHUNGBUK NATIONAL UNIVERSITY

M.S., KONKUK UNIVESITY

Ph.D., UNIVERSITY OF MASSACHUSETTS AMHERST

Directed by: Professor Rafael A. Fissore

Calcium channels at the plasma membrane have been suggested to mediate Ca^{2+} influx during egg activation. The transient receptor potential (TRP) Ca^{2+} channel, TRPV3, is differentially expressed in oocytes during maturation, being fully active at MII stage. Specific stimulation of TRPV3 channels in mouse eggs promotes Ca^{2+} influx sufficient to induce egg activation and parthenogenesis. In chapter 2, we explore the function and distribution dynamics of the TRPV3 channel protein during oocyte maturation. Using dsRNA, TrpV3 overexpression, and inhibitors of protein synthesis, we modified the native expression of the channel and showed that the TRPV3 protein is synthesized and translocated to the plasma membrane during maturation. We demonstrated that 2-APB at the concentration used to promote Ca^{2+} influx in eggs, specifically and reversibly targets TRPV3 channels, and does not block the IP_3 receptor. Finally, we showed that TRPV3 channels functionally interact with the actin cytoskeleton indicating an actin-based

regulation of its expression on the plasma membrane. Our results indicated that TRPV3 is a target of 2-APB in eggs, a condition that can be used to induce parthenogenesis. The association of endogenous TRPV3 channels with the actin cytoskeleton is a novel finding, and suggests that the rearrangements of actin that occur during maturation could regulate both plasma membrane presence and function of TRPV3 Ca^{2+} channels involved in oocyte maturation and fertilization. We show that TRPV3 is required for strontium influx because TRPV3-KO eggs failed to conduct Sr^{2+} or undergo strontium-induced activation. We propose that TRPV3 is a major mediator of calcium influx in mouse eggs and is a putative target for artificial egg activation.

In chapter 3, we conducted studies to determine if expression of the testis-specific PLCZ1 correlated with low success or fertilization failure after ICSI in patients with normal parameters after standard semen analysis (SA). The presence of PLCZ1 in sperm was ascertained using western blotting and immunofluorescence (IF) analysis. The ability of sperm to initiate changes in the intracellular concentrations of $[Ca^{2+}]_i$ was also examined. Male partners of couples with failed or low success ICSI fertilization but with normal SA parameters showed low expression levels of PLCZ1 as determined by western blotting and reduced fluorescent signal during IF studies. In addition, fewer of these males' sperm showed PLCZ1 expression and were able to initiate robust $[Ca^{2+}]_i$ oscillations upon injection into eggs. In the second part of this chapter, we examined two infertile brothers exhibiting normal sperm morphology but complete fertilization failure after intra cytoplasmic sperm injection (ICSI). Whole exomic sequencing evidenced a missense homozygous mutation in PLCZ1, converting Ile 489 into Phe (Ile489Phe). We showed that the mutation is deleterious, leading to absence of the protein in sperm.

Injection of cRNA into GV and MII oocytes showed that the protein was mislocalized and produced highly abnormal Ca^{2+} transients and early embryonic arrest. Altogether these alterations are consistent with our patients' sperm inability to induce oocyte activation and initiate embryo development. In contrast, no mutations were identified in *WBP2NL* and PAWP presented normal expression and localization. Overall we demonstrate in humans that the absence of PLCZ1 alone is sufficient to prevent oocyte activation irrespective of the presence of PAWP. Additionally, it is the first mutation located in the C2 domain of PLCZ1, a domain involved in targeting proteins to cell membranes, opening the door for structure function studies to define the conserved amino acids on the β1 strand of the C2 domain that might regulate the selectivity of PLCZ1 for its lipid substrate(s).

TABLE OF CONTENTS

Page

LIST OF TABLES

Table Page

LIST OF FIGURES

CHAPTER 1

BACKGROUND

1.1 Egg Activation

Increases in the intracellular concentration of free Ca^{2+} ($[Ca^{2+}]_i$) triggers the initiation, progression and/or completion of a range of cellular processes, including fertilization, muscle contraction, secretion, cell division, and apoptosis (1). In order to survive and proliferate, cells must communicate with each other and within organisms, and changes in $[Ca^{2+}]_i$ allow them to quickly respond to environmental or metabolic challenges and cues with reactions that regulate cell fate and function. In the case of Ca^{2+}, myriad proteins have acquired the ability to bind Ca^{2+}, which allows them to interpret and transform these elevations into cellular decisions and functions.

In most species, oocytes through the process of maturation, prepare for fertilization and initiation of embryogenesis. In mammals, fully-grown oocytes remain arrested until fertilization at the metaphase of the second meiotic division (MII) (2, 3). During fertilization, sperm triggers a series of increases in the levels of $[Ca^{2+}]_i$, which are termed Ca^{2+} oscillations that are responsible for oocyte activation (4). Oocyte or egg activation is the process that transforms a ready-to-be-fertilized MII oocyte, also known as an egg, into a competent zygote capable of supporting embryo development to term. Egg activation, is characterized for many events including the resumption and progression of meiosis, cortical granule (CG) exocytosis, prevention of polyspermy, release of the polar body, sperm head decondensation and PN formation and translation, accumulation, and degradation of specific mRNAs and proteins (5) (Figure 1-1). Increases in $[Ca^{2+}]_i$ are the universal signal of egg activation in all species investigated to date (6). Importantly, to

support the long-persistence of oscillations, which are the hallmark of mammalian fertilization, Ca^{2+} influx is necessary to refill the internal stores and maintain the oscillations in all mammals (7-9).

The $[Ca^{2+}]_i$ responses that underlie egg activation offer a great deal of diversity regarding their spatiotemporal configuration, reflecting both the plasticity of the Ca^{2+} signaling machinery as well as the dissimilar Ca^{2+} requirements for egg activation among species. In general, species can be categorized either as displaying a single $[Ca^{2+}]_i$ rise, in the case of sea urchins, starfish, frogs, and fish, or showing multiple $[Ca^{2+}]_i$ increases, also known as oscillations, in the case of nemertean worms, ascidians, and mammals (10, 11). Research has found that Src-family kinases (SFKs) and phospholipase Cγ (PLCγ) are involved in the activation of the phosphoinositide pathway and production of inositol 1,4,5, -triphosphate (IP_3) during fertilization in sea urchins, starfish, and frogs, reflecting the contribution of a presently unknown plasma membrane receptor/signaling complex (12, 13). Inositol 1,4,5-triphosphate (IP_3)-mediated Ca^{2+} release from intracellular stores in the endoplasmic reticulum (ER) is primarily responsible for the generation of the $[Ca^{2+}]_i$ wave and oscillations during fertilization in mammals. During these oscillations, the production of IP_3 production is upregulated, which mediates Ca^{2+} release via its cognate receptor (IP_3R), located in the ER, and in this form makes possible the occurrence of $[Ca^{2+}]_i$ oscillations(14).

Research now suggests that in mammals the initiation of oscillations may be accomplished by a novel mechanism whereby the signaling molecule/cargo, known as the sperm factor (SF), is released by the sperm into the ooplasm after fusion of the gametes. Importantly, the SF is not IP_3 or Ca^{2+} and rather contains a protein moiety (15-18). The

mammalian SF's molecular identity appeared to have been resolved when a new member of the PLC family, a sperm-specific isoform named PLCZ (19), was reported to reproduce the responses of the sperm. Nevertheless, the recent proposal of PAWP as an alternative SF has raised some doubts about the true identity of the mammalian SF.

External Ca^{2+} is required to fill the internal stores from where Ca^{2+} is increased internally. External can be incorporated into cells through channels and/or transporters. One of the first characterized channels in mouse eggs (20) was the T-Type Voltage-gated Ca^{2+} channel (21). The role of these channels in fertilization remains elusive (22), as changes in membrane potential during mouse fertilization are negligible (23) and the resting potential of mouse eggs is close to the activation threshold of these channels, which suggests that a large majority of them might be inactive in MII eggs before and after fertilization. Therefore, the identity of the channels that mediate influx to support the oscillations in mammals remains unknown.

1.2 TRP channels

The transient receptor potential (TRP) proteins are the second largest class of non-selective cation channels. The founding member of the TRP family was identified nearly 40 years ago in Drosophila (24-26), which was defective in light sensing and exhibited only transient light-induced receptor potentials (TRP) instead of the normal persistent response (27). TRP channels are widely expressed in somatic cells. The TRP channel superfamily contains 28 mammalian members subdivided in six subfamilies: TRP canonical (TRPC; TRPC1-7), TRP vanilloid (TRPV; TRPV1-6), TRP melastatin (TRPM; TRPM1-8), TRP ankyrin (TRPA; TRPA1), TRP polycystin (TRPP; TRPP2, 3, 5), and

TRP mucolipin (TRPML; TRPML1-3) (28). All TRP channels are primary six-transmembrane segments polypeptide subunits. The permeable cation pore is located between the fifth and sixth transmembrane domains (Figure 1-2) (29). TRP channels can sense a variety of stimuli such as light (26, 30, 31)[Montell C Neuron 1989, Hardie RC Neuron 1992, Xue T Nature 2011], odors (32, 33), taste (34, 35), acids (36, 37), temperature (38, 39), gravity (40), auditory stimuli (41, 42), as well as mild and noxious mechanical forces (43-46). The stimuli that activate TRPs do so through a multistep of downstream cellular signal pathways, or through a single step via Ca^{2+} entry and/or membrane depolarization (46). TRP channels are also involved in cellular homeostasis and growth control, regulation of cell fate and survival, immune and inflammatory mechanisms, and endocrine and exocrine secretory processes (28).

1.2.1 TRPV family

Based on homology, the TRPV (vanilloid) family comprises six ion channels. There are four main groups: TRPV1/TRPV2, TRPV3, TRPV4, and TRPV5/6. This family is named after the first mammalian member of the TRPV subfamily, which binds vanilloids (27). Among the TRPV channels, TRPV1, 2, 3 and 4 have striking temperature sensitivities. Indeed, TRPV1 is activated at > 43°C; TRPV2 at >52°C; TRPV3 at 33°C; and TRPV4 at >30°C (27). These thermo-TRPVs are modestly permeable to Ca^{2+}, whereas TRPV5 and TRPV6 are the only highly Ca^{2+} selective channels in the TRP family. Nevertheless, functions of all of these channels are tightly regulated by $[Ca^{2+}]_i$ and phosphoinositides (27, 47).

1.2.2 TRPV3

The voltage-independent member of the TRP channel family, TRPV3, was recently reported to be functionally active in mouse eggs (48). TRPV3 shares 43% sequence similarity with TRPV1. The initial characterization of TRPV3 expression was carried out in somatic tissues and the brain, spinal cord, testis, skin, oral cavity, and gastrointestinal tract showed high levels of expression (49, 50); reviewed in (51). TRPV3 was found to be activated by innocuous warm temperatures above 33°C (27, 49, 50, 52). The role of TRPV3 as a thermosensor is still not completely understood. TRPV3 knockout mice exhibit strong deficits in responses to innocuous and noxious heat but not in other sensory modalities (27, 53).

In mice, TRPV3 is involved in the formation and maintenance of the physical-chemical skin barrier. TRPV3 forms a signaling complex with the receptor of epidermal growth factor (EGFR) and transforming growth factor-α (TGF-α). Activation of EGFR leads to increased TRPV3 channel activity, which in turn stimulates TGF-α release resulting in the formation of the barrier (54). Lack of the *trpv3* gene in mice results in particular hair phenotypes (wavy hair coat and curly whiskers) (54). Functional TRPV3 channels were identified in cultures of hair follicle-derived outer root sheath keratinocytes, in which the activation of TRPV3 and the concomitant elevation of $[Ca^{2+}]_i$ resulted in inhibition of cell growth and the onset of cell death (55).

Native TRPV3 currents were first reported in keratinocytes, where exposure to 100 μM 2-Aminoethoxydiphenyl borate (2-APB), a known activator of the TRPV3 channel, only caused whole cell currents when cells were sensitized with temperature (56). Remarkably, TRPV3 channels are expressed in MI oocytes and MII eggs are capable of

generating strong and measurable whole cell currents after 2-APB treatment without temperature exposure, suggesting different regulation or sensitization of native TRPV3 channels in eggs (48).

1.3 Sperm factor

In mammals, repetitive $[Ca^{2+}]_i$ transients are induced soon after sperm-oocyte fusion (7, 57), which trigger the events of egg activation (58). Furthermore, the amplitude and number of $[Ca^{2+}]_i$ rises might affect gene expression at later stages of embryo development and even after postnatal development (59). The mechanism by which the sperm induces $[Ca^{2+}]_i$ oscillations involves IP_3 (58, 60). IP_3 is generated by phospholipase C (PLC), which causes hydrolysis of phosphatidyl inositol 4,5-bisphosphate ($PI(4,5)P_2$). How the PLC is activated during fertilization has been investigated for several decades, and three major hypotheses have been proposed (61-63). The first is the 'membrane receptor hypothesis', which suggested that an egg surface receptor was engaged by a sperm resulting in the production of a signaling pathway that activated PLC and triggered Ca^{2+} release (64). Another idea is the 'conduit hypothesis', which proposed that extracellular Ca^{2+} flowed into the egg during sperm and gamete fusion, although this notion was quickly abandoned once it was shown that $[Ca^{2+}]_i$ increases occurred in the absence of external Ca^{2+}. The third hypothesis is the 'sperm factor hypothesis', which since the advent of intracytoplasmic sperm injection (ICSI), which demonstrated that activation could happen in the absence of interaction of the gametes, is considered the mechanism whereby fertilization initiates $[Ca^{2+}]_i$ oscillations. In support of this hypothesis, injection of sperm cytosolic extracts into eggs results in $[Ca^{2+}]_i$ responses

similar to those observed during fertilization in many species, including sea urchin (65), ascidian (66), chicken (67), hamster (68), mouse (69), rat (70), cow (16), pig (71), human (72), and rabbit (73).

1.3.1 PLCZ

Saunders et al. showed evidence that phospholipase C zeta (PLCZ) might be the sperm-borne oocyte-activating factor. For example, microinjection of cRNAs encoding for mouse PLCz1 (19) or recombinant PLCz1 protein (74) induced $[Ca^{2+}]_i$ oscillations highly reminiscent of those during fertilization. Furthermore, depletion of PLCZ form sperm extracts removed the ability of these extracts to initiate oscillations. (19). It was also demonstrated that the content of PLCz1 in a single sperm was compatible with the concentrations required to induce oscillations (19). Others reported that reducing sperm PLCz1 levels by a transgenic RNA interference resulted in perturbation in patterns of $[Ca^{2+}]_i$ oscillations after fertilization and reduced litter size (75). PLCZ1 has been detected in all mammalian species investigated to date, including mouse (19, 70), rat (70), human (70, 76), and also in some non-mammalian species (65-67).

1.3.2 Structure and Function of PLCZ

There are 13 known mammalian PLC isozymes classified according to their structure into six groups: PLC-beta (PLCβ 1-4), -gamma (PLCγ 1, 2), -delta (PLCδ 1, 3, 4), -epsilon (PLCε), -zeta (PLCζ), and –eta (PLCδ 1, 2) (77-79), of which PLCζ is the smallest (80). PLCZ is composed of four EF-hand (EF1-EF4) domains in the N terminus, catalytic X and Y domains, and a C2 domain in the C terminus, which are domains

common to all other PLCs. However, PLCZ lacks the N-terminal PH domain that is found in PLCβ, -γ, -δ, and –ε, which underlies their interaction with membrane phospholipids and the localization of those PLCs to the PM (81).

PLCZ has a very distinct functional property, which is the high Ca^{2+} sensitivity of its in the PIP_2 hydrolyzing activity. PLCZ and PLCδ1, which exhibits comparatively high homology with PLCZ, have a similar affinity for $PI(4,5)P_2$, but PLCZ is more sensitive to Ca^{2+} than PLCδ1, which in other words means it can hydrolyze PIP_2 at lower, basal, concentrations of Ca^{2+} (82). These properties are thought to depend on the N-terminal EF-hand domains, as the absence of the all EF hands results in complete loss of the PIP_2 hydrolyzing activity and $[Ca^{2+}]_i$ oscillations inducing activity of PLCZ1 (83). EF1 and EF2 are also important for PLCZ activity because deletion of these domains remarkably reduces PLCZ activity (83). However, point mutations in EF1 or EF2 do not cause a marked decline in the Ca^{2+} sensitivity of the PIP_2-hydrolyzing activity (83), suggesting the two EF-hand domains play a structural role to form the active conformation rather than being a Ca^{2+}-binding site for the catalytic activity (83) (Figure 1-3).

The C2 domain, which consists of approximately 37 amino acids in the C terminal end of PLCZ, is required for PLC activity and Ca^{2+} oscillatory activity, as its deletion causes complete loss of PLC activity (83). The C2 domain has been characterized as a membrane-associating and intermolecular interaction domain in a variety of proteins (84). It has been suggested that the C2 domain plays part in the Ca^{2+}-dependent subcellular membrane targeting for several lipid-metabolizing enzymes (85, 86). Therefore, there is a possibility that the C2 domain of PLCZ also functions as its PIP_2 binding site. On the other hand, it has been also reported that the C2 domain does not

play a direct role in the interaction with PIP_2 because in *in vitro* studies PLCZΔC2 showed binding to $PI(4,5)P_2$ with equivalent affinity to wild-type PLCZ (87). Instead, it has suggested that the X-Y linker region PLCZ, which shows strong binding to $PI(4,5)P_2$ might be the substrate targeting enzyme for PLCZ1 (87) (Figure 1-3).

The X and Y domains are associated with the catalytic activity common to all phosphoinositide-specific PLCs. It has been reported that the X and Y catalytic domains are capable of binding and hydrolyzing PIP_2 because even with the XY catalytic domains alone, that is without the other domains of the enzyme, *in vitro* studies show it exhibits well over half of the activity of full-length PLCZs (82) (Figure 1-3).

The linker region connects the X and Y domains. This domain in PLCZ is longer than in other PLCs, and it appears to host a nuclear localization signal sequence, which is thought to be a binding site for the nuclear transport receptor, and explains the ability of mouse PLCZ to undergo nuclear translocation (88, 89). Consistent with this, following fertilization and PN formation, PLCZ accumulates into the PN (90, 91), and this localization contributes to the termination of the oscillations around the time of the time of PN formation in mouse zygotes (2). Therefore, it has been suggested that the translocation of PLCZ plays a important role in the cessation of $[Ca^{2+}]_i$ oscillations observed at the interphase of a cell cycle in mouse zygotes (91, 92). Curiously, mPLCz1 is thus far the only member able to translocate to the PN, as human, rat, medaka fish (70), horse (93) and bovine PLCZs (94) are unable to accumulate in the PN despite the containing the highly conserved nuclear localization signal. Therefore, the physiological function of PLCZ translocation to the PN and the termination of the oscillations at the PN stage remain unclear.

1.3.3 Localization of PLCZ in sperm

The localization of PLCZ in the sperm of several mammalian species has been reported and it appears variable. A word of caution is needed here, as in most cases the antibodies used show cross reactivity with unknown proteins, therefore raising questions regarding the accuracy of the reported information. For example, in mouse sperm, PLCz1 localization was reported in both post-acrosomal region (95) and acrosomal regions (96), which was also the case for hamster sperm (96), whereas in rat sperm the localization seemed mostly to concentrate, in the acrosomal region (97). In human sperm, PLCZ1 was found in the equatorial (98) and equatorial and post-acrosomal regions (99). In large domestic species, whereas in the bull appeared almost exclusively in the equatorial region (95), in equine sperm appeared in the acrosome, equatorial region, head-midpiece junction and tail of equine sperm (100), which was similar to the distribution in pig sperm (101). In addition to the specificity of the antibodies, the localization of PLCZ1 may be affected by the status of sperm, i.e., whether or not capacitated or acrosome reacted. For instance, in humans, the proportion of sperm displaying the equatorial/acrosomal location distribution decreased, whereas the equatorial/post-acrosomal pattern increased after capacitation and ionophore treatment (102). Presently, it is not not known whether PLCZ protein undergoes redistribution during these events or the accessibility of the antibodies changes during capacitation and acrosome reaction.

1.3.4 PAWP

In 2007, Dr. Oko and colleagues reported that a novel alkaline extractable protein of the sperm head that exclusively resides in the post-acrosomal sheath region of the perinuclear theca (PT) might also be capable of inducing oscillations in mammalian eggs (103). Molecular cloning of PAWP has been reported in humans, mice and cows (103). It consists of 309 (human), 354 (mouse) and 313 amino acids (cow), and the N-terminal half of PAWP shares a 49% sequence similarity to WW domain binding protein 2. As for the C-terminal half of PAWP, Wu et al. (2007) showed that it contains an unidentified repeating motif (YG*X*PP*X*G (where *X* represents any residue). The protein was named PAWP (Postacrosomal sheath WW domain-binding protein). PAWP was detected in the cytoplasmic droplets of spermatids beginning to undergo elongation in mice, rabbits, pigs, cows, rhesus monkeys and humans using a PAWP antibody (103-105). Upon injection of recombinant human PAWP or alkaline PT extracts into porcine, bovine, macaque, and *Xenopus* oocytes, the authors revealed high incidence of PN formation and suggested PAWP mihgt be a candidate to be a sperm factor. On the other hand, co-injection of PAWP with a competitive peptide containing the PPXY motif prevented the effects of PAWP on activaiton on several species. To extend those results, the investigators examined whether injection of PAWP could induce oscillations. To that end, Aarabi et al. demonstrated that injection of recombinant human PAWP caused a $[Ca^{2+}]_i$ release in Xenopus oocytes (106), and also oscillations in mouse eggs (107). Nevertheless, given the lack of sequence homology to known signaling molecules, it remains unknown how this protein could trigger oscillations. Towards that end, attempts to replicate the results with PAWP in mouse oocytes have failed (108, 109), and a recent reported PAWP null mice line showed normal spermatogenesis and fertility (110).

Therefore, the role of PAWP at best remains thus uncertain in the mouse, although the possibility that a human oocyte specific factor is needed was not ruled out. Indeed, numerous studies have shown that testis and reproductive tissues evolve faster than other tissues leading to noticeable differences between species (111).

CHAPTER 2

THE ROLES OF TRPV3 CHANNELS IN MOUSE EGGS

Summary

Mammalian fertilization is initiated when a sperm fuses with a mature metaphase II (MII) oocyte, also known as an egg, and triggers a plethora of finely controlled processes identified as egg activation. The completion of early and late events of egg activation is driven by and depends on a series of repetitive $[Ca^{2+}]_i$ oscillations, which rely on Ca^{2+} influx. Ca^{2+} channels at the plasma membrane have been suggested to mediate Ca^{2+} influx during egg activation. The TRP Ca^{2+} channel TRPV3 is differentially expressed in oocytes during maturation, being fully active at the MII stage. Specific stimulation of TRPV3 channels in mouse eggs promotes Ca^{2+} influx sufficient to induce egg activation and parthenogenesis. Here, we explore the function and distribution dynamics of the TRPV3 channel protein during oocyte maturation. Using dsRNA, TrpV3 overexpression, and inhibitors of protein synthesis, we modified the native expression of the channel and showed the TRPV3 protein is synthetized and translocated to the plasma membrane during maturation. We demonstrated that 2-APB at the concentrations used to promote Ca^{2+} influx in eggs, specifically and reversibly targets TRPV3 channels, and it does not block the IP_3 receptor. Finally, we showed that TRPV3 channels functionally interact with the actin cytoskeleton indicating an actin-based regulation of its expression on the plasma membrane. Our results show that TRPV3 is a target of 2-APB in eggs, a condition that can be used to induce parthenogenesis. The association of endogenous TRPV3 channels with the actin cytoskeleton is a novel finding, and suggests that the rearrangements of actin that occur during maturation could regulate both plasma

membrane presence and function of TRPV3 Ca^{2+} channels involved in oocyte maturation and fertilization. We show that TRPV3 is required for strontium influx because TRPV3-KO eggs failed to conduct Sr^{2+} or undergo strontium-induced activation. We propose that TRPV3 is a major mediator of Ca^{2+} and/or other divalent cations influx in mouse eggs and is a putative target for artificial activation of mouse eggs.

2.1 Introduction

Under natural conditions, egg activation starts with fertilization and includes initiation of calcium ($[Ca^{2+}]_i$) oscillations, which trigger egg activation (reviewed in (5)). $[Ca^{2+}]_i$ increases are the universal signal of egg activation in all species investigated to date (6), whereas Ca^{2+} influx is necessary to support the long-lasting oscillations in mammals, which are the hallmark of mammalian fertilization (7, 8). External Ca^{2+} can be incorporated into cells through channels and/or transporters. One of the first characterized channels in mouse eggs were the T-type Voltage-gated Ca^{2+} channels (CaV 3.2; (21)); although, the function remains elusive as CaV 3.2-deficient female mice are fertile (22). Changes in membrane potential during fertilization are negligible (23), and the resting membrane potential of mouse eggs is close to the activation threshold of the CaV channels, which suggests that a large proportion of them might be inactivate in eggs before and after fertilization. The voltage-independent member of the TRP channel family, TRPV3, was also reported to be functionally active in mouse eggs (48). Native TRPV3 currents were first reported in keratinocytes, where addition of 100 μM 2-APB, a known activator of TRPV3 channels, elicited measurable changes in whole cell currents only in cells previously sensitized by temperature (56). Remarkably, TRPV3 channels

expressed in MI oocytes and eggs respond to 2-APB treatment with quantifiable whole cell currents without previous temperature exposure, suggesting different regulation or sensitization of native TRPV3 channels in mouse eggs (48). In this study, we artificially overexpressed the wild type channel tagged with fluorescent fusion protein to evaluate its localization in mouse oocytes and eggs. We showed that the exogenous and endogenous channel protein is synthetized during maturation and is translocated to the plasma membrane (PM) where it is fully responsive to 2-APB at the MII stage.

Since its initial use as specific inhibitor of the IP_3R1 (112), an ubiquitously expressed channel that mediates intracellular Ca^{2+} release in most cell types (1), 2-APB has been shown to block (or to activate, depending on the concentration and isoform) Ca^{2+}-ATPase pumps, SERCA (113), and other channels (114), including TRP channels where it was described as an "unspecific" blocker (115) 2-APB was also shown to activate TRPV1, TRPV2 and TRPV3 (116), and in fact, it is the most used activator of TRPV3 channels (56, 116). 2-APB is also an agonist of ORAI3 (117), one of the proteins that are molecular correlates, together with STIM, of the Store-Operated Ca^{2+} channels or CRAC channels (114). 2-APB was therefore also used to test the presence of ORAI3 in mouse oocytes and eggs, and the Ca^{2+} influx promoted by 2-APB in these cells was taken as confirmation of ORAI3 expression (118). Nevertheless, a previous report showed that 2-APB was unable to promote Ca^{2+} influx in *TrpV3-KO* eggs (at 100 μM (48)), suggesting TRPV3 is the only channel responsible for mediating the effects of 2-APB in mouse eggs. Using molecular and functional assays we show that the agonist effect of 2-APB in mouse oocytes and eggs is specifically mediated by TRPV3. We also demonstrated that

concentrations of 2-APB known to inhibit Ca^{2+} influx (119) do not block the function of IP_3R1 in oocytes.

Actin is a major cytoskeletal protein found ubiquitously within eukaryotic cells. Actin-based cytoskeleton complexes are involved in the dynamic of channels at the PM including endocytosis/exocytosis and intracellular trafficking (120), and can also modulate the activity of channels while on the membrane surface (121). Cytoplasmic actin filaments have been shown to function in mitosis and meiosis, especially in oocytes, eggs and blastomeres (122). These functions are related with positioning and assembly of the meiotic spindle as well as general organization and redistribution of organelles (122, 123). To that end, actin interacts with the ARP2/3 protein complex that becomes activated in the cortical region, where it nucleates a thick cortical actin layer termed "actin cap", which is essential for cytoplasmic flow (124). The reorganization of the cytoplasm during maturation correlates with changes in the functional expression of TRPV3 channels (48), which suggests an association between actin reorganization, redistribution, and incorporation of these channels into the PM. In this study, we hypothesized that TRPV3 channels actively interact with the actin cytoskeleton in mouse oocytes and eggs. Our results propose a close functional relationship between actin and TRPV3 channel presence in the PM, suggesting that intact microfilament organization may regulate the function of TRPV3 and other PM channels involved in Ca^{2+} homeostasis in oocytes and eggs.

Mammalian eggs can be parthenogenetically activated by a variety of artificial stimuli. Replacement of external Ca^{2+} by 5-10 mM strontium (Sr^{2+}) has been extensively used to induce egg activation in rodents (7, 125). This procedure is not associated with

chromosome abnormalities and is capable of promoting full-term development when combined with somatic cell nuclear transplantation (126). Importantly, it is unknown what channel(s) mediates the influx of Sr^{2+} in mouse oocytes, although the temperature regulation of TRPV3 channels and the reported sensitivity of Sr^{2+} influx to temperature makes them ideal candidates (48).

2.2 Results

2.2.1 Functional expression of TRPV3 channels progressively increases during oocyte maturation

Since significant changes take place in Ca^{2+} signaling in oocytes and eggs (2, 14, 127), we explored changes in TRPV3 functional expression in oocytes at different stages of maturation. During the GV stage, addition of 100 μM 2-APB did not induce a measurable current (Figure 2-1A) in these cells, and Ca^{2+} imaging studies confirmed those findings (Figure 2-1A and D). Once oocytes had undergone germinal vesicle breakdown (GVBD) and progressed to MI (Figure 2-1B), application of 2-APB evoked a TRPV3 current (Figure 2-1B) of 23 ± 2pA/pF (Figure 2-1D, left panel) as well as a $[Ca^{2+}]_i$ increase (Figures 2-1B and D). At MII (Figure 2-1C), when eggs become competent to mount oscillations in response to fertilization, TRPV3 channels responded to 2-APB with a current of 73 ± 6 pA/pF (Figure 2-1C and D), which is significantly higher than in MI eggs. Thus, TRPV3 more densely populates the MII membrane compared to the MI membrane (in channels/ μm^2). Despite their much smaller surface area (120 ± 7pF versus 226 ±9.5 pF, Figure 2-1D, middle panel) and higher TRPV3 channel density, $[Ca^{2+}]_i$

increases in MII eggs were similar in magnitude to those in MI (Figure 2-1C), reflecting the lower sensitivity of Ca^{2+} measurements compared with direct voltage clamp recordings of currents to monitor transport of ions across the PM, which is due to native Ca^{2+} buffers and variations in resting membrane potential in unclamped oocytes. Addition of Ionomycin, a Ca^{2+} ionophore that under Ca^{2+} -free conditions causes Ca^{2+} release from the intracellular stores, induced a response in all stages of maturation (Figure 2-1A-C, lower panel), confirming the healthy status of the our cells. Our results therefore show that the number of TRPV3 channels increase during oocyte maturation, being undetectable with electrophysiological recordings in the GV stage and reaching maximal absolute numbers of functional channels in the MII stage (0.1 channels/μm^2 in MII, assuming an equal open probability, P_0= 0.5 for both stages). They also show that ion channel density in oocytes and eggs is very low compared to excitable cells in which these values are typically 10^3- to 10^4 – fold larger (128).

2.2.2 Carvacrol, a TRPV3 agonist, induces $[Ca^{2+}]_i$ responses and activation in mouse eggs.

Carvacrol, the major ingredient in oregano, elicits TRPV3 mediated currents in heterologously expressing cells and in primary keratinocytes (54). Because heterozygous (V3-Het) eggs had robust TRPV3 currents in response to 2-APB, we performed functional studies in eggs isolated from V3-Het and knockout (V3-KO) littermates. Addition of 50 μM carvacrol to V3-Het eggs evoked a substantial increase in $[Ca^{2+}]_i$ (Figure 2-2A, left panel) and responded with an additional $[Ca^{2+}]_i$ increase following addition of 200 μM 2-APB. In contrast, eggs from V3-KO mice failed to respond to

either agonist (Figure 2-2A, right panel). We next tested whether stimulation of TRPV3 channel causes egg activation. Incubation of wild type (WT) and V3-Het eggs with 50 μM carvacrol provoked parthenogenesis as PN formation was observed within 5 hr after carvacrol treatment in roughly half of the mature eggs (Figure 2-2B and C). Cleavage to the 2-cell stage was observed 24 hr after treatment (67% ± 3% in WT eggs and 56% ± 4% in V3-Het eggs, Figure 2-2B and D).

2.2.3 TRPV3-mediated Ca^{2+} influx is not required for maintenance of Ca^{2+} oscillations.

The fertilization-associated $[Ca^{2+}]_i$ oscillations that underlie activation of mammalian eggs are thought to be triggered by the sperm-specific PLCZ. PLCZ activates the egg's phosphoinositide pathway to generate IP_3, which, in turn, gates the endoplasmic reticular Ca^{2+}-permeant IP_3R (11, 19). Although the first few oscillations of Ca^{2+} rely on internal Ca^{2+} stores, the persistence of the Ca^{2+} oscillations requires Ca^{2+} influx (7, 23). To ascertain whether TRPV3 channels are required for these oscillations in response to fertilization, we examined sperm-induced Ca^2 oscillations in V3-KO and V3-Het MII eggs. We observed the first $[Ca^{2+}]_i$ transients 5-10 min after addition of sperm (Figure 2-3A; see (129)). No differences were found for in vitro fertilization success, assessed as the rate of 2-cell formation between V3-KO and V3-Het eggs (Figure 2-3B). We next examined whether the activity of TRPV3 channels was required to support oscillations induced by injection of Plcz cRNA. These oscillations, which were monitored for 6 hr, were similar in V3-KO and V3-Het MII eggs with respect to time of initiation, amplitude, frequency, and duration (Figure 2-3C). These data suggest that PLCZ does not

substantially potentiate TRPV3 as a mechanism of its action on Ca^{2+} oscillations. However, addition of 200 μM 2-APB to V3-Het eggs that were undergoing oscillations at 37°C dramatically increased Ca^{2+} influx and prevented $[Ca^{2+}]_i$ from returning to baseline, immediately blocking oscillations in V3-KO eggs (Figure 2-3C). Finally and as expected, the addition of the TRPV3 agonist, carvacrol (50 μM), to oscillating WT eggs increased Ca^{2+} influx and immediately halted the oscillations by preventing the return of $[Ca^{2+}]_i$ back to baseline.

2.2.4 TRPV3 channels mediate Sr^{2+} influx and subsequent egg activation

Sr^{2+} has been widely used to induce parthenogenesis in rodent eggs (130, 131). The channel that mediates Sr^{2+} influx has not been reported in any species, and whether Sr^{2+} and Ca^{2+} permeate the same channels in mouse eggs is unknown. To ascertain whether the TRPV3 channel mediates Sr^{2+} influx, we recorded the heat-activated TRPV3 current in V3-Het and V3-KO cells in the presence of an extracellular solution containing 10 mM $SrCl_2$ and normal $[Ca^{2+}]$ (~10 μM) (Figure 2-4A). The absence of inward Sr^{2+} current in V3-KO eggs correlates with the lack of $SrCl_2$-induced oscillations in these eggs (Figure 2-4B) and their inability to become activated in media supplemented with $SrCl_2$, as assessed by 2-cell formation (Figure 2-4C and D). Nearly all WT eggs (89%±11%) and over half of V3-Het eggs (61% ± 5.3%) became activated in these experiments.

2.2.5 2-APB promotes repetitive $[Ca^{2+}]_i$ rises by promoting Ca^{2+} influx

To confirm that $[Ca^{2+}]_i$ increases induced by 2-APB are caused by Ca^{2+} influx and are not due to off target effects of the drug (113), we exposed MII eggs to sequential 10 min

pulses of 2-APB interspersed with intervals without it in Ca^{2+} containing media. This treatment resulted in immediate $[Ca^{2+}]_i$ increases with $[Ca^{2+}]_i$ levels remaining elevated throughout the presence of the agonist. Washout of 2-APB caused a rapid return of $[Ca^{2+}]_i$ values to basal levels (Figure 2-5 *left panel*). Exposure to 2-APB in the absence of extracellular Ca^{2+} failed to cause any $[Ca^{2+}]_i$ increase, although re-addition of Ca^{2+} was followed by a progressive rise in $[Ca^{2+}]_i$ until reaching peak levels (Figure 2-5, *right panel*). These results show that 2-APB- induced $[Ca^{2+}]_i$ increases in MII eggs are due to Ca^{2+} influx and are caused by selective opening of TRPV3 channels by 2-APB.

2.2.6 Inhibition of protein synthesis undermines the response to 2-APB in oocytes and eggs

GV oocytes do not express TRPV3 channels on the PM, although the channel is functionally present in eggs, suggesting that protein translation and/or translocation of the channel to the PM takes place during the late stages of maturation. To more closely investigate the dynamics of TRPV3 function during maturation, we performed *in vitro* maturation and examined the response to 2-APB at different time points during the process. Maturation was conducted in the presence and/or absence of cycloheximide (CHX), a protein synthesis inhibitor, as we assumed that preventing protein translation would reduce the availability of TRPV3 channels. CHX was added 4 hr after the initiation of maturation, to allow initial synthesis of cyclin B, a member of the maturation promoting factor (MPF) complex, to ensure better progression through meiosis [S Brunet, 2005]. At the same time, we supplemented the media with colcemid (COL), a microtubule polymerization inhibitor that by preventing the formation of the spindle

should favor cyclin synthesis and avoid transition into interphase (132). We anticipated that this was necessary as in the presence of lower levels of cyclin B and MPF activity following CHX treatment, MI oocytes may prematurely enter interphase instead of remaining arrested at M-phase; COL does not interfere with initiation and persistence of oscillations at the MII stage (2). Therefore, after maturation for 8, 10 or 12 hr, control oocytes and oocytes treated only with COL responded to 2-APB for the first time at 8 hr post-initiation of maturation with a small and transient $[Ca^{2+}]_i$ increase (Figure 2-6*, left, upper panel; middle, upper panel*). Two additional hours of maturation (10 hr post initiation of the essay), greatly enhanced $[Ca^{2+}]_i$ responses to 2-APB, with the rises being large and sustained (Figure 2-6*, left middle panel; middle, middle panel*). The responses to 2-APB treatment increased even further by 12 hr of maturation, which is the time at which oocytes reach the MII stage, and the responses had amplitudes nearly twice as large as those at 10 hr $[Ca^{2+}]_i$ levels remained at peak values throughout the monitoring period (Figure 2-6*, left bottom panel; middle bottom panel*). Oocytes matured in the presence of CHX+COL also initially responded to 2-APB by 8 h post maturation, comparable to controls. However, $[Ca^{2+}]_i$ responses to 2-APB by 10 and 12 hr post maturation were greatly reduced in CHX- treated cells both in persistence (10 hr) and amplitude (12 hr) (Figure 2-6*, middle and bottom right panels*). These results suggest that protein synthesis of TRPV3 channel occurs during middle and late stages of maturation, rendering mouse eggs sensitive to Ca^{2+} influx stimulated by 2-APB.

2.2.7 Overexpression of TRPV3 promotes Ca^{2+} influx in GV oocytes

Given the stimulatory effects of 2-APB towards TRPV3 channels (116), we tested the function of RFP-TRPV3 channels. As expected, in non-injected GV oocytes, 200 μM 2-APB failed to trigger an increase in $[Ca^{2+}]_i$, (Figure 2-7A, *left panel* (48)), whereas it triggered a $[Ca^{2+}]_i$ increase in GV oocytes injected with *Rfp*-m*TrpV3* (Figure 2-7A, *right panel*) suggesting TRPV3 is the only channel responsible for Ca^{2+} influx in mouse oocytes.

To extend these results given that TRPV3 accumulates during maturation, we performed the converse experiment and attempted to prevent expression of TRPV3 channels during maturation (48) using double strand (ds) RNA technology. To this end, GV oocytes were injected with dsRNAs targeting the endogenous *TrpV3* mRNA or *Venus* (control) and the impact on *TrpV3* RNA levels was evaluated using RT-PCR. Injection of dsRNA-*TrpV3* effectively decreased RNA levels (Figure 2-7 B, *left panel,* lane 7; Figure 2-7 B*, right panel*), whereas *Venus* dsRNA had no effect on the levels of *TrpV3* mRNA (Figure 2-7 B, *left panel*, lane 5; Figure 2-7 B, *right panel*). Following *in vitro* maturation, we examined the ability of these eggs to respond to 2-APB stimulation. As previously shown, control non-injected eggs (48) and DsRNA-*Venus* injected eggs showed the expected $[Ca^{2+}]_i$ increase after addition of 2-APB (Figure 2-7 C, *left panel* [I. Carvacho, 2013]; Figure 2-7 D, *right panel*), whereas eggs injected dsRNA-*TrpV3* showed reduced responses (Figure 2-7 C, *right panel*), confirming the role of this channel in mediating responses to 2-APB.

2.2.8 TRPV3 channels localize to the PM of oocytes, eggs and zygotes

Previous studies using whole-cell patch-clamp methods showed TRPV3 channels are expressed on the PM of MI oocytes and MII mouse eggs (48). However, the subcellular localization and trafficking of TRPV3 during maturation was not characterized, in part due to the lack of specific antibodies. To overcome this limitation, we injected RFP-*TrpV3* mRNA into GV oocytes and incubated them for 8 hr in media containing IBMX to allow protein translation. GV oocytes were then allowed to resume meiosis and reach the MII stage while the localization of RFP-*TrpV3* throughout maturation was monitored. Endogenous TRPV3 channels are not expressed on the PM of GV oocytes, at least as defined by functional evidence provided by electrophysiological and Ca^{2+} monitoring studies (48) (Figure 2-7 A, *left panel*); although, exogenous TRPV3 channels were observed on the PM of GVs injected with *TrpV3* mRNA (Figure 2-8, *Upper panel*, GV). Following completion of maturation at the MII stage, RFP-TRPV3 channels remained on the PM (Figure 2-8, *Middle panel*, MII); although there appeared to be more cytoplasmic staining, possibly associated with trafficking of the channel and/or excess of protein synthesis caused by the overexpression (Figure 2-8*, Middle panel*, MII). Consistent with an excess of functional TRPV3 channels in MII oocytes injected with *TrpV3* mRNA, a small percentage of these oocytes, ~10-15%, failed to arrest and spontaneously progressed to the PN stage (Figure 2-8, *lower panel*, PN), in contrast to control non-injected oocytes, which always arrested at the MII stage

2.2.9 Actin cytoskeleton regulates the function of TRPV3 channels in the egg membrane

Functional interaction between TRP channels and the actin cytoskeleton is well established (133, 134); although it is unknown whether interactions between TRPV3 channels and the actin microfilament occur and if they might affect TRPV3 function and/or distribution. To explore these possibilities, we exposed eggs to LatA, which is an actin polymerization inhibitor that modifies the organization of the egg cortex (135). As expected, in control conditions, 2-APB increased $[Ca^{2+}]_i$ in all cells (Figure 2-9A*, left panel*), whereas eggs exposed to LatA (5 μM, 30 min) showed lower responses to 2-APB (Figure 2-9A *right panel*), which was also clearly delayed (Figure 2-9A*, right panel*; Figure 2-9B). We next examined the effect of LatA on oscillatory responses, which are induced in mouse eggs by incubation in 5-10 mM Sr^{2+} (131, 136, 137). TRPV3 channels have been shown to mediate Sr^{2+} oscillations in mouse MII eggs (48), and the expectation was that disruption of cortical actin might affect Sr^{2+}-induced oscillations. Consistent with a role of actin on TRPV3 function, Sr^{2+}-induced oscillations were reversibly blocked by LatA treatment (Figure 2-9C).

In agreement with the Ca^{2+} imaging results, analysis of TRPV3 distribution following using confocal microscopy showed changes in its cellular localization following treatment with LatA- (Figure 2-10 A-L). In control GVs and MII eggs injected with RFP-*TrpV3* mRNA, the exogenous protein showed a clear PM localization (Figure 2-10 A, E, I), which was disrupted by addition of LatA (Figure 2-10 B, F, J). Addition of LatA reduced the presence of TRPV3 on the PM and increased its presence in the ooplasm, and these changes in distribution are reflected by the ratio of fluorescence intensity between cytoplasm and PM and are proportional to the duration of the LatA treatment (Figure 2-10 C and D, G and H, K and L; *, $P<0.05$) (138). In short, the longer the duration of

exposure to LatA, the greater the redistribution of TRPV3 from the PM to the ooplasm, as evidenced in MII eggs exposed to LatA for 2 hr (Figure 2-10 L). All together these results suggest a direct and/or indirect interaction between TRPV3 and the actin cytoskeleton, which is capable of affecting the function and distribution of TRPV3, and possibly other channels on the PM.

2.2.10 2-APB does not block the function of IP_3R1 in mouse eggs

In a previous study we showed that $[Ca^{2+}]_i$ oscillations induced by injection of *mPLCζ* mRNA in *TrpV3-KO* eggs were nearly identical to those of wild type eggs with an exception: addition of 2-APB did not block *mPLCζ* cRNA induced oscillations in wild type eggs, whereas it blocked *mPLCζ* induced $[Ca^{2+}]_i$ oscillations in *TrpV3*-KO eggs (48). Interpretation of those results indicates that in *TrpV3-KO* eggs, 2-APB becomes an inhibitor of the channel(s) that support influx at fertilization, with *mPLCZ* mRNA being used as a proxy for fertilization. However, as previously mentioned, 2-APB is a broad spectrum inhibitor of the TRP family of channels, of the SERCA pump (113) and even of IP_3R1 (112), and inhibition of oscillations by 2-APB in *TrpV3*-KO eggs is due to inhibition of IP_3R1 cannot be ruled out. To test the effect of 2-APB on the mentioned receptor, we injected eggs with caged IP_3 which is released by pulses of UV light and causes $[Ca^{2+}]_i$ responses (Wakai T, 2012). In control eggs, repeated UV pulses caused single and sharp $[Ca^{2+}]_i$ increases (Figure 2-11, *upper panel*]), and similar responses were observed in eggs treated with 50 μM 2-APB (Figure 2-11. *lower panel*); although, $[Ca^{2+}]_i$ levels seemed to return to baseline in a protracted manner, probably due to partial

activation of TRPV3 channels on the PM by 2-APB. Thus, at the concentration tested, 2-APB does not affect IP_3R1 function in mouse eggs.

2.3 Discussion

Ca^{2+} signaling plays a pivotal role in many physiological processes including fertilization and early embryo development. Increases in $[Ca^{2+}]_i$ induce egg activation in all animals studied to date, and these increases are mostly induced by fertilization and sperm entry (6), but they can also be induced by mechanical stimulation (139). In mammals, the fertilization Ca^{2+} signal last for several hours and the number of oscillations and/or overall magnitude of the Ca^{2+} increases is directly related with successful completion of all events of egg activation and embryo development to term (59, 140). Extracellular Ca^{2+} influences the frequency and magnitude of the $[Ca^{2+}]_i$ responses (7) and is required for complete egg activation (8). Therefore, detailed study of the Ca^{2+} entry pathways is essential to better understand the Ca^{2+} dynamics during maturation and fertilization. We examined the contribution of a TRP channel to Ca^{2+} influx in mouse oocytes and eggs during maturation and fertilization. Using voltage clamp and Ca^{2+} imaging measurements of WT and V3-KO mouse oocytes, we show that TRPV3 becomes the major Ca^{2+} entry pathway in these cells as they mature. Ca^{2+} permeation via TRPV3, as induced by temperature elevation, and the TRPV3 agonists 2-APB and carvacrol, was confirmed using TRPV3 knockout mice. Notably, TRPV3 channels are the major mediators of $SrCl_2$ influx during strontium-induced activation in mouse eggs. $SrCl_2$ failed to induce oscillations or egg activation in TRPV3-null eggs. In line with this, we have shown functional expression of the TRPV3 channel during

maturation, with initiation of expression coinciding with resumption of meiosis (48). TRPV3 channels are consequently able to mediate Ca^{2+} influx in mouse eggs and its specific activation provokes Ca^{2+} influx capable of inducing parthenogenetic egg activation. Here, we examined the localization and functional activity of the TRPV3 channel using gain- and loss-of-function approaches. Besides confirming the direct stimulation of TRPV3 by 2-APB, we show it is a useful tool for further studies related with Ca^{2+} channels expression and function in oocytes and eggs, as it does not affect the function of IP_3R1. Using fluorescence and Ca^{2+} imaging assays we show TRPV3 channels functionally interact with the actin cytoskeleton, and our results suggest other channels involved in Ca^{2+} influx during maturation and fertilization may have similar associations with the cytoskeleton. Future studies should address this possible association. Also, given the sensitivity of TRPV3 channels to 2-APB, we propose future experiments to elucidate the channels underlying fertilization-induced influx should be performed in *TrpV3* knock-down or *TrpV3*-KO oocytes and to avoid the confounding effects of native TRPV3 channels, which are not required for sperm-induced $[Ca^{2+}]_i$ responses.

The small T-type, CaV3.2, currents in eggs does not appear to be necessary or sufficient for Ca^{2+} oscillations. In any case, the normally depolarized egg membrane potential ensures that they are primarily inactivated (20, 141). Thus, Ca_v channels would most likely be important during an acute depolarizing stimulus, such as fertilization in some species (142). Interestingly, commonly used Ca_v1(L-type) and Ca_v3 (T-type) channel-blocking drugs are not known to be associated with human female infertility.

Another potential source of Ca^{2+} entry, CRAC currents, might be active at the GV stage of mouse oocytes, but their function decreases as maturation progresses (119). Expression of Stim1 and Orai1 was detected in mouse oocytes and eggs (119), but to date, no Stim1 or Orai1subtype female heterozygous or KO mice are reported to be subfertile. Because $Orai1^{-/-}$ and $Stim1^{-/-}$ mice die prenatally, tissue- and age specific genetic deletion would clarify this issue. Direct measurements of CRAC current under voltage clamp would likely clear up these inconsistencies, but the size of eggs makes this task difficult due to the size of background currents. In our studies, if CRAC currents are present, they are ≤ 3 pA/pF (in 20 mM $[Ca^{2+}]_e$), but still large enough to be significant in maintaining cytoplasmic and ER levels. We found that addition of a specific CRAC (Orai1, Orai3) channel blocker during in vitro maturation of Het-V3 and V3-KO oocytes did not affect germinal vesicle breakdown (GVBD); although, we did observe a slight decrease in the percentage of polar body extrusion in both groups. Further experiments, such as tissue-specific deletion of Orai subunits, are necessary to clarify the function of CRAC channels during maturation.

2.3.1 Functional expression of TRPV3 channels during mouse oocyte maturation

At the germinal vesicle stage of oocyte development, TRPV3 currents were undetectable, and consistent with this observation, conditions that activate TRPV3 fail to induce Ca^{2+} influx. By the MI stage, however, small TRPV3 currents were recorded, and these became significantly larger (in both net amplitude and density) in MII oocytes. Thus, during maturation, increases in TRPV3 functional expression coincide with meiotic progression during maturation. $[Ca^{2+}]_e$ is required for progression beyond GVBD during

oocyte maturation (14); without $[Ca^{2+}]_e$, the formation of the polar body is inhibited and oocytes fail to progress past MI (143). In vivo, the immature GV stage oocyte maintains direct communication with the surrounding cumulus and granulosa cells through gap junctions, permitting heterologous metabolic and electrical coupling (127). However, spontaneous Ca^{2+} oscillations recorded in GV stage oocytes are not dependent on the surrounding follicle cells (144).

Although TRPV3 currents coincide with meiotic progression during maturation, the TRPV3 channel function is not required for this process. The striking fact is that V3-KO female mice have normal fertility and number of offspring to skin and hair rather than mating or reproduction. Constitutively active TRPV3 mutations cause hair loss and increase susceptibility to dermatitis and inflammatory skin lesions in rodents (145, 146), although without apparent defects in female fertility. The Olmsted syndrome, a rare human congenital disorder producing palmoplantar keratoderma, alopecia, and severe itching, is associated with TRPV3 gain-of function mutations. However, it is unclear whether female fertility is affected.

2.3.2 Stimulation of TRPV3 channels leads to egg activation

Activation of TRPV3 by carvacrol and 2-APB induces Ca^{2+} entry, which can parthenogenetically activate eggs. Treatment with Ca^{2+} ionophores such as Ionomycin or A213187 can result in embryos with decreased or impaired developmental competence. The long-term ramifications on offspring are unknown (147), even though these manipulations are used in patients who have low fertilization potential (148, 149). Thus, the understanding of TRPV3 expression and function in human eggs may be an

opportunity to improve artificial oocyte activation (AOA) via specific activation of TRPV3 channels rather than the use of nonspecific ionophores.

2.3.3 Sr^{2+} induced egg activation and TRPV3 channels

Strontium induces egg activation by promoting oscillations in $[Ca^{2+}]_i/[Sr^{2+}]$, perhaps by sensitizing the egg IP_3R1 receptors. These $SrCl_2$-induced calcium oscillations are distinct from those provoked by the sperm (or by adenophostin, a nonhydrolyzable agonist of the IP_3R) and do not induce downregulation of the IP_3R (150, 151). The mechanism or Sr^{2+} gating of the IP_3R1 is thus the TRPV3 channel, because it mediates Sr^{2+} influx into rodent eggs. It has been suggested that Sr^{2+} could sensitize IP_3Rs and facilitate Ca^{2+} oscillations, perhaps by substituting for Ca^{2+} in the potentiation of IP_3Rs (152, 153). Strontium-induced egg activation is mediated by CaMKIIγ, as CaMKIIγ$^{-/-}$ eggs failed to respond to Sr^{2+} treatment, likely due to a failure to resume meiosis II (154).

The fact that V3-KO eggs do not to respond to Sr^{2+} is clear evidence that under the conditions in which Sr^{2+} -induced activation was measured (37°C, 10 mM $SrCl_2$ in the extracellular media, ~10 μM [Ca]), TRPV3 is required for measurable strontium permeation. This does not mean that TRPV3 is the only strontium-permeable channel in the egg plasma membrane. In fact, Ca_v channels present in the egg plasma membrane are permeable to Sr^{2+} as shown by Hirano et al. (155), but Ca_v3 channels are largely inactivated at the eggs' resting membrane potentials. Because the egg membrane potential remains stable at potentials in which Ca_vs are inactivated (23), we did not observe measurable Sr^{2+} permeation via Ca_v, positioning TRPV3 as the major mechanism for Sr^{2+} -induced egg activation in mice.

2.3.4 Regulation and function of TRPV3 channels in mouse oocytes and eggs

Muscarinic receptors couple to the Gq/11 proteins in mouse eggs activate PLCβ (156) and initiate PIP2 hydrolysis. This, in turn, generates IP_3 and the PKC activator, diacylglycerol (157). Muscarinic agonists induce membrane potential changes (158) and a series of small $[Ca^{2+}]_i$ oscillations in mouse eggs (159). Stimulation of PKC activity greatly enhances the frequency of these oscillations (160). These same pathways also modify TRPV3 channels: in somatic cells, carbachol (161), diacylglycerol, phorbol-12-myristate-13-acetate, and PLC-coupled receptor-catalyzed PIP2 hydrolysis (162) all modulate TRPV3 activity. Ca^{2+}, via calmodulin, also activates CaMKII to modulate oscillatory changes during fertilization (163) and govern exit from MII (164). Ca^{2+}/calmodulin initially inhibits TRPV3 activity, perhaps explaining sensitization of TRPV3 to repetitive stimulation by mediating Ca^{2+}-dependent initial channel inhibition (165). In summary, there is good evidence that PLC activation regulates both oocyte and egg TRPV3 and $[Ca^{2+}]_i$.

The male-specific PLCz, which more effectively generates PIP2 production in eggs, is likely to be the upstream activator of TRPV3 (129). Accordingly, we expect that PLCz overexpression would potentiate endogenous egg TRPV3 current. In spite of the expression of TRPV3 in MII mouse eggs and its predicted nearly constitutive function at 37°C, TRPV3-mediated Ca^{2+} influx is seemingly dispensable for maintaining PLCz-induced $[Ca^{2+}]_i$ oscillations or for fertility, because V3-KO females show normal oscillatory responses in eggs and after fertilization.

What is the function of TRPV3 in oocytes and eggs? One possibility is that TRPV3 channels constitutively conduct low levels of Ca^{2+} to maintain Ca^{2+} homeostasis. Nevertheless, given the importance of these functions, eggs may have a redundant system that may explain the unchanged oscillation pattern and fertility in V3-KO eggs. It is probable that an unknown G protein receptor may be activated to induce PLCβ activation and modulate TRPV3 activity. Less probable, but more intriguing, is that highly temperature-sensitive TRPV3 may function to "reawaken" egg maturation/activation in mammals that significantly lower their body temperatures during hibernation, and that TRPV3 is thus not functionally relevant in mammals that do not hibernate. Increasing ambient temperatures above 32°C would increase TRPV3 activity and prime progression to MII. Finally, it is possible that there are unknown endogenous direct activators of oocyte and egg TRPV3. Future studies will examine the expression of TRPV3 in other species, such as humans, as well as the regulation of TRPV3 function.

2.3.5 2-APB activates TRPV3 channels without altering IP_3R1 function in mouse oocytes.

The actions of 2-APB on Ca^{2+} channels are both stimulatory and inhibitory. Its main agonist activity towards channels of the TRP channel family has been associated with the closely related members of the vanilloid subgroup (TRPV1, 2 and 3. (116)). 2-APB also potentiates TRPM6 and has a bimodal action on TRPM7, with high micromolar concentrations inhibiting TRPM7, whereas concentrations greater than 1 mM potentiating TRPM7 currents (166). In addition, low concentration of 2-APB were shown to potentiate ORAI1 and activate ORAI3 (114), which are the proteins that constitute the

ion channels of the CRAC or SOCE current, and whose expression has been reported in mouse eggs (119).

In light of the broad actions of 2-APB, it is necessary to identify the channel(s) targeted by it in oocytes and eggs. Using electrophysiology and null mice, we have shown that TRPV3 was functional in mouse oocytes and eggs and it was responsible for the action of 2-APB (48). Here, we extended those results by showing that expression of TRPV3 in GV oocytes, which lack endogenous TRPV3 on the PM, confers responsiveness to 2-APB, confirming the specificity of the channel as the target of 2-APB. We also show the response to 2-APB depends on extracellular Ca^{2+}, which is consistent with findings showing that eggs incubated in its presence at 37 °C undergoes parthenogenetic activation.

The purported actions of 2-APB are not limited to targets on PM channels, but it has also been described to target intracellular molecules and channels. In fact, 2-APB was first investigated as an inhibitor of IP_3R1 (112). IP_3R1 plays a crucial role in fertilization, and specific antibodies to it blocked $[Ca^{2+}]_i$ responses associated with sperm entry and egg activation (60). While the actions of 2-APB on IP_3R1 have not been investigated in mouse oocytes and eggs, addition of 2-APB was shown to block fertilization-induced oscillations in eggs from *TrpV3-KO* mice. The possibility that results could be due to inhibition of IP_3R1 cannot be ruled out. Our results show that this is not the case, as 2-APB not only did not abrogate Ca^{2+} release induced by cIP_3, but actually increased it, which is possibly due to activation of some TRPV3 channels on the PM by 2-APB. Thus, our data show that the main action of 2-APB on WT eggs is on TRPV3 channels where it promotes Ca^{2+} influx. Importantly, given that 2-APB behaves as a channel inhibitor in

eggs of the *TrpV3*-KO mice (48), it could be a very useful tool to identify the channels that underlie the sperm-induced oscillations in mouse eggs.

2.3.6 Actin microfilaments and functional expression of TRPV3 channels

The physiological regulation and natural agonists of TRPV3 channels are not well characterized (51); although, a few interacting partners are known, including calmodulin (165), epidermal growth factor receptor (EGFR) (167), and TRPV1, which reportedly forms heteromeric channels with TRPV3 (50). The cytoskeleton, especially actin, has also been shown to interact and modulate the function of members of the TRP family (134), and of other ion channels (120). Related to TRPV3 activity is the impaired function of TRPV4 caused by addition of LatA, which affects the regulation of cell volume (133). In mouse oocytes and eggs, the role of actin on PM channels has not yet been explored. Research shows evidence of an association between actin organization and Ca^{2+} homeostasis, as in starfish oocytes, LatA induced Ca^{2+} mobilization that resulted in fast discharge of cortical granules similar to responses caused by fertilization (168). In rat basophilic leukemia (RBL) cells, $[Ca^{2+}]_i$ oscillations and IP_3 synthesis are directly associated with oscillations of cortical actin polymerization and cycles of vesicle secretion (169). Our results in mouse eggs demonstrate TRPV3 channels and the actin cytoskeleton are also interconnected, as depolymerization of actin reduced the recycling of TRPV3 channels to the PM, which was evidenced by the loss of TRPV3 expression on the PM and increased presence in the cytoplasm. Remarkably, where the effects of LatA on actin organization became evident after a few hours of exposure to the drug, the effect of LatA on TRPV3 responses to 2-APB or Sr^{2+}oscillations was faster, approximately

within 20 minutes of addition of LatA. We speculate this "fast" action of LatA might be due to altered permeability of the channels caused by disruption of the cortical microfilaments, which also reportedly occurs for SOCE, whose current is impaired by disruption of the actin cortical layer subjacent to the PM without substantial breakdown of the actin cytoskeleton (170). It is unknown whether the function of TRPV3 channels in mouse eggs is regulated by other factors known to regulate these channels in somatic cells, such as hydrolysis of PIP_2 (162) or by the polymerization-depolymerization cycles of cortical actin. Future studies should investigate this possibility along with the prospect that actin also regulates the activity of other channels involved in Ca^{2+} influx during maturation and fertilization.

2.3.7 TRPV3 responsiveness to 2-APB and Sr^{2+}

It is known that TRPV3 mediates Sr^{2+} influx in unfertilized eggs and as shown here, it is also the target of the stimulatory effects of 2-APB on Ca^{2+} influx in these cells (48). It is noteworthy that only in rodent eggs- mice and rats- Sr^{2+} exposure causes oscillations and egg activation (136). Moreover, exposure of bovine eggs to Sr^{2+} does not result in egg activation or oscillations. Further, evidence in the literature suggests that Sr^{2+} might not be a reliable parthenogenetic agent in humans, which implies that these cells also do not display oscillations in response to Sr^{2+} treatment (171). Therefore, there exists the possibility that the response to 2-APB treatment and the ability of Sr^{2+} to initiate oscillations are associated. The residues that mediate the responsiveness of TRPV3 to 2-APB are known (116) and are well conserved among mammals, which suggest that this might not underlie the differences between oocytes of different species. Therefore, it is possible that different residues determine ability to conduct Sr^{2+}; although, this seems

very unlikely considering that the pore region within related channels (same family) is, in general, conserved (172). Alternatively, not all mammalian oocytes might express TRPV3 channels, which would prevent Sr^{2+} influx altogether, as well as responses to 2-APB. Lastly, despite Sr^{2+} influx, IP_3R1s in those species might be less sensitive to the stimulatory effects of Sr^{2+} and therefore might not be capable of promoting additional Ca^{2+} release to induce a whole-cell Ca^{2+} increase. Future studies should determine how the responsiveness to 2-APB and Sr^{2+} influx are associated, as it might lead to the development of better parthenogenetic agents. I would like to attempt a rescue experiment using V3-KO mice. I plan to inject *TRPV3* cRNA into GV oocytes of V3-KO mice, and I will induce Sr^{2+} activation and 2-APB mediated Ca^{2+} influx 12 to 24 hr after the injection of the cRNA.

We have already published some of these data in Cell Reports (2013), and other data were accepted to publish in Cell Calcium (2015).

2.4 Materials and Methods

2.4.1 Animal care and welfare

Animals used for gamete collections for this study were handled according to the National Research Council's Animal Care and Welfare guidelines. The Institutional Animal Care and Used Committee at the University of Massachusetts approved these procedures.

2.4.2 Collection of mouse oocytes

GV oocytes were collected from the ovaries of 6- to 10-week-old CD-1 female mice 44–46 hr after injection of 5 IU of pregnant mare serum gonadotropin (PMSG; Sigma). Cumulus intact GV oocytes were recovered in a HEPES–buffered Tyrode's lactate solution (TL-HEPES) containing 5% heat-treated fetal calf serum (FCS; Gibco) and 100 μM isobutyl-I-methylxanthine (IBMX). Cumulus cells were removed by repetitive pipetting and denuded oocytes were matured in vitro for 12–14 hr in IBMX-free Chatot, Ziomek, and Bavister (CZB) [Chatot CL J reprod fertilization 1989] media that were supplemented with 3 mg/ml bovine serum albumin (BSA) or 0.1% polyvinyl alcohol (PVA; Sigma, St Louis, MO) under mineral oil at 37°C in a humidified atmosphere of 5% CO_2. MII oocytes were collected from the oviducts 12–14 hr after administration of 5 IU of human chorionic gonadotropin (hCG), which was administered 46–48 hr after PMSG. Cumulus cells were removed with 0.1% bovine testes hyaluronidase (Sigma).

2.4.3 TRPV3 plasmid and dsRNA preparation

Mouse *TrpV3* (m*TrpV3* cDNA) construct kindly provided by the lab of Dr. D Clapham (Boston Children's Hospital-Harvard Medical School). *TrpV3* was subcloned into a pcDNA6B/his-myc B vector between the XhoI and AgeI restriction sites. To determine the subcellular distribution of the protein in oocytes and eggs, the sequence encoding *TrpV3* was tagged on the N-terminal end with the sequence encoding for the fluorescence protein Ruby. Double stranded RNA (dsRNA) oligonucleotides against the *TrpV3* gene was synthesized by the MEGAclear Kit (or Cell to cDNA Kit). DNA fragments of approximately 520 bp in length containing coding sequences for the protein to be

"knocked down" were amplified using PCR. Each PCR primer will contain a 5' T7 RNA polymerase-binding site (TAA TAC GAC TCA CTA TAG GG) preceding the targeted sequences. The sequences used for primer construction are as follows: *TrpV3*, GenBank accession no. NM145099, sense-primer: CATCA CCCTG ACCCT TGTCT; antisense-primer: GCTGA AGCTG CCATA GGAAC. A plasmid target to the fluorescent protein Venus was used as a control (T7 Venus 5F': TAA TAC GAC TCA CTA TAG GG GACGT AAACG GCCAC AAGTT, T7 Venus 3R': CCC TAT AGT GAG TCG TAT TA GGATC TTGAA GTTGG CCTTG). The PCR products were purified using the MEGAclear kit (Ambion). Purified PCR products were used as templates by a MEGASCRIPT T7 transcription kit (Ambion) to produce dsRNA (173). The dsRNA products were ethanol-precipitated and resuspended in water. The dsRNAs were annealed by incubation at 65 °C for 30 min followed by slow cooling to room temperature. The concentrations of dsRNAs was adjusted to 1-2 μg/μl, with aliquots stored at -80 °C.

2.4.4 TRPV3KO mice

These mice were generated in the lab of Dr. David Clapham and details are published in Cell Reports eggs (48).

2.4.5 Microinjections

Microinjections were performed as described previously (174). dsRNAs or cRNA were centrifuged, and the top 1-2 μl. used to prepare micro drops from which glass micropipettes will be loaded by aspiration. dsRNAs or cRNA were delivered into oocytes by pneumatic pressure (PLI-100 picoinjector, Harvard Apparatus, Cambridge, MA). Each

oocyte was received 5 - 10 pl, which is approximately 1- 3% of the total volume of the egg. Injected GV oocytes were allowed for maximal translation up to 8 hr in CZB in medium supplemented with IBMX, after which IBMX was washed off to allow for resumption of maturation for 12 hr. For downregulation of *TrpV3* mRNA, dsRNAs were injected at the GV stage and held there in IBMX for 8 hr, after which maturation was allowed to resume. Evaluation of mRNA degradation was performed using the Cell to cDNA kit (Ambion), after which relative expression levels of transcripts were compared.

2.4.6 Parthenogenetic egg activation

For TRPV3-mediated egg activation, eggs were incubated at 37°C for 10 min in 50 μM Carvacrol in CZB medium or for 30 min in 200 μM 2-APB in modified Krebs-Ringer bicarbonate medium. In both cases, the media was FCS-free 0.1% PVA (poly-vinyl alcohol, Sigma). In studies using MII eggs, activation was induced by exposure to 2.5 μM Ionomycin (A.G. Scientific) for 5 min in Ca^{2+}-free CZB media followed by incubation for 4 hr in CZB (0.1% PVA) supplemented with cycloheximide (CHX, 20 μg/ml, EMD Biosciences). All procedures were in humidified 5% CO_2 at 37°C. For Sr^{2+} activation, eggs were incubated for 2 hr in Ca^{2+} -free CZB medium supplemented with 10 mM $SrCl_2$. Eggs were then washed and transferred to HTF medium and cultured to the 2-cell stage.

Eggs were evaluated for signs of activation 5 and 24 hr after treatment under phase contrast microscopy. Activated eggs were classified according to the following criteria: (1) PN group, consisted of zygotes forming a single PN with first and second polar bodies (5 hr post treatment); (2) cleaved group, eggs undergoing immediate cleavage after 24 hr.

Eggs without second polar bodies, PN formation, or those failing to cleave were considered as un-activated MII eggs. Fragmented eggs were excluded from analysis.

2.4.7 $[Ca^{2+}]_i$ measurements

$[Ca^{2+}]_i$ monitoring was performed as previously described (174). $[Ca^{2+}]_i$ was measured using the Ca^{2+} sensitive dyes Fura-2-acetoxymethyl ester (Fura 2-AM, Molecular Probes; Invitrogen) or Fluo-4-AM (Invitrogen). Oocytes were loaded with 1.25 μM Fura-2AM (Fluo) supplemented with 0.02% pluronic acid (Molecular Probes) for 20 min at room temperature. Oocytes were placed in micro-drops of TL-HEPES on a monitoring glass bottom dish (Mat-Tek Corp.) under mineral oil. Eggs were monitored simultaneously using an inverted microscope (Nikon) outfitted with fluorescence measurement capabilities. Fura 2-AM were excited between 340 nm and 380 nm by a filter wheel (Ludl Electronic Products Ltd.), and fluorescence was captured every 20 s. To estimate TRPV3 channel protein functional expression, oocytes were treated with 50, 100, 200 μM 2-APB, and Ca^{2+} responses monitored in Ca^{2+} or in Ca^{2+} free TL-HEPES.

To test for IP_3-induced Ca^{2+} release, 0.25 mM Caged-IP_3 (cIP_3; Molecular Probes) was injected into MII oocytes. Injected oocytes were loaded with 1 μM Fluo-4AM for 20 min and photolysis were performed 1-2 hr after microinjection of cIP_3 in Ca^{2+} free TL-HEPES +EGTA. cIP_3 photolysis was released by pulses of 360 nm wavelength UV light provided using a 75W Xenon arc lamp, which also produce the 488 nm wavelength required to excite Fluo-4. Emitted light above 510 nm were collected by a cooled

Photometrics SenSys CCD camera (Roper Scientific). Acquisition of fluorescence ratios will be analyzed by SimplePCI software 5.2.1 (Hamamatsu) (118).

2.4.8 Preparation of pharmacological agents

Latrunculin A (Lat-A), Cyclohexamide (CHX), Colcemid (COL), and 2-Aminoethoxydiphenyl borate (2-APB) were from Calbiochem. The stock solutions were dissolved in dimethyl sulfoxide (DMSO; Sigma) and further diluted in CZB or TL-HEPES medium to their final concentration (Lat-A; 5 μM, CHX; 10 μg/ml, Col; 5 μM, and 2-APB; 200 μM).

2.4.9 Confocal microscope imaging

Live-cell imaging of oocytes/eggs expressing fluorescent-tagged proteins were performed with a confocal laser-scanning microscope (LSM 510 META, Carl Zeiss Microimaging Inc., Germany) using a 63 X 1.4 NA oil-immersion objective lens, and as previously performed in the lab (14). Images were acquired with LSM software (Carl Zeiss Microimaging Inc., Germany). Oocyte/eggs expressing TRPV3 tagged with Ruby fluorescent protein were collected at variable times of maturation and attached to glass bottom dishes while incubated in HCZB medium. The measurement of fluorescence intensity was analyzed using ImageJ64.

2.4.10 Electrophysiology

Whole-cell currents were measured at 22°C - 24°C using an Axopatch 200B amplifier digitized at 20 kHz (Digidata 1320A) and filtered at 5 kHz. Electrophysiology recordings

were performed on the same day of egg isolation up to 8 hr post surgery. Eggs were maintained in human tubal fluid medium (HTF, EMD Millipore) at 37°C and 5% Co2. For temperature ramps, the perfusate was heated using a TC-324B temperature controller and SH-27B solution heater (Warner Instrument Corporation). Data were analyzed using Clampfit (Molecular Devices) and Origin 7.0 (Origin Lab). Pipettes of 1-3 MΩ resistance were made from glass capillaries (593600, A-M Systems). Series resistance was compensated by 60%-80%. The intracellular solution contained 152 mM Cs-methanesulfonate, 1 mM Cs-BAPTA, 10 mM HEPES, 2 mM Mg ATP, 8 mM NaCl, and 0.3 mM NaGTP (pH 7.3-7.4). The external solution contained 125 mM NaCl, 6 mM KCl, 20 mM $CaCl_2$ 1.2 mM $MgCl_2$, and 20 mM HEPES-NaOH (pH 7.3-7.4). The response to 2-aminoethoxydiphenyl borate (2-APB, Sigma) was measured in an external solution containing 140 mM NaCl, 10 mM HEPES, 10 mM Glucose, 4 mM KCl, 1 mM $MgCl_2$, and 2 mM $CaCl_2$. In order to avoid chloride currents (Qu and Hertzell, 2000), a solution of Na-gluconate was used in the temperature response experiments and in the Sr^{2+} permeability experiments. The osmolality of all solutions was 290-300 mOsm. All voltages were corrected for measured junction potentials present between the internal and external solution before seal formation. TRPV3 currents were activated by voltage ramps from -100 mV to 100 mV (600 ms, every 2 s), in the presence of 2-APB or temperature ramps. The holding potential (HP) was -80 mV. For Sr^{2+} permeability recordings and to avoid T-type voltage gated Ca^{2+} channels, ramps are from +100 mV to -100 mV with a HP of 0 mV.

2.4.11 Statistical Analysis

Data collected in these studies were used for evaluation of statistical significance. The prism software (GraphPad Software) was used to perform statistical comparisons using student's *t*-test, or ANOVA, or the appropriate test for the data under analysis. All data were presented as mean ± SEM. Significant differences were considered at *P* values <0.05.

CHAPTER 3

THE ROLES OF PLCZ1 IN HUMAN FERTILITY

Summary

In mammals, sperm-oocyte fusion initiates Ca^{2+} oscillations leading to a series of events called oocyte activation, which is the first stage of embryo development. Ca^{2+} signaling is elicited by the delivery of an oocyte-activating factor by the sperm. A sperm-specific PLCZ1 has emerged as the likely candidate to induce oocyte activation. Recently, PAWP, a sperm-born tryptophan domain-binding protein coded by WBP2NL, was proposed to serve the same purpose. The first part of this study was conducted to determine if expression of the testis-specific PLCZ1 correlated with low success or fertilization failure after ICSI in patients with normal parameters after standard semen analysis (SA). Standard semen analysis was performed to determine sperm parameters in male partners, whereas females were evaluated for antral follicle counts (AFC), day 3 FSH levels and peak estradiol (E2) levels. The presence of PLCZ1 in sperm was ascertained using western blotting and immunofluorescence (IF) analysis. The ability of sperm to initiate changes in the intracellular concentrations of $[Ca^{2+}]_i$, which is characteristic of mammalian sperm, was performed after injection of human sperm into mouse eggs loaded with the Ca^{2+} sensitive dye fura-2 AM. Male partners of couples with failed or low success ICSI fertilization but with normal SA parameters showed low expression levels of PLCZ1 as determined by western blotting and reduced fluorescent signal during IF studies. In addition, fewer of these males' sperm showed PLCZ1 expression and were able to initiate robust $[Ca^{2+}]_i$ oscillations upon injection into eggs. In the second part of this study, we examined two infertile brothers exhibiting largely

normal SA parameters, including sperm morphology, but complete fertilization failure after intra cytoplasmic sperm injection (ICSI). Whole exomic sequencing evidenced a missense homozygous mutation in PLCZ1, converting Ile 489 into Phe (Ile489Phe). We showed that the mutation is deleterious, leading to absence of the protein in sperm. Mislocalization of the protein when injected in mouse GV and MII oocytes produced highly abnormal Ca^{2+} transients and early embryonic arrest. Altogether these alterations are consistent with our patients' sperm inability to induce oocyte activation and initiate embryo development. In contrast, no mutations were identified in WBP2NL and PAWP presented normal expression and localization. Overall we demonstrate in humans that the absence of PLCZ1 alone is sufficient to prevent oocyte activation irrespective of the presence of PAWP. Additionally, it is the first mutation located in the C2 domain of PLCZ1, a domain involved in targeting proteins to cell membranes, opening the door for structure function studies to define the conserved amino acids on the β1 strand of the C2 domain that might regulate the selectivity of PLCZ1 for its lipid substrate(s).

3.1 Introduction

Fertilization causes eggs to leave their meiotic arrest and initiate embryo development. The universal signal whereby the sperm induces the initiation of development is an increase in the intracellular concentration of free calcium $[Ca^{2+}]_{i,}$ which was demonstrated to be a sufficient and necessary stimulus to trigger oocyte activation and embryo development in all species studied to date (175). In mammals, this Ca^{2+} signal unfolds in a manner of repeated short-lived rises, which are also known as $[Ca^{2+}]_i$ oscillations, that last in excess of 4 hr in the mouse and as long as 20 hr in other species including humans (11). It is thought that activation of the phosphoinositide pathway (PI) in the egg by a

sperm-derived phospholipase C (PLC) enzyme underlies the oscillations by hydrolyzing phosphatidylinositol 4,5-bisphosphate (PIP_2) into inositol triphosphate (IP_3) and diacylglycerol (DAG). IP_3 promotes Ca^{2+} release by binding to the inositol 1,4,5-triphosphate receptors (IP_3R1) located in the endoplasmic reticulum (ER) membrane, which is the Ca^{2+} store of the cell (176, 177). The $[Ca^{2+}]_i$ oscillations induce the exit from the meiotic arrest, the metaphase II stage (MII), and the initiation of the events of activation that render eggs into zygotes (140, 164). Despite this pivotal role, a persistent question has been by what mechanism does the sperm initiate and sustain the $[Ca^{2+}]_i$ oscillations?

Current evidence suggests that after fusion the sperm delivers into the egg's cytosol a factor that is responsible for triggering $[Ca^{2+}]_i$ oscillations. It is thought this factor is capable of activating the PI pathway and induces production of IP_3. Evidence suggests that the factor is a male-specific PLCZ1, which was first discovered following a screen for expression of sequence tags related to PLCs in testis (19). It was subsequently shown that expression of cRNAs encoding for PLCZ1 in eggs initiated oscillations reminiscent of those induced by normal fertilization (19, 174). Additional studies demonstrated expression of PLCZ1 in the testes of other mammals and PLCZ1 cRNAs were able to induce oscillations in eggs of homologous and heterologous species including human PLCZ1 into human eggs (19, 62). Further, injection of sperm extracts depleted of PLCZ1 failed to initiate oscillations (19, 174). Despite this evidence, demonstration of the unique and primary role of PLCZ1 on mammalian fertilization needs confirmation from genetic models where the gene is purposely eliminated. However, the inability thus far to obtain a PLCZ1 KO animal model capable of producing mature sperm has prevented

assigning to this molecule the exclusive role for oocyte activation, while leaving open the possibility that other sperm factor may be required (178).

Towards that end, PAWP has been proposed as an alternative or complementary pathway for eggs activation based on findings that injection of recombinant PAWP induced oscillations comparable to those of fertilization (105). Nevertheless, attempts to replicate those studies in mouse eggs failed (108, 109) and no defects, including egg activation, were reported for sperm of PAWP null mice (110). The role of PAWP remains thus uncertain, although the possibility that a human oocyte specific factor is needed was not ruled out. Indeed, numerous studies have shown that testis and reproductive tissues evolve faster than other tissues leading to noticeable differences between species (111).

Human clinical studies have proven a valuable asset to gain insight into the role of PLCZ1 in fertilization and fertility. For example, approximately 1-3% of ICSI procedures result in fertilization failure and nearly 80% of these failures display "unsuccessful egg activation" (179, 180). Examination of patients with repeated ICSI failure revealed that in the majority of cases their sperm were unable to consistently initiate $[Ca^{2+}]_i$ responses and showed low expression levels of PLCZ1 (98). Subsequent studies extended the association between PLCZ1 and infertility, as it was found that one case of failed ICSI was linked to point mutations in the catalytic domains of PLCZ1, which undermined the ability of the enzyme to initiate robust oscillations (99, 181). Interestingly, in the initial studies, most of the PLCZ1-associated defects appeared linked to severe defects of sperm morphology, especially globozoospermia, which is characterized by round-headed sperm that lack most of the acrosomal content (148). Nevertheless, in our present observations we noted a few cases of ICSI failure in patients with grossly normal semen analysis (SA)

including normal morphology. In the first part of this study we examined the association of PLZ1 expression and ICSI failure in patients with normal SA parameters. We also examined whether the sperm of these patients showed uniform or inconsistent ability to initiate $[Ca^{2+}]_i$ oscillations. We found that the sperm of patients with normal SA but failed fertilization (FF) after ICSI expressed low levels of PLCZ1 and had dissimilar $[Ca^{2+}]_i$-inducing oscillatory ability; a minority of sperm are capable of initiating robust responses, whereas the majority of sperm are capable of only inducing mediocre or no responses at all. Invariably, in these sperm, the equatorial distribution of PLCZ1 was compromised. Thus, our results show in cases of ICSI failure with normal SA values only a few sperm are capable of initiating robust $[Ca^{2+}]_i$ responses and their selection will likely yield better fertilization outcomes. In the second part of the study, we examined two infertile brothers showing complete fertilization failure after ICSI. Exome sequencing enabled us to find a missense homozygous mutation in PLCZ1, converting Ile 489 into Phe, and structure-functional models reveal a conformational change that might affect binding to substrate(s). Using Western blotting (WB), immunofluorescence (IF), live fluorescence and Ca^{2+} imaging, we show that the mutation is deleterious, leading to mislocalization of the protein, lower enzymatic activity and lower rates of oocyte activation and embryo development. In contrast, no mutations were identified in WBP2NL and PAWP showed normal expression and localization. Overall we demonstrate in humans that the absence of PLCZ1 alone is sufficient to prevent oocyte activation irrespective of PAWP. Moreover, it is the first mutation located in the C2 domain of the enzyme, an important domain targeting proteins to lipid membranes, opening the door for better structure function analysis of PLCZ1 and of proteins that

carry this domain.

3.2 Results

3.2.1 Clinical parameters of failed-fertilization (FF) ICSI patients

Four couples seeking infertility treatment at Baystate Medical Center during 2010-2012 (one couple was referred from the Fertility and Reproductive Health Center, UCLA, CA) had either one or two failed ICSI cycles or low (<25%) fertilization after this procedure. Baystate performs ~500 A.R.T cycles per year and therefore these three cases represented approximately 1% of the patient population, which is in line with national statistics for failed fertilization cases after ICSI (182). Table 1 summarizes the main female clinical and SA parameters information regarding the couples under consideration. Clinical information is also presented as a form of control from a contemporaneous couple that underwent successful fertilization (SF) after ICSI and from another contemporaneous patient with abnormal semen parameters, oligoasthenoteratozoospermia (OAT), which failed ICSI. Female clinical parameters are limited to a few values indicative of their response to stimulation protocols, such as AFC, peak E_2 levels before day 10 of stimulation, day 3 FSH and number of eggs retrieved. The obtained values were mostly unremarkable leading us to suspect the cause of unsuccessful fertilization might be of male origin. Male parameters from SA examination were also unremarkable, as parameters for FF1-FF3 patients were comparable to those of the control patient SF1; sperm parameters for the OAT male were expected to be abnormal. The only consistent and significant finding for FF1-FF3 patients was the low

fertilization rates after ICSI, which given the known association between failed ICSI and defects in PLCZ1 expression (98, 99), prompted us to examine the patients' sperm for PLCZ1 expression and localization as well as ability to initiate $[Ca^{2+}]_i$ responses in mouse eggs.

3.2.2 Morphology and $[Ca^{2+}]_i$-inducing oscillatory activity of sperm of FF patients

As previously discussed and as shown in Figure 3-1, the sperm of patients FF1, FF2 and FF3 displayed unremarkable morphology, meaning that it was similar to that displayed by the sperm of a cohort control patient SF1, whereas the morphology of sperm from the OAT patient was abnormal, showing a combination of pyriform heads and amorphous shapes (Figure 3-1, OAT, left and right panels, respectively).

To elucidate whether these sperm with grossly normal sperm morphology but failed ICSI showed reduced ability to initiate $[Ca^{2+}]_i$ oscillations, we performed ICSI using the sperm of each patient and mouse eggs as the recipient cells. While all spermatozoa from the control patient initiated $[Ca^{2+}]_i$ responses (13/13), only 50 to 70% of the FF patients' sperm initiated responses (Figure 3-2). Importantly, while 8/13 sperm from the control patient initiated the expected vigorous, +++, $[Ca^{2+}]_i$ responses; only 1/8, 2/10 and 0/24 sperm from FF1, FF2, and FF3 patients, respectively, initiated this type of response. In the case of the SF1 patient, the rest of the sperm initiated moderate, ++, responses, whereas all the rest of FF1-3 sperm initiated moderate to low, ++, $[Ca^{2+}]_i$ responses. Expectedly, sperm from the OAT patient were only capable of initiating these moderate to low $[Ca^{2+}]_i$ responses (3/8; Figure 3-2). Altogether, the results show that whereas the morphology of sperm associated with ICSI failure is highly variable, they share a defect

to initiate robust $[Ca^{2+}]_i$ oscillations. It is noteworthy nevertheless that a small minority ~10 to 20% of the sperm from patients that failed ICSI were still capable of initiating robust $[Ca^{2+}]_i$ responses in mouse eggs.

3.2.3 Expression and localization of PLCZ1 in the sperm of FF patients

To determine whether the low $[Ca^{2+}]_i$ -oscillatory activity of FF patients correlated with low expression levels of PLCZ1 and/or mislocalization of PLCZ1, we performed western blotting and IF studies using a specific anti-PLCZ1 antibody. Immunoblot studies revealed that all patients that repeatedly failed ICSI displayed reduced expression of PLCZ1, which was especially noticeable in sperm from FF3 and OAT patients (Figure 3-3); it is worth noting that these two patients' sperm were the only ones in the study unable to initiate robust $[Ca^{2+}]_i$ responses.

Examination of the localization of PLCZ1 in the same patients revealed that the majority of SF, control, sperm (63%, 41/65) showed the expected equatorial localization characteristic of PLCZ1 in human sperm (Figure 3-4) (98). The PLCZ1 signal was detectable in only 25% (12/47) of FF1 sperm, 21% (18/86) of FF2 sperm and 12% (2/17) of FF3 sperm. As expected, only 5% (2/36) of the OAT sperm showed PLCZ1 reactivity. In addition, the intensity and distribution of PLCZ1 was highly abnormal in FF sperm (Figure 3-4). For instance, while FF1 sperm displayed PLCZ1 distribution consistent with its uniform equatorial localization, albeit of low intensity, PLCZ1 localization in FF2 sperm was arranged in discontinuous patches along the equatorial band, whereas in FF3 sperm the presence of PLCZ1 in the equatorial region was negligible, although some reactivity was observed on the base of the head, which is denoted by an arrowhead.

Sperm from the OAT patient, as expected, showed uncharacteristic distribution of PLCZ1 (Figure 3-4; bottom two rows).

3.2.4 Identification of a homozygous PLCZ1 mutation in two brothers with recurrent oocyte activation failure

In the previous study, we did not perform genome analysis of the patients failing ICSI. However, we did in the subsequent study, as we encounter infertility in two brothers. Specifically, two Tunisian brothers and their respective wives sought medical advice from infertility clinics in Tunis between 2008 and 2014. The brothers were born from first cousin parents and have one fertile brother with children conceived spontaneously and two fertile sisters. The brothers showed sperm parameters well above the low reference limits set by the WHO guideline [World Health Organization, 2010]; even although patient 1 (P1) had higher than normal number of sperm with acrosome defects (Figure 3-5). To investigate this in more detail, we examined acrosome morphology using an anti-acrosin antibody and found that the acrosome was absent in ~50% of sperm of both brothers. The acrosomal abnormality found in the patients was most likely due to a premature acrosome reaction and not to a lack of acrosome biogenesis because the shape of sperm head was normal and not globozoospermic (Figure 3-6A). Finally, DNA quality was assessed using three different methods: chromomycin A3 (CMA3), aniline blue (AB) and terminal deoxynucleotidyl transferase (TdT)-mediated deoxyuridine triphosphate (dUTP)-nick-end labeling (TUNEL), which allowed evaluation of DNA protamination, histone content and DNA fragmentation, respectively. Although higher than in fertile control men, the percentages of positive sperm were below 20% for all methods (Figure

3-6B). Although these sperm parameters are compatible with spontaneous conception, the clinical outcome following several ART procedures for both brothers was fertilization failure. P1 had two unsuccessful attempts of artificial insemination and sperm from both brothers was used subsequently for ICSI. In total, three ICSI cycles were carried out with 20 MII oocytes being injected; however, none of the oocytes displayed signs of activation such as extrusion of the second polar body (Table 2). Since both brothers were married to unrelated women we excluded the possibility of a female factor. We therefore proceeded to whole exome sequencing to identify a possible genetic defect(s) that could explain the observed fertilization failures. Given the parental consanguinity, we focused on homozygous mutations. After exclusion of frequent variants only four common homozygous variants were identified in both brothers (Figure 3-7A). Three variants, located in EPS8, RP11- 021N1.1 and LKAAEAR1, had no expected deleterious effect. The fourth variant was a missense mutation on PLCZ1, c.1465A>T located in exon 13, changing an Ile at position 489 into a Phe (Ile489Phe) (Figure 3-8A). Given that PLCZ1 has been suggested to be necessary for oocyte activation in mammals, this mutation could underlie the patients' phenotype. The presence of the mutation was validated by Sanger sequencing, which also found both affected brothers to be homozygous for the mutation, whereas the 3rd, fertile brother was heterozygous for the same mutation (Figure 3-7B). The c.1465A>T variant was absent from over 60,000 individuals described in the ExAC database (http://exac.broadinstitute.org), which confirms it is not a polymorphism and that missense variations occurring at this localization would likely cause negative selection throughout evolution. We verified the conservation of the concerned amino acid and found Ile489 to be well conserved throughout evolution (Figure 3-8B), suggesting

that this mutation could be deleterious.

3.2.5 Deleterious effects of the identified mutation

To assess the impact of the mutation on protein expression, PLCZ1 expression and localization were first studied on sperm from both patients. IF was performed with a specific anti-human PLCZ1 polyclonal antibody. Whereas the sperm of fertile patients showed a band of strong staining on the postacrosomal area and more diffuse staining over the acrosome (Figure 3-8C1), there was no staining detectable in the sperm from the patients, except for a few sperm showing a faint punctuate staining over the acrosome (Figure 3-8C2), which suggested the mutant PLCZ1 was absent or present at a very low concentration. Absence of PLCZ1 in the patients' sperm was confirmed by Western blotting, where a single band at the expected MW of PLCZ1 was noticeable in the control lane, although there was no corresponding band in the patients' lanes (Figure 3-8D) despite loading similar number of sperm (Figure 3-8E). These results suggest that during spermatogenesis Ile489Phe PLCZ1 displays defects in stability, trafficking and/or anchoring. To examine these possibilities, cRNAs of human WT and Ile489Phe Venus-tagged PLCZ1s were first injected into mouse GV oocytes, which given their cell cycle arrest, permit comparisons of protein distribution at the same stage of the cell cycle. WT PLCZ1 exhibited a homogeneous distribution in the ooplasm, which partly co-localized with the endoplasmic reticulum, which was marked by ER-DsRed (Figure 3-9A). Conversely Ile489Phe PLCZ1 displayed an uneven distribution, characterized by large patches near the nucleus and decreased peripheral localization; the distribution of the patches did not overlap the distribution of the ER (Figure 3-9B). These results suggest

that the mutation does not affect the stability of PLCZ1, although its trafficking and/or anchoring ability appeared altered. To further test the later, we took advantage of a property of mouse Plcz1 (mPlcz1) which, following pronuclear (PN) formation, is translocated into the PN (90, 91). WT and Ile527Phe mPlcz1 cRNAs (the equivalent mutation of Ile489Phe human PLCZ1 (hPLCZ1)) were injected into MII eggs, which were activated by the oscillations initiated by the translated proteins. Following PN formation, as expected, WT mPlcz1 accumulated in the PN. In contrast PN formation was delayed by ~ 3 hr when the mutant Ile527Phe mPlcz1 was injected, presumably due to lower oscillation frequency, and the mutant protein failed to localize to the PN (Figure 3-9C). These results suggest the mutation modifies PLCZ1's anchoring and/or trafficking properties in oocytes and zygotes, and these properties might be also altered during spermatogenesis, which could explain the absence of Ile489Phe PLCZ1 in patients' sperm.

We next assessed the enzymatic activity of the mutated human and mouse PLCZ1s, by examining the Ca^{2+}responses elicited by injection of their cRNAs in mouse eggs. WT hPLCZ1 initiated high frequency oscillations in all injected eggs (Figure 3-10A); in contrast, the activity of the mutated PLCZ1 was strongly decreased between 10 to 100-fold (54%, n=17/31) or abolished (76%, n=14/31) (Figure 3-10B) and the activity of the Ile489Phe hPLCZ1 was decreased irrespectively of the concentrations of cRNA injected (Figure 3-10C). These results suggest that possible traces of hPLCZ1 may not be sufficient to activate oocytes. To confirm this hypothesis, both WT and mutant cRNAs were injected into mouse eggs, and rates of PN formation and cleavage to the 2-cell stage were evaluated; Ile489Phe hPLCZ1 showed a greatly reduced ability to induced oocyte

activation and zygotes failed to progress to the blastocyst stage (Figure 3-10D). Similar results were obtained with mPlcz1, as Ca^{2+} responses triggered by mIle527Phe were weaker than WT Plcz1, with a longer lag time, and reduced frequency (Figure 3-11AB), which compromised pre-implantation embryo development (Figure 3-11CD).

3.2.6 Mutation alters the C2 domain

To assess the possible impact of the mutation on the structure of hPLCZ1, a 3D structure of hPLCZ1 was modeled from the crystallographic structure of rPLCdelta1 (42% identity, 59% homology). The model shows that Ile489 is at the interface of the EF-hand and C2 domains, and it appears too distant from the catalytic domain to directly affect its function (Figure 3-12A). Using molecular dynamics simulations of the hPLCZ1 and hPLCZ1-Ile489Phe models, we observed that the larger size of Phe over Ile (203 vs 169 Å3) initially results in a displacement of its intradomain neighbors (Y582, F601, Y603, and R487) by sculpting a more accommodating space, and second in establishing a unique interdomain hydrophobic contact with I76 from the proximal EF-hand 2 helix (Figure 3-12BC). The notable outcomes of these perturbations are the formation of an aromatic-rich concave-like subsite capable of associating with lipophilic molecules or protein surfaces (Figure 3-13) and a significant shift of the EF2 domain toward C2 (12.2 vs 10.7 Å for CαI76–CαI489 and CαI76– CαF489 distances, respectively), reinforced by the newly formed H-bond between the newly displaced Y582 and Y80 of EF2 (Figure 3-13B). Significantly, this tighter interdomain arrangement returns back to the original looser status when Phe489 is mutated back to Ile489 in the course of a simulation (Figure 3-14). Because EF-hands and C2 domains have been shown to be important for

enzymatic activity of PLCZ1 and its nuclear translocation (88), this unique interdomain interaction supports the observed deleterious effect of the mutation.

3.2.7 PAWP does not rescue PLCZ1 mutation.

The PAWP protein encoded by WBP2NL has been proposed to participate in oocyte activation and we therefore examined it for possible mutations. Analysis of exome data from P1 and P2 failed to find any deleterious variant in WBP2NL. It is however well known that exome sequencing only covers 80-90% of all targeted sequences. WBP2NL coverage was thus verified and we observed that for both patients all exons and exon borders had a minimal coverage of 40X; therefore unambiguously confirming the absence of deleterious variants in WBP2NL in the patients (Figure 3-15). Consistent with these results, we confirmed by Western blotting normal expression of PAWP (Figure 3-16A) from sperm extracts of patients and a fertile control prepared from the same number of sperm (Figure 3-16B). We also examined PAWP localization by IF and in agreement with previous reports, PAWP reactivity appeared as a compact band around the equatorial/post-acrosomal area in the sperm of a control fertile human (Figure 3-16B1) and in the sperm of both patients (Figure 3-16B2). These results show that PAWP is unable to support activation of human oocytes when PLCZ1 is absent and/or non-functional. To extend these results to mice, we examined the expression of PAWP in the sperm of Dpy19l2 KO males whose sperm are globozoospermic, do not contain Plcz1, and where ICSI of these sperm fails to induce oocyte activation (183, 184). We show that PAWP expression is normal in these sperm (Figure 3-17), showing that even though PAWP is present in the injected globozoospermic mouse sperm, it is unable to rescue

oocyte activation. Altogether, these experiments demonstrate that PAWP is not able by itself to initiate oocyte activation in humans or mice.

3.3 Discussion

In this study we first investigated the underlying functional defects of sperm from three patients that either had low or failed fertilization after ICSI during cycles performed in calendar years 2010 and 2012 despite having normal SA parameters. None of the patients conceived during this period. We found these sperm largely failed to initiate robust $[Ca^{2+}]_i$ oscillations, although two of these three patients had ~10% of sperm capable of initiating moderate $[Ca^{2+}]_i$ responses in mouse eggs. The expression levels of PLCZ1 were severely reduced in all patients and, more importantly, in the few sperm that expressed PLCZ1 the distribution and/or intensity were affected. Our results suggest that abnormal PLCZ1 expression is likely to underlie most cases of ICSI failure, even when SA parameters are grossly normal.

3.3.1 ICSI Failure and sperm morphology

ICSI is a highly successful technique that overcomes the most severe cases of male infertility. Nevertheless, low fertilization or fertilization failures after ICSI occur in ~4% of ICSI cases (148, 179), and the great majority of those cases show a consistent phenotype; namely, absence of egg activation (185). In addition, research has shown that ICSI failure is observed in a disproportionate number of patients with globozoospermia (148, 186). While the precise molecular defect(s) that underlie these patients' infertility

remains to be resolved; these sperm tend to have defects in the organization of the sperm head, including the perinuclear theca and the equatorial regions (187), which are the sites where purportedly PLCZ1 is located (98, 188). We first reported that globozoospermic sperm from patients that failed ICSI showed reduced or absent expression of PLCZ1 (98). A recent study has extended the association of globozoospermia and infertility to the mouse in the form of the loss or point mutations in the *DPY19L2* gene, which encodes for an inner nuclear membrane protein. The lack of normal DPY19L2 expression has been associated with disruption of the sperm perinuclear area, globozoospermia and subsequent infertility (189, 190). Thus, it appears that abnormal sperm head organization, especially in the perinuclear theca and equatorial regions, which may affect the anchoring and/or the stability of PLCZ1, is associated with inability of the sperm to initiate $[Ca^{2+}]_i$ responses and egg activation. Interestingly, the OAT patient, who was used as a negative control in this study, fell in this category.

ICSI failure has also been reported to occur in a few patients with apparent normal gross sperm morphology (99, 148). In one case, after careful analysis of the PLCZ1 gene sequence, point mutations that undermined the activity of the enzyme were found in the catalytic region of PLCZ1, providing a molecular explanation for the lack of egg activation and infertility observed in the patient (6, 99). We found three patients that despite displaying normal gross sperm morphology and SA parameters failed or had low fertilization after ICSI. The sperm of these patients displayed greatly reduced PLCZ1 expression, which might underlie the failure to initiate $[Ca^{2+}]_i$ responses regardless of whether or not point mutations were present in PLCZ1; nevertheless, we cannot exclude the possibility that mutations in the enzyme of those patients could further compromise

the function of the enzyme. Also, because we did not carry out EM studies, we cannot exclude the possibility of abnormal perinuclear theca organization in these sperm contributing to the abnormal expression and/or distribution of PLCZ1 in those patients. A recent study from another group also found reduced expression of PLCZ1 in patients that failed ICSI, although they also found variable expression levels in control, fertile patients (6). Quantification of PLCZ1 expression in that study was performed by immunofluorescence; whereas in our previous (98) and current study quantification was performed by immunoblotting, and the differences in methodology may account for the large variation observed in that study (6). Further, it is worth pointing out that in the aforementioned study the level of PLCZ1 expression was low in all infertile patients and the variability of PLCZ1 expression among failed ICSI patients was also lower than among fertile patients (6). Therefore, in the presence of failed fertilization after ICSI, low PLCZ1 levels remain highly predictive of repeated fertilization failure. Collectively, our results suggest that regardless of sperm morphology, patients that repeatedly fail ICSI or have low fertilization rates, especially those where acceptable numbers of eggs are retrieved, are likely to exhibit defects on the ability to induce $[Ca^{2+}]_i$ oscillations associated with defects in PLCZ1 expression and/or function.

3.3.2 $[Ca^{2+}]_i$ responses, PLCZ1 expression and low ICSI success

In a previous study we found that sperm from patients with repeated ICSI failure when injected into mouse oocytes were mostly unable to initiate $[Ca^{2+}]_i$ oscillations; in all cases, this was associated with reduced expression of PLCZ1 (98). In that study, the sperm of the patients examined displayed severe globozoospermia or obvious morphology defects

that, as we reported then and was later confirmed by other studies, correlate with the loss of PLCZ1 (98, 99). In the present study, we focused on patients that despite showing grossly normal sperm morphology and SA parameters were unable to fertilize ICSI. Whether or not these types of ICSI failure are also associated with reduced ability to induce $[Ca^{2+}]_i$ responses and defective PLCZ1 expression has not been closely investigated. We found that ~20% of these sperm were capable of initiating robust $[Ca^{2+}]_i$ responses and another 20% had the capacity to initiate moderate to low $[Ca^{2+}]_i$ responses; while 30 to 50% of the sperm were unable to initiate $[Ca^{2+}]_i$ responses. None of the sperm of the single patient in the study with abnormal morphology were able to initiate robust responses, although ~60% of the sperm induced moderate to low responses. Collectively, this data fits nicely with western blots results showing that the levels of PLCZ1 expression in these patients were ~40 to 80% lower than those of control sperm. It is worth noting that $[Ca^{2+}]_i$ monitoring was performed in mouse eggs, which are believed to be more sensitive to IP_3 than human eggs, and therefore only those sperm capable of initiating robust responses in mouse eggs might be capable of initiating moderate $[Ca^{2+}]_i$ responses in human eggs, which might explain that fertilization failure observed in these patients.

Next we addressed the question of whether the low expression of PLCZ1 was uniform in every sperm or rather was due to a few sperm expressing normal amounts of PLCZ1 and others expressing none. To accomplish this, we examined PLCZ1 expression in individual sperm using IF. In patients FF1, FF2 and FF3, less than 30% of the sperm showed reactivity after IF, which was in marked contrast to the nearly 70% of the sperm that displayed reactivity in the control patient. In the OAT patient with abnormal

morphology less than 5% of the sperm displayed reactivity. Thus, our results suggest that patients that have low fertilization after ICSI, not only are the overall expression of PLCZ1 reduced, but the number of sperm expressing PLCZ1 is also affected. Similar results have recently been reported in a larger study evaluating PLCZ1 expression in sperm from control and failed fertilization patients (6). Given that single sperm are selected and injected during the ICSI procedure, the possibility of identifying and using those sperm that express PLCZ1 and are capable of initiating $[Ca^{2+}]_i$ responses is intriguing and may increase the chances of successful fertilization. Selection of these sperm could be aided by approaches such as motile sperm organelle morphology examination (MSOME) that enables evaluation of nuclear morphology in motile spermatozoa in real time and under high magnification. The selected sperm could then be used for intracytoplasmic injection (191, 192). A recent manuscript showed that such a selection might be associated with higher levels of PLCZ1 expression (181).

In summary, we found that low fertilization and failed fertilization after ICSI can occur in patients with normal gross sperm morphology and is likely associated with defects in PLCZ1 expression and/or function. Despite that the proportion of sperm expressing PLCZ1 being severely reduced in these patients, some sperm retain PLCZ1 expression and are capable of initiating robust $[Ca^{2+}]_i$ responses. These findings have clinical implications, as selection of the $[Ca^{2+}]_i$ oscillation-competent sperm may overcome the severe fertilization defects observed in patients with repeated low fertilization or failed ICSI.

Our previous studies did not address the role of PAWP, which has been proposed as an alternative sperm factor candidate (105, 107). Nevertheless, controversial results have

been published, as a group other than the group proposing the role of PAWP has failed to replicate the results (108, 109). Further, it is presently unclear how PAWP can lead to the production of IP_3 and Ca^{2+} responses. Also we did not examine the genomic status of the *PLCZ1* gene in our patients. Genetic diseases are a unique way to demonstrate the role of a protein in a disorder, and our understanding of reproduction, including gametogenesis and fertilization, has benefited from the genetic characterization of several phenotypes of male and female infertilities (193). In humans, a link between oocyte activation failure and PLCZ1 was first reported in patients displaying abnormal expression and localization of PLCZ1 in sperm (98), however, these patients exhibited severe teratozoospermia genetic defects were not found. The first genetic evidence was provided by Heytens et al., who found a heterozygous mutation in the Y catalytic domain of PLCZ1 at position 398, which caused significant decrease in enzymatic activity (99). It was unclear how this heterozygous mutation could cause infertility. Subsequently, another heterozygous mutation was found in the X catalytic domain at position 233, resulting in compound heterozygosity, which reinforced the link between PLCZ1 and oocyte activation failure (181). We show the first identified homozygous mutation in PLCZ1 leading to oocyte activation failure and infertility. Importantly, it is the first whole exomic analysis of a patient presenting oocyte activation failure, enabling us to identify most, if not all, of the genetic variants. We identified only four common homozygous variants shared by both brothers, though three of them were not expected to have deleterious effects, which is in contrasting to the missense mutation found in PLCZ1. This mutation was not associated with teratozoospermia and the numbers of normal sperm were well above lower reference limits (WHO laboratory manual for the examination and processing of human semen-

fifth edition). Moreover, the sperm of both brothers showed only slightly reduced DNA quality, ruling this out as the cause of oocyte activation failure (194, 195). Altogether, these results indicate that PLCZ1 plays a direct role in mammalian oocyte activation.

Unlike PLCZ1, we show that the PAWP gene was unchanged and the expression and localization of the protein were normal. There is no evidence that PAWP is defective in the patients' sperm. This conclusion was reinforced by results using a mouse model of globozoospermia, Dpy19l2 KO males, exhibiting normal expression of PAWP, despite their sperm being unable to induce oocyte activation after ICSI (183, 184). Our results, thus, do not support the notion that PAWP alone triggers Ca^{2+} responses and oocyte activation (107); instead, they confirm the importance of PLCZ1 for this function in human. Finally, molecular modeling of WT and mutant PLCZ1s offers possible insights into the atomic-level perturbations caused by the nominally homologous I489F mutation. Molecular dynamics simulation suggests that the large size of the PHE residue results in displacements of neighboring side chains around the previously buried (ILE) position, which is predicted to lead to several short, and even long-range, outcomes. Among these, the shift by approximately 1.5 Å of the EF2-hand helix 1 toward C2 - driven by novel hydrophobic and H-bonding interactions, and the opening of an aromatic-rich surface patch capable of associations with hydrophobic counterparts - is the most direct structural effects for explaining the functional outcome of the mutation which led to abnormal distribution of PLCZ1, inability to translocate to the PNs, and reduced enzymatic activity. By changing the structural properties of the C2 domain, this mutation likely modifies PLCZ1/lipidic membrane interactions; a hypothesis in accordance with our results showing that PLCZ1 is not retained in sperm and on the reticulum of GV oocytes. The

Ile489, and likely its neighbors, are thus crucial for the selectivity of the PLCZ1 C2 domain and may explain a unique property of PLCZ that targets intracellular PIP2 localized in the reticulum; contrary to somatic PLCs that hydrolyze mostly the PIP2 localized in the internal leaflet of the plasma membrane (196).

Our results will provide clarification on the mechanism of infertility in these patients and these data might provide important insights about factors that regulate the function of PLCZ1. Future studies should determine how rescue the I489F mutant, we propose the following double mutants (I489F/Y582F, I489F/Y80F).

A significant portion of these data has already been published in the Journal of Assisted Reproduction Genetics (2014) (197). The data involving the characterization of $PLCZ1^{I489P}$ expression and function were submitted to Human Molecular Genetics (2015).

3.4 Materials and Methods

3.4.1 Patients

Following institutional IRB approval, infertile couples undergoing Assisted Reproductive Technologies at Baystate Medical Center (Springfield, MA) for ICSI were consented for PLCZ1 analysis of the husbands' sperm after one or two failed or low fertilization ICSI cycles. Clinical information regarding antral follicle count (AFC), day 3 FSH levels and peak Estradiol (E2) levels for the three patients were also obtained and are presented in Table 1. Patients underwent either a long luteal protocol using the GnRH-analogue (GnRH-a), leuprolide acetate (LA) (Lupron; TAP Phamaceuticals Inc., Chicago, IL) or a microdose stimulation protocol using the same analogue (198, 199).

In PLCZ mutation studies, sperm were obtained from patient consulting at the fertility department of Grenoble (France) or Clinique des Jasmins (Tunis, Tunisia), following approval by the ethical committee and informed consent from the patients. All patients gave an informed consent for the conservation of the remnant sperm in the Germetheque biobank and their use in studies on human fertility in accordance with the Helsinki Declaration on human experimentation. Dpy19l2 KO mice were obtained from the Mutant Mouse Regional Resource Center (MMRRC), University of California, Davis, CA.

3.4.2 Semen analysis

Freshly ejaculated semen was collected and analyzed for motility, concentration, viability, and morphology as previously described by us (98). Morphology was evaluated according to strict Kruger criteria. Sperm were then washed by centrifugation on a 40%/80% PureCeption Percoll gradient (Sage BioPharma, Bedminster, NJ) and the recovered pellet was washed three times in PBS, after which sperm were prepared for the different functional or biochemical assays.

3.4.3 Detection of PLCZ1 immunoblotting

Western blotting was performed as previously published by our laboratory (98). Patients' sperm were diluted to appropriate concentrations, 2X sample buffer was added and the samples were kept at –80°C until use. Thawed samples were boiled for 3 minutes, mixed well and loaded onto 7.5% SDS-PAGE gels and resolved polypeptides were transferred onto PVDF membranes (Millipore, Billerica, MA) using a Mini Trans-Blot Cell (Bio-Rad, Hercules, CA). The membranes were blocked in 6% nonfat dry milk in

PBS–0.1% Tween and incubated overnight at 4°C with the MI-305 antibody (1:500); this was followed by 1 hour of incubation with a horseradish peroxidase–labeled secondary antibody (Bio-Rad). Immunoreactivity was detected using chemiluminescence per manufacturer's instructions (PerkinElmer, Waltham, MA) using a Kodak Image Station 440CF. Western blotting procedures were repeated at least 2 times per sample.

3.4.4 $[Ca^{2+}]_i$ monitoring

$[Ca^{2+}]_i$ monitoring was carried out as described by our laboratory (98). In brief, mouse eggs were loaded with fura-2-acetoxymethyl ester (Fura 2-AM, Molecular Probes; Invitrogen) prior to performing the ICSI procedure after which eggs were transferred to a monitoring dish (Mat- Tek Corp., Ashland, MA) containing microdrops of TL-HEPES medium under mineral oil. Eggs were monitored simultaneously using a 20X objective on an inverted microscope (Nikon) outfitted for fluorescence measurements and a temperature-controlled stage. Excitation wavelengths were alternated between 340 nm and 380 nm using a filter wheel (Ludl Electronic Products Ltd., Hawthorne, NY) and fluorescence ratios were taken every 20 seconds. After passing through a 510-nm barrier filter, the emitted light was collected by a CoolSNAPES digital camera (Roper Scientific, Tucson, AZ). SimplePCI imaging software was used to run all the hardware and capture images (Hamamatsu, Sewickley, PA). $[Ca^{2+}]_i$ values are reported as the ratio of 340 nm:380 nm fluorescence in the whole egg. $[Ca^{2+}]_i$ oscillatory activity of human sperm was scored as previously reported by our laboratory from 0 to +++ according to the number of $[Ca^{2+}]_i$ rises detected within 1 hr of initiating the monitoring (98).

3.4.5 Immunofluorescence

Patients' sperm were fixed in freshly made 3.7% PFA-DPBS and kept at 4°C in DPBS until use, then the suspension was spotted onto 0.1% poly l-lysine (Sigma-Aldrich, St. Louis, MO) pre-coated multi-well slides (Thermo Scientific, Waltham, MA). Attached sperm were permeabilized with 0.1% (v/v) Triton X-100–DPBS (Triton X-100; Sigma-Aldrich) for 5 min at 4°C. Slides were blocked in DPBS+5% normal goat serum (GIBCO, Invitrogen) and incubated overnight at 4°C with the same primary anti-PLCZ1 antibody MI-305, (1:30) in 5% normal goat serum (98). Washes were performed with 0.1% (v/v) Tween 20–DPBS followed by 1 hr incubation at room temperature in an Alexa Fluor 555–labeled secondary goat anti-rabbit antibody (1:200) (Invitrogen). Samples were counterstained with 5 μg/ml Hoechst 33342 (Sigma-Aldrich) and mounted using mounting media (Vector Laboratories, Burlingame, CA). Fluorescence images were captured with a Zeiss Axiovert 200M microscope outfitted with a ×63 oil immersion objective and a Hamamatsu Orca-AG cooled CCD Camera controlled by AxioVision software 4.6 (Zeiss, Maple Gove, MN). Figures were assembled in PowerPoint (Microsoft, Redmond, WA).

3.4.6 Generation of constructs and preparation of cRNA

Human and mouse PLCZ1 constructs were kind gifts from Dr. K. Fukami (Tokyo University of Pharmacy and Life Science, Japan) and Dr. K. Jones (University of Southampton, UK), respectively. WT h and mPLCZ1-venus sequences were subcloned into a pcDNA6/Myc-His B (Invitrogen, Carlsbad, CA) between EcoRI and XbaI restriction sites. hPLCZ1 Ile489Phe and mPlcz1 Ile527Phe were generated by

substituting Ile to Phe using the Gibson Assembly Cloning Kit (New England Bio Labs, Ipswich, MA), as previously reported (200). Before performing in vitro transcription, the sequences of all constructs and presence of mutation sites were confirmed by DNA sequencing. pDsRed2-ER was kindly provided by Dr. M Trebak (Pen State Hershey College of Medicine, Hershey, PA). The ER-targeting sequence of calreticulin, DsRed2 and the KDEL ER retention sequence were ligated to pcDNA6/Myc-His B. Plasmids were linearized outside of the coding region with PmeI and in vitro transcribed using mMESSAGE/mMACHINE T7 Kit (Ambion, Austin, TX). Poly-A tail was added to the mRNAs using a Tailing Kit (Ambion).

3.4.7 Preparation of mouse eggs

MII eggs were obtained from superovulated 6- to 10-week-old B6D2F1 (C57BL/6J × DBA/2J) female mice as described by our laboratory (139). Eggs were collected in a HEPES-buffered Tyrode's lactate solution (TL-HEPES) supplemented with 5% heat-treated FCS (GIBCO; Invitrogen, Carlsbad, CA). Cumulus cells were removed with 0.1% bovine testes hyaluronidase (Sigma-Aldrich) and eggs incubated in CZB medium at 36.5°C under 5% CO_2 until the time of injection. All animal studies were approved by the Animal Care and Use Committee.

3.4.8 ICSI of mouse eggs

MII eggs were injected with patient sperm as described by Kimura and Yanagimachi (201) and (202) using a piezo micropipette-driven unit (PiezoDrill; Burleigh Instruments Inc., Rochester, NY). Spare sperm from patients as well as routine sperm analysis

samples were washed with microinjection buffer (MIB) and frozen at –80°C until injection, which was performed within a week of collection. Prior to ICSI, human sperm were thawed and mixed 1:1 with MIB containing 12% PVP. ICSI was performed in HEPES-buffered CZB medium supplemented with 0.1% polyvinyl alcohol (MW = 30–80 kDa).

3.4.9 Exome Sequencing and bioinformatics analysis

Genomic DNA was isolated from saliva using Oragen DNA extraction kit (DNAgenotech®, Ottawa, Canada). Coding regions and intron/exon boundaries using the Agilent SureSelect were enriched using the "all Exon V5 kit" (Agilent Technologies, Wokingham, UK). DNA sequencing was undertaken at the Genoscope, Evry, France, on the HiSeq 2000 from Illumina®. Sequence reads were aligned to the reference genome (hg19) using MAGIC software. Duplicate reads and reads that mapped to multiple locations in the exome were excluded from further analysis. Depth of sequence coverage was calculated using « in-house » Perl script calculating separately forward and reverse reads. Reads with sequence coverage under 10 in at least one of forward or reverse reads were excluded. Single nucleotide variation (SNV) and small insertion/deletion (indels) were identified and filtered for quality using an « in-house » software tool that allowed the production of a list of variants present in the studied patients. Candidate variants were identified using a combination of bioinformatics tools. All were filtered by comparison to EVS, the 1000 Genomes Project (1KG) and the ExAc consortium, and those with a minor allele frequency (MAF) greater than 0.05 for EVS and 0.01 for ExAc were excluded. We also compared these variants to an « inhouse » database of 56 control exomes obtained

from subjects from the same geographic origin as our two patients (North Africa). All variants present in homozygous state in this database were excluded. We used Variant Effect Predictor (VEP) to predict the impact of the selected variants on transcripts. We only retained the variant impacting splice donor / receptor region or causing frameshift, inframe insertion / deletion, stop gain, stop loss or missense.

3.4.10 Confocal microscopy of florescent-PLCZ1

Live-cell images of oocytes expressing fluorescently tagged proteins were captured with a confocal laser-scanning microscope (LSM 510 META, Carl Zeiss) using a 63 X 1.4 numerical aperture oil-immersion objective lens. Images were reconstructed using LSM software (Carl Zeiss). Eggs were maintained in HCZB medium and those expressing Venus-hPLCZ1 and DsRed-ER proteins were imaged at the GV stage; whereas expression of Venus-mPlcz1 and DsRed-ER proteins was imaged in PN stage zygotes.

3.4.11 Parthenogenetic oocyte activation experiments

Oocytes were activated by injection of cRNA PLCZ1 (0.01 µg/µl, concentration in the pipette) into the ooplasm. After cRNA microinjection, oocytes were cultured in KSOM/EAA, supplemented with 5 µg/mL cytochalasin B (CB) to diploidize the parthenotes. The cRNA PLCZ1 injection volume was 5 to 10 pL, which is approximately 1%–3% of the total egg volume. Pronucleus formation was checked at 6 h after ICSI, and outcomes were scored up to the blastocyst stage.

3.4.12 Homology modeling

A homology model for hPLCZ1 was generated with the Prime homology modeling workflow (version 3.8, Schrödinger, LLC) using the structure of rPLCD1, in complex with inositol-1,4,5-triphosphate and associated Ca^{2+} (pdb code: 1DJX) as the template. Briefly, all sequences (1DJX, rPLCD1, and hPLCZ1) were initially aligned by the BLAST homology search. First, a contiguous template structure was generated by replacing the missing 445–486 loop in the rPLCD1 structure with a peptide bond between the proximal (per 1DJX) G444 and K487 and minimization of the resulting loop using the OPLS2005 force field within Prime. Next, a similar operation resulted in the exclusion of the basic loop from the catalytic domain of hPLCZ1 (304–344) by linking residues 303 ad 345 to recreate a contiguous mode. A single-chain, liganded model, comprising the residues 64–303 and 345– 608, was then built via the energy-based algorithm in Prime to construct and refine non-identical residues and loops with deletions and insertions.

3.4.13 Molecular dynamics simulations

Both the resulting complex and pre-minimized I489F mutant were subjected to an unconstrained 1.2-ns, molecular dynamics procedure within Desmond (version 4.0, D. E. Shaw Research & Schrödinger, LLC). A NPT ensemble was built at 300K and 1 atm with neutralized (by 10 Cl^- ions) system and further Na^+/Cl^- ions to simulate 150 mM concentration in an explicit SPC solvent model. The interactions that both I489 and the corresponding phenylalanine were participating throughout the simulations were identified using the Simulated Interaction Diagram routine within Desmond. Topological changes were detected using Simulated Event Analysis program by monitoring the

CαI76–CαI489 and CαI76–CαF489 distances and root mean square fluctuations (RMSF) as a function of simulation time. The mutant structure from the final frame was modified back to contain I489, and a simulation under the identical conditions was conducted to ascertain the persistence of the mutant's conformation.

CHAPTER 4

CONCLUSIONS

The first aim of our studies focused on examining the role of TRPV3 channels in Ca^{2+} homeostasis in oocytes and eggs. During maturation, TRPV3 is differentially expressed in oocytes, being only fully active at MII stage. At this stage, specific stimulation of TRPV3 channels promotes Ca^{2+} influx sufficient to induce egg activation. Subsequently, we used TrpV3 overexpression, DsRNA, and inhibitors of protein synthesis to modify the native expression of the channel to learn about its precise timing of expression and function. We showed that TRPV3 protein is synthesized and translocated to the plasma membrane during maturation. We also demonstrated that 2-APB promotes Ca^{2+} influx, and reversibly targets TRPV3 channels, without blocking the IP_3 receptor. Lastly, we showed that TRPV3 channels functionally interact with the actin cytoskeleton indicating an actin-based regulation of its expression on the plasma membrane. Together, our results suggest that TRPV3 is a target of 2-APB in mouse eggs, which can be used to induce parthenogenesis. The association of endogenous TRPV3 channels with the actin cytoskeleton is a novel finding, and suggests that the rearrangements of actin that occur during maturation could regulate both the plasma membrane presence and function of TRPV3 and other Ca^{2+} channels involved in oocyte maturation and fertilization. Future studies should attempt to develop better activators of this channel to be used in parthenogenesis in mouse and rats. In addition, studies should focus on discovering other plasma membrane channels in mouse as well as in other mammalian eggs that could possibly participate in the support of fertilization-initiated oscillations. This knowledge could then be used to develop activators or inhibitors for these channels that will find

application in the clinic as methods of parthenogenesis or, conversely, as possible targets for non-hormonal contraception.

Studies in the second aim focused on the role of PLCZ1 in Ca^{2+} homeostasis. We show that the expression level of PLCZ1 in sperm is directly related to the sperm's ability to induce $[Ca^{2+}]_i$ responses. For example, male partners of failed or low success after ICSI fertilization showed low expression levels of PLCZ1 or mislocalized PLCZ1 even tough their semen analysis parameters were normal. Further, in our last study we showed that PLCZ1 might be the only molecule required for the initiation of oscillations during fertilization, as the only defect found in two infertile brothers exhibiting normal sperm morphology but complete fertilization failure after ICSI was a mutation in the coding sequence of PLCZ1. Using whole exomic sequencing of these brothers found a missense homozygous mutation in PLCZ1, converting Isoleucine 489 into Phenylalanine (Ile489Phe); this mutation was not found on a third brother who was fertile. We showed the mutation was deleterious, leading to absence of the protein in sperm. In addition, injection of a cRNA into mouse GV and MII oocytes with a point mutation similar to that found in those patients, showed the protein was mislocalized and produced highly reduced Ca^{2+} transients and early embryonic arrest. Altogether these alterations are consistent with our patients' sperm inability to induce oocyte activation and initiate embryo development. Furthermore, it is the first mutation located in the C2 domain of PLCZ1, a domain involved in targeting proteins to cell membranes, opening the door for structure function studies to define the conserved amino acids on the β1 strand of the C2 domain that might regulate the selectivity of PLCZ1 for its lipid substrate(s). Finally, these patients showed normal expression of the PAWP protein, which was suggested to

also participate in inducing oscillations in mouse eggs. Therefore, our results together with the findings of a PAWP KO mouse strongly suggest that PAWP is not involved in initiating Ca^{2+} responses in mammalian oocytes.

Despite our findings directly demonstrating the involvement of PLCZ1 in oocyte activation in mammalian, important aspects of its activation and function remain to be discovered. For example, how is the protein maintained seemingly inactive in sperm until the time of fertilization? Where is the localization of is substrate in eggs? Lastly, and more specific to our results, we still do not know why $PLCZ^{I489F}$ induces infertility. Is this due to misfolding of the protein that leads to its degradation? What about the reasons behind its lower activity and abnormal distribution? Does the mutation change the affinity of the substrate? Finding answers to some of these questions might provide important insights into the functioning of PLCZ1, which should contribute to alleviate human male infertility.

APPENDIX A

TABLES

TABLE 1

Table 1. Fertilization, pregnancy outcomes, stimulation and sperm parameters in patients with successful (SF1) and unsuccessful (FF1-3 and OAT) fertilization ICSI outcomes

	Female Parameters						Sperm parameters[3]		
Patients	**Age (years)**	**Day3 FSH (IU)**	**Peak E2 (pmol/l)**	**AFC[1]**	**Fertilization (#2PN/#OOC[2])**	**Pregnancy (Y/N)**	**Motility (%)**	**Concentration (X 10^6)**	**Morphology (%)**
SF1	29	5.3	1526	21	10/11	Y	74	45.75	5
FF1	39	8.5	2303	7	0/6;2/8	N	47	23	4.5
FF2	36	5.9	2102	19	0/6	N	55	73	5
FF3	30	8.7	1167	11	1/5	N	49	41	6
OAT[4]	42	6.2	3132	18	1/13	N	17	4.2	2

[1] AFC. Antral follicular count.
[2] PN stands for pronuclei. Ooc stands for oocytes.
[3] Sperm parameters were evaluated according to WHO standard
[4] OAT stands for Oligoasthenoteratozoospermia

TABLE 2

Table 2. ICSI outcomes following stimulation cycles with sperm from patient 1 (P1) and patient 2 (P2). N (number). P1 and P2 are brothers.

Patient and procedure	Year	N of follicles	N of abnormal oocytes (GV, M1, atretic).	N of mature oocytes injected	N of 2PN oocytes
P1 ICSI - Jasmin clinic	2011	9	4	5	0
P1 ICSI - Jasmin clinic	2012	9	2	7	0
P2 ICSI - Jasmin clinic	2012	14	6	8	0

APPENDIX B

FIGURES

FIGURE 1-1

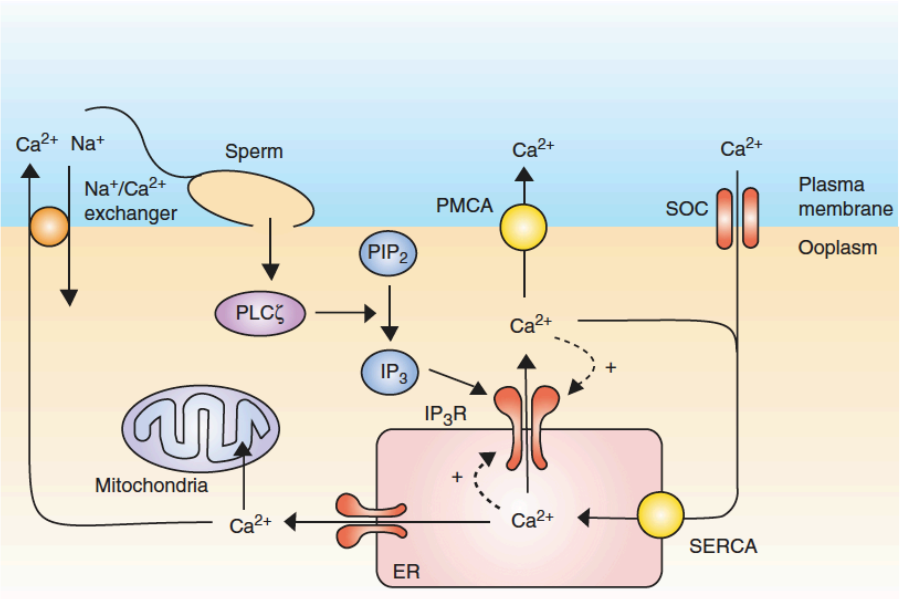

Figure 1-1. Proposed mechanisms the initiation of oscillations in mammalian eggs. Temporal course of activation events in mouse eggs with a characteristic $[Ca^{2+}]_i$ response and candidate molecules involved in $[Ca^{2+}]_i$ oscillation and Ca^{2+} homeostasis. Image (Wakai et al., 2011)

FIGURE 1-2

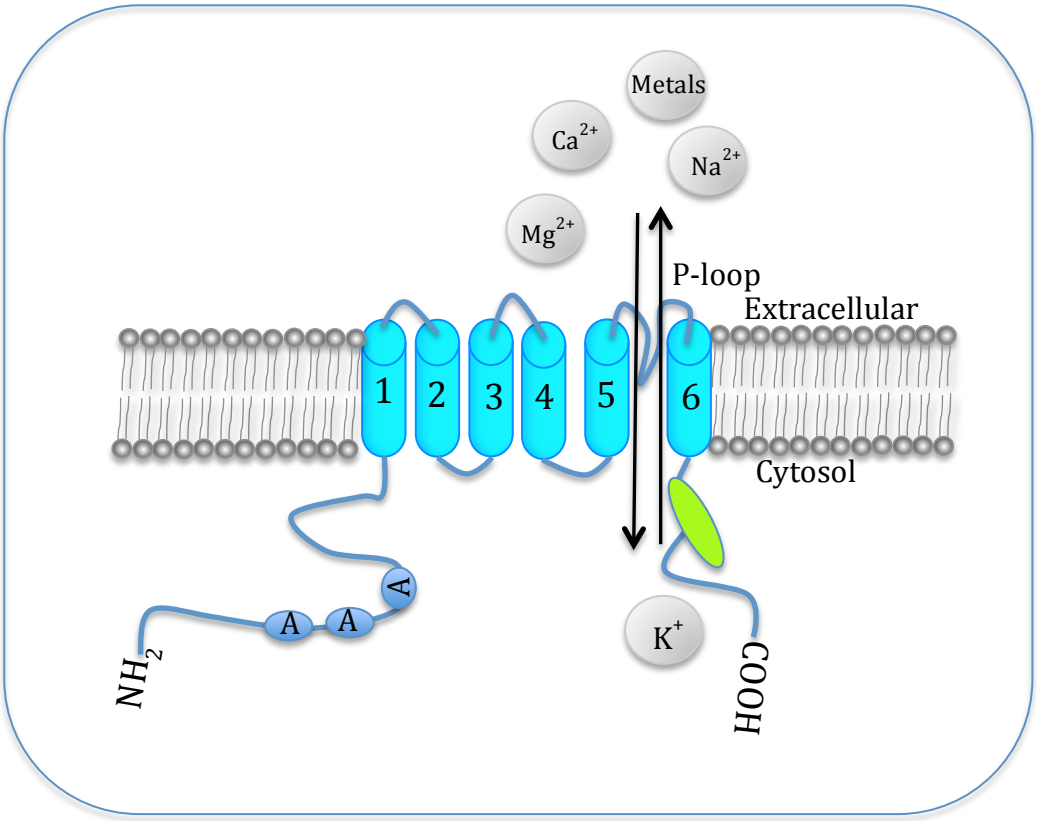

Figure 1-2. Schematic architecture of TRP channels

FIGURE 1-3

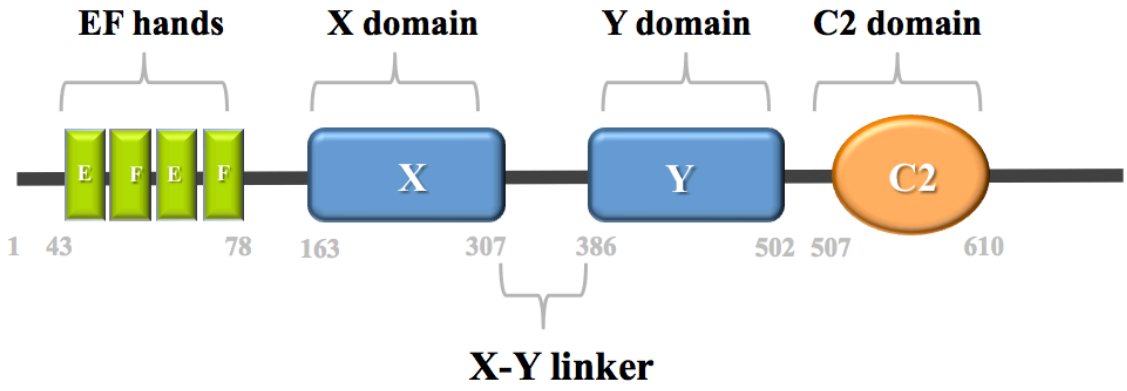

Figure 1-3. Schematic architecture of PLCZ1

FIGURE 2-1

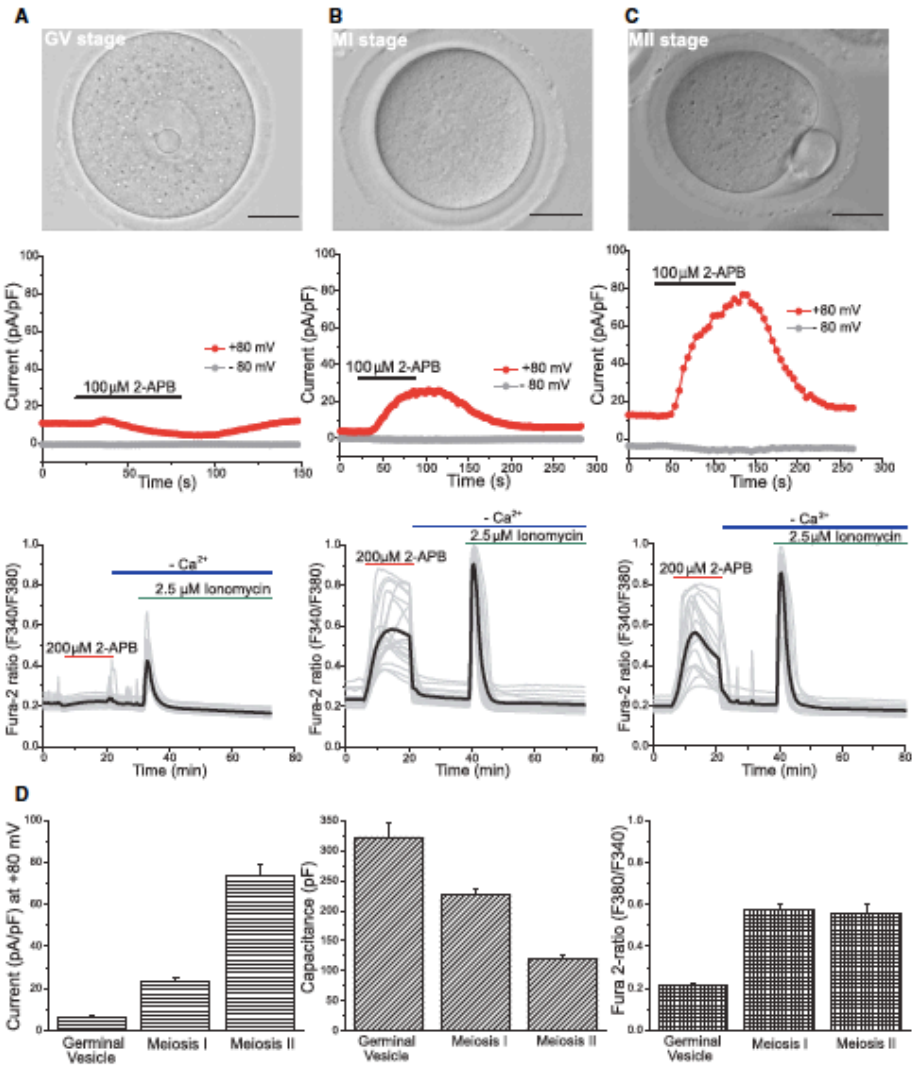

Figure 2-1. TRPV3 in response to 2-APB during oocyte maturation (A-C) Upper panels: Germinal vesicle (GV) oocyte, Meiosis I (MI) and Meiosis II (MII) eggs. Scale bar: 50 mm. Middle panel: Whole-cell patch-clamp recording in response to 100 mM 2-APB (black bar). Lower panel: Changes in $[Ca^{2+}]_i$ induced by 200 mM 2-APB (red bars; black = averaged trace. GV, n=19; MI, n=19; MII, n=16) and ionomycin (green bars) in nominal Ca^{2+}-free solutions (blue bars). (D) Summary of parameters measured at different stages of oocyte maturation. Left panel: peak current measured at +80 mV in response to 100 mM 2- APB (GV, n=4; MI, n=3; MII, n=4). Middle panel: Whole-cell capacitance measurements (pF) (GV, n=4; MI, n=5; MII, n=10). Right panel: Peak fura-2 ratio, reflecting relative $[Ca^{2+}]_i$. Data are averages ± S.E.M. Scale bar: 50 mm.

FIGURE 2-2

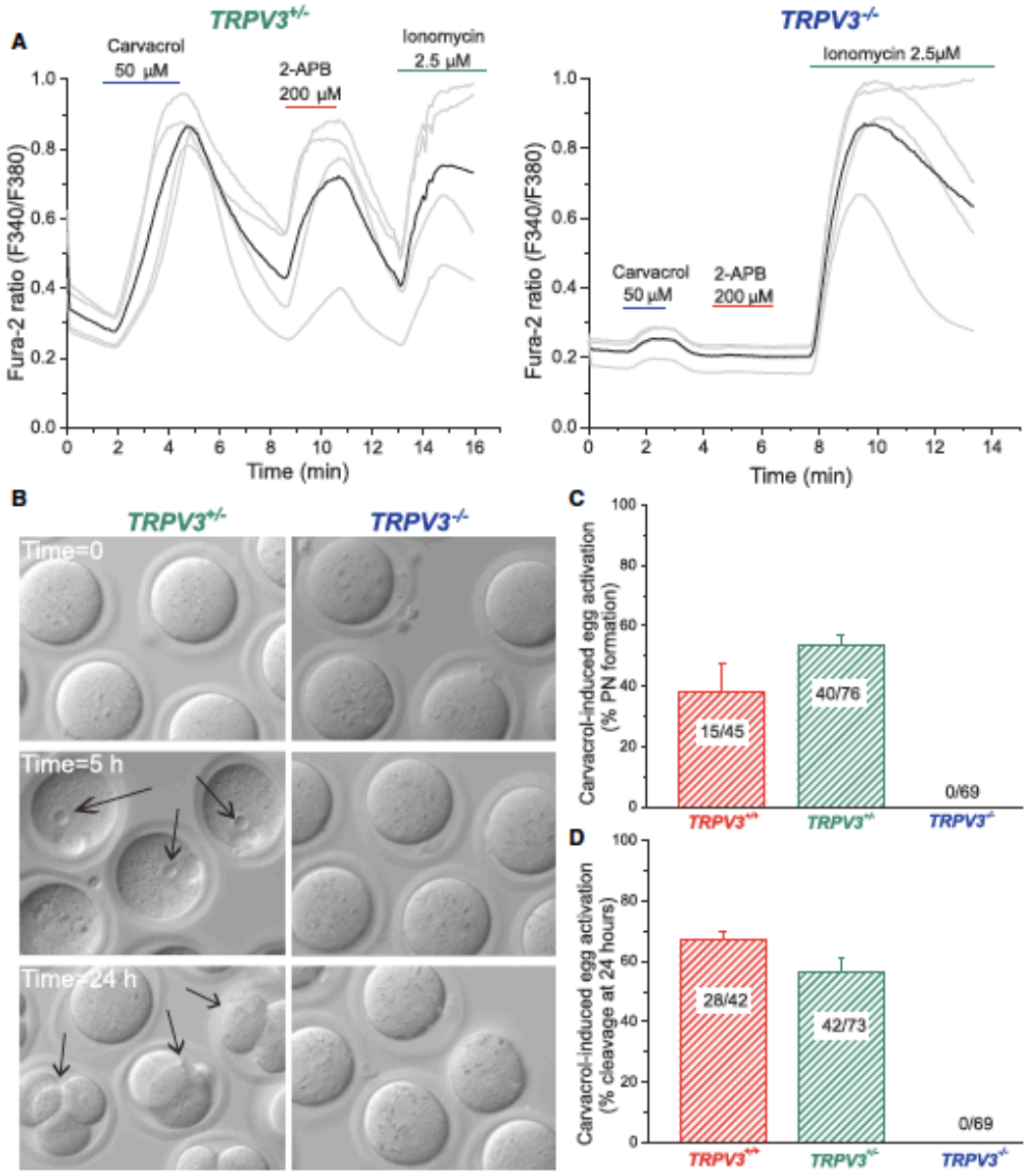

Figure 2-2. The TRPV3 channel agonist, carvacrol, induces Ca^{2+} responses and activation in MII mouse eggs. (A) Changes in $[Ca^{2+}]_i$ induced by TRPV3 channels activated by 50 mM carvacrol (violet), 200 mM 2-APB (red), and ionomycin (green) in $TrpV3^{+/-}$ and $TrpV3^{-/-}$ cells (V3-Het, n=4; V3-KO, n=4). (B) Activation of $TrpV3^{+/-}$, but not $TrpV3^{-/-}$ eggs, by treatment with 50 mM carvacrol (37°C, 10 min). Arrows indicate PN formation (5 hr, left panel) and cell cleavage (24 hr, left panel). (C) Percentages of PN formation in WT ($TrpV3^{+/+}$, CD1 strain), heterozygous ($TrpV3^{+/-}$) and V3-KO ($TrpV3^{-/-}$) eggs 5-6 hr after carvacrol activation. Numbers of eggs undergoing PN formation/total number of eggs is indicated. (D) Percentage of eggs cleaved after 24 hr exposure to carvacrol.

Numbers of 2, 3, or 4-cell blastomeres over the total number of eggs is indicated. Data are averages ± S.E.M.

FIGURE 2-3

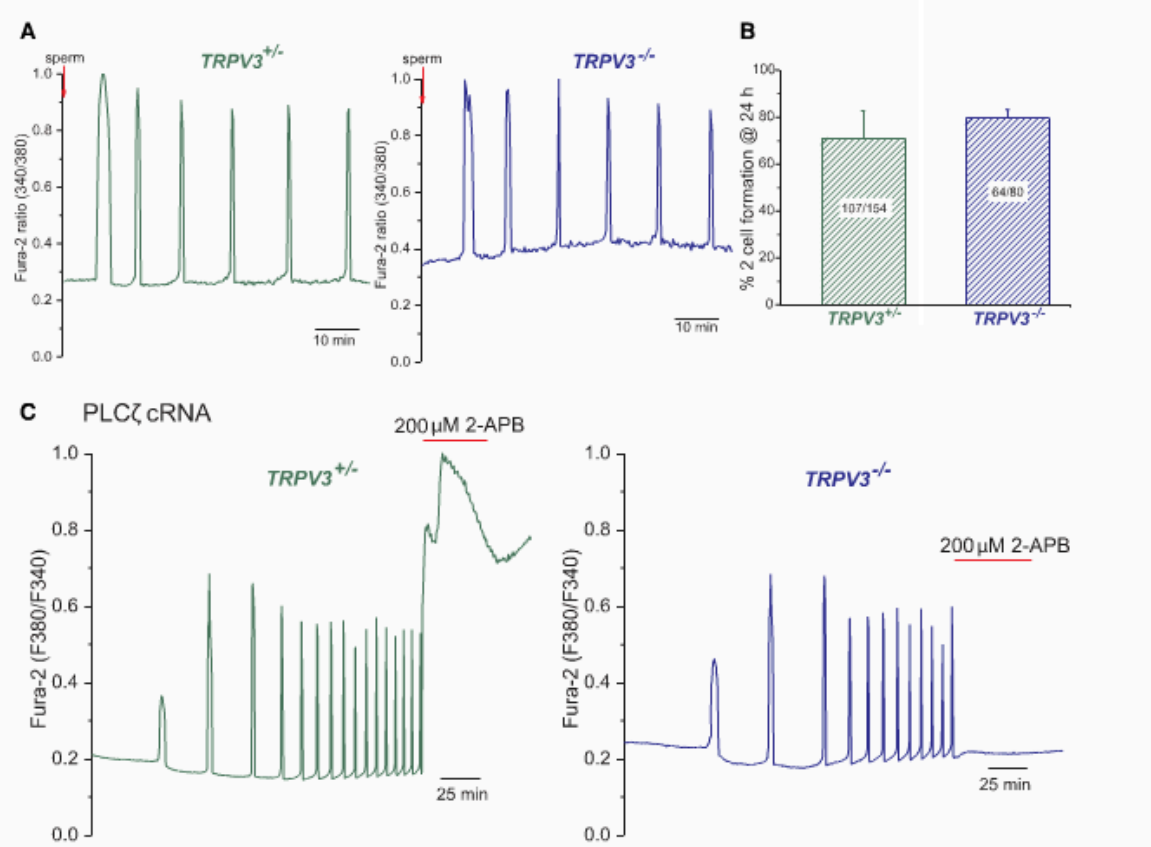

Figure 2-3. Calcium influx through TRPV3 channels does not contribute to early development in mouse eggs. (A) Oscillations induced by sperm fertilization in heterozygous (left, TrpV3$^{+/-}$, green line, n=12/24 have 5-6 oscillations in 60 min) and V3-KO (right) eggs (blue line, n=9/18 have 5-6 oscillations in 60 min). (B) In vitro fertilization (IVF) rates measured by 2-cell formation after 24 hr of fertilization showed no difference between V3- Het and V3-KO eggs (71 ± 12 for V3-Het vs. 80 ± 4 for V3-KO eggs, $p > 0.05$). Numbers of 2-cell blastomeres/total number of eggs is indicated. Data are averages ± S.E.M. (C) $[Ca^{2+}]_i$ responses were induced by injection of 0.01 mg/ml mPLCz cRNA (similar responses were obtained by 0.05 mg/ml mPLCz cRNA injection). $[Ca^{2+}]_i$ oscillations (37°C) in a control egg (TrpV3$^{+/-}$, left panel, n=8) and KO egg (TrpV3$^{-/-}$, right panel, n=3). 200 mM 2-APB (red bar) was applied at the end of the experiment.

FIGURE 2-4

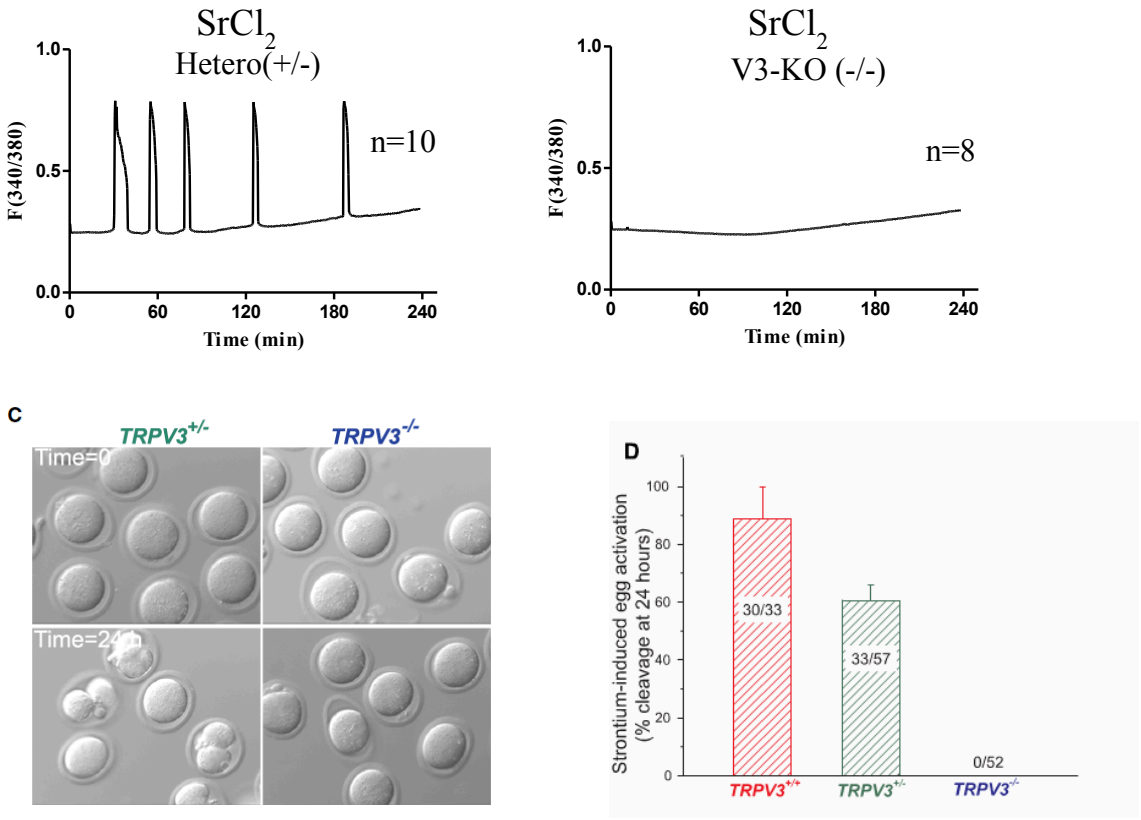

Figure 2-4. TRPV3 channels mediate Sr^{2+} influx and subsequent egg activation. (A) Results of whole-cell patch-clamp recording (37°C) of MII eggs from heterozygous ($TrpV3^{+/-}$, green symbols, n=4) and TrpV3-KO ($TrpV3^{-/-}$, blue symbols, n=4) mice. Current-voltage (I-V) relation in 10 mM $SrCl_2$. Inset: Averaged current at -80 mV. (B) Oscillations induced by Sr^{2+} in a $TrpV3^{+/-}$ egg (green line, n=6), but not in a TrpV3-KO egg (blue line, n=8). (C) Sr^{2+} induces cleavage in V3-Het (left) but not in V3-KO (right) eggs. (D) Percentage of cleaved eggs after 24 hr of 10 mM Sr^{2+} treatment. Numbers of 2, 3, or 4-cell blastomeres/total number of eggs is indicated. Data are averages ± S.E.M.

FIGURE 2-5

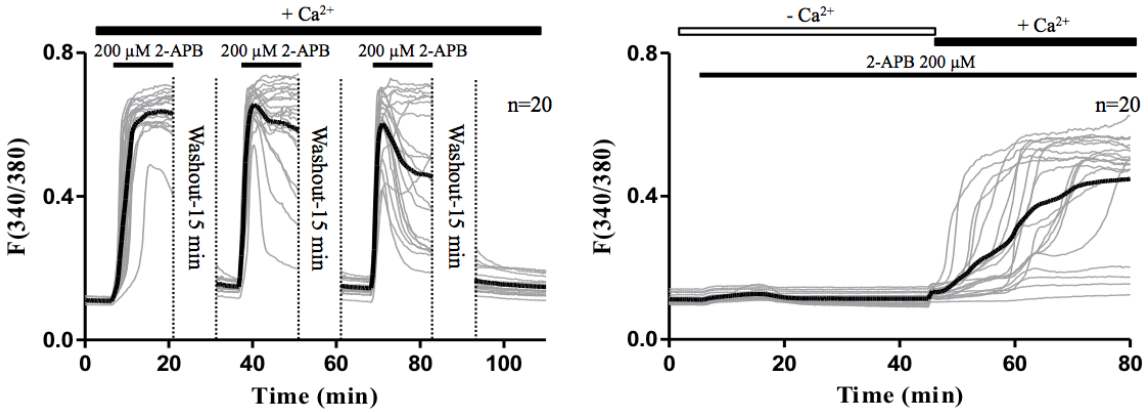

Figure 2-5. 2-APB increases $[Ca^{2+}]_i$ in mouse eggs by promoting Ca^{2+} influx. Changes in $[Ca^{2+}]_i$ were induced by repeated application of 200 µM 2-APB in Ca^{2+}-containing media (*left panel*) or in Ca^{2+} free-media (*right panel*). Note that in Ca^{2+} free-media application of 2-APB failed to induce $[Ca^{2+}]_i$ changes. Re-addition of Ca^{2+} caused a delayed increase in $[Ca^{2+}]_i$ (*right panel*).

FIGURE 2-6

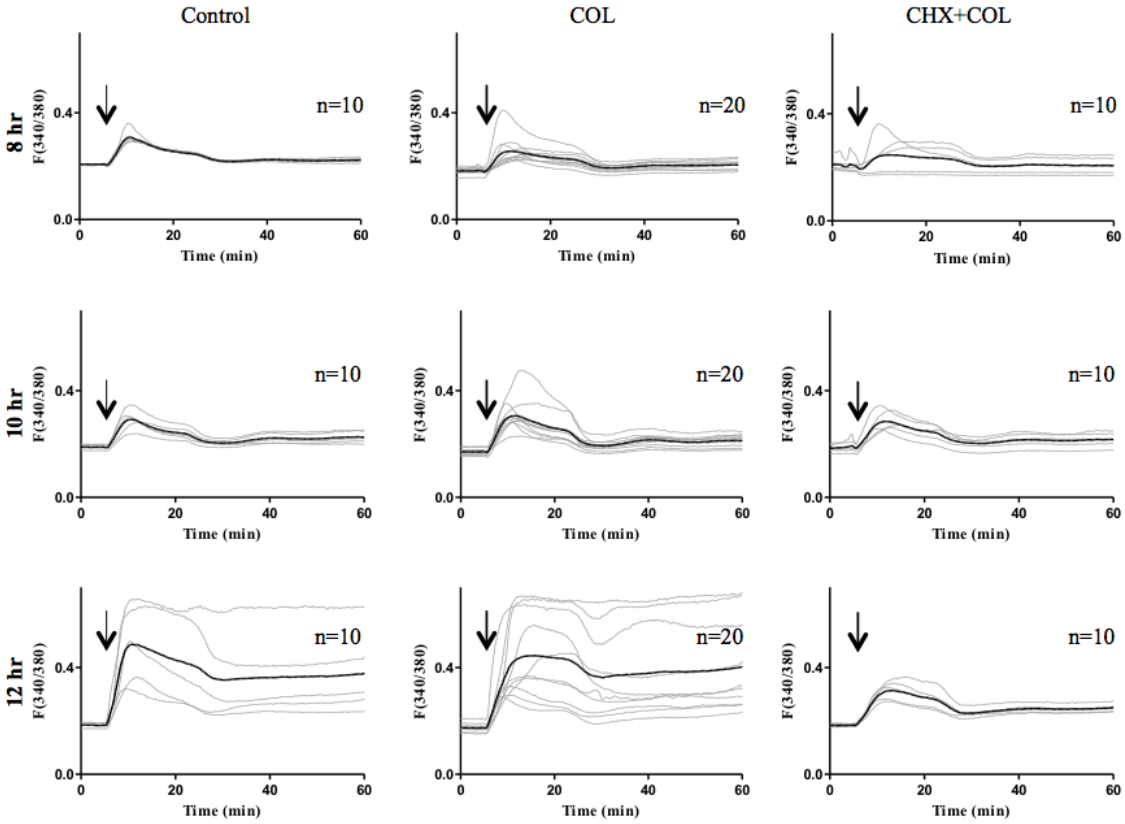

Figure 2-6. Inhibition of protein synthesis decreases response to 2-APB in oocytes. GV oocytes were matured *in-vitro* and responses were evaluated at different time points in the presence/absence of colcemid (COL) and cycloheximide (CHX) plus colcemid (COL). Oocytes were exposed to 200 µM 2-APB and $[Ca^{2+}]_i$ responses generated at each time compared. Traces from control (non-treated) oocytes are on *left panels;* oocytes treated with COL are *on the middle panels, and* traces for CHX and COL-treated oocytes are on *right panels* (CHX+COL, 20 µg/ml and 0.2 µg/ml, respectively). Changes in $[Ca^{2+}]_i$ were measured at 8, 10 and 12 hr of maturation. Numbers of eggs are indicated in each graph.

FIGURE 2-7

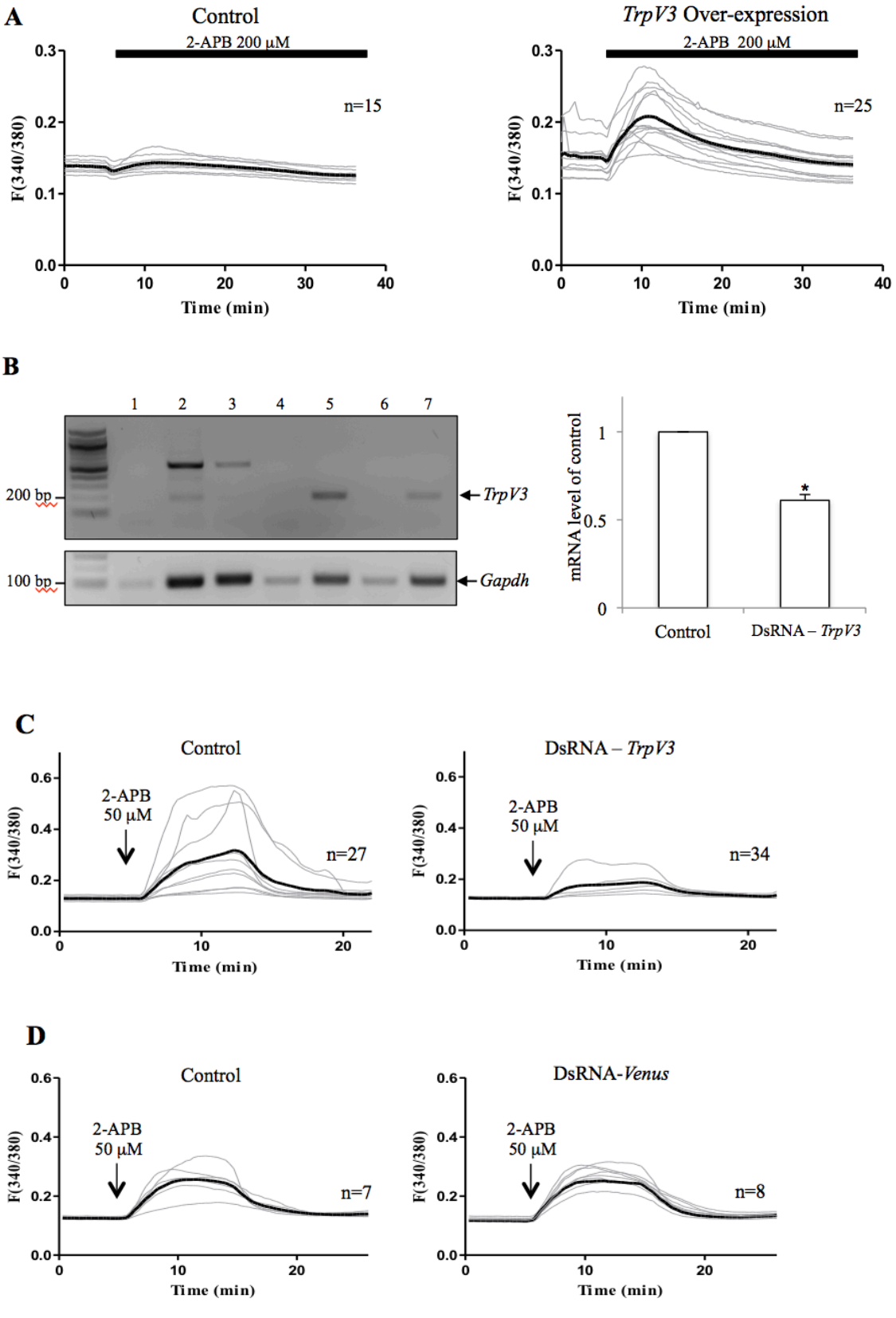
A
Control
2-APB 200 µM
n=15
F(340/380)
Time (min)
TrpV3 Over-expression
2-APB 200 µM
n=25
F(340/380)
Time (min)
B
1 2 3 4 5 6 7
200 bp
TrpV3
100 bp
Gapdh
mRNA level of control
Control
DsRNA – TrpV3
C
Control
2-APB 50 µM
n=27
F(340/380)
Time (min)
DsRNA – TrpV3
2-APB 50 µM
n=34
F(340/380)
Time (min)
D
Control
2-APB 50 µM
n=7
F(340/380)
Time (min)
DsRNA-Venus
2-APB 50 µM
n=8
F(340/380)
Time (min)

Figure 2-7. 2-APB causes an increase in $[Ca^{2+}]_i$ in GV oocytes over-expressing TRPV3 channels, but down-regulation of endogenous TRPV3 reduces response to 2-APB in mouse eggs. **(**A) Non-injected GV oocytes failed to show $[Ca^{2+}]_i$ responses to 2-APB treatment (*left panel*), whereas oocytes injected with *TrpV3* mRNA responded with an increase in $[Ca^{2+}]_i$ (*right panel*). (B-D) Down-regulation of native TRPV3 channels compromises the response of eggs to 2-APB. B. RT-PCR from GV oocytes showing *TrpV3* mRNA levels in control and ds-injected GV oocytes. Lanes: 1. Negative control (No RT reaction), 2. Positive control (T cell cDNA high concentration, sizes: 575 bp and 230 bp), 3. Positive control (T cell cDNA low concentration, size: 587 bp), 4. No RT ds-*Venus* control- GVs, 5. Ds-*Venus* cDNA –GVs (size: 230 bp), 6. No RT ds*TrpV3* control, 7. ds*TrpV3* –GVs (size: 230 bp). *Right Panel*: Bar graph showing relative levels of m*TrpV3* normalized to the control mRNA levels of m*TrpV3*. (D) Changes in $[Ca^{2+}]_i$ induced by exposures to 2-APB, 50 μM (black arrows) in control non-injected eggs (*left panel*), and ds*TrpV3* RNA injected MII eggs (*right panel*). (D) Changes in $[Ca^{2+}]_i$ induced by exposures to 2-APB, 50 μM (black arrows) in control non-injected eggs (*left panel*), and ds*Venus* RNA injected MII eggs (*right panel*).

FIGURE 2-8

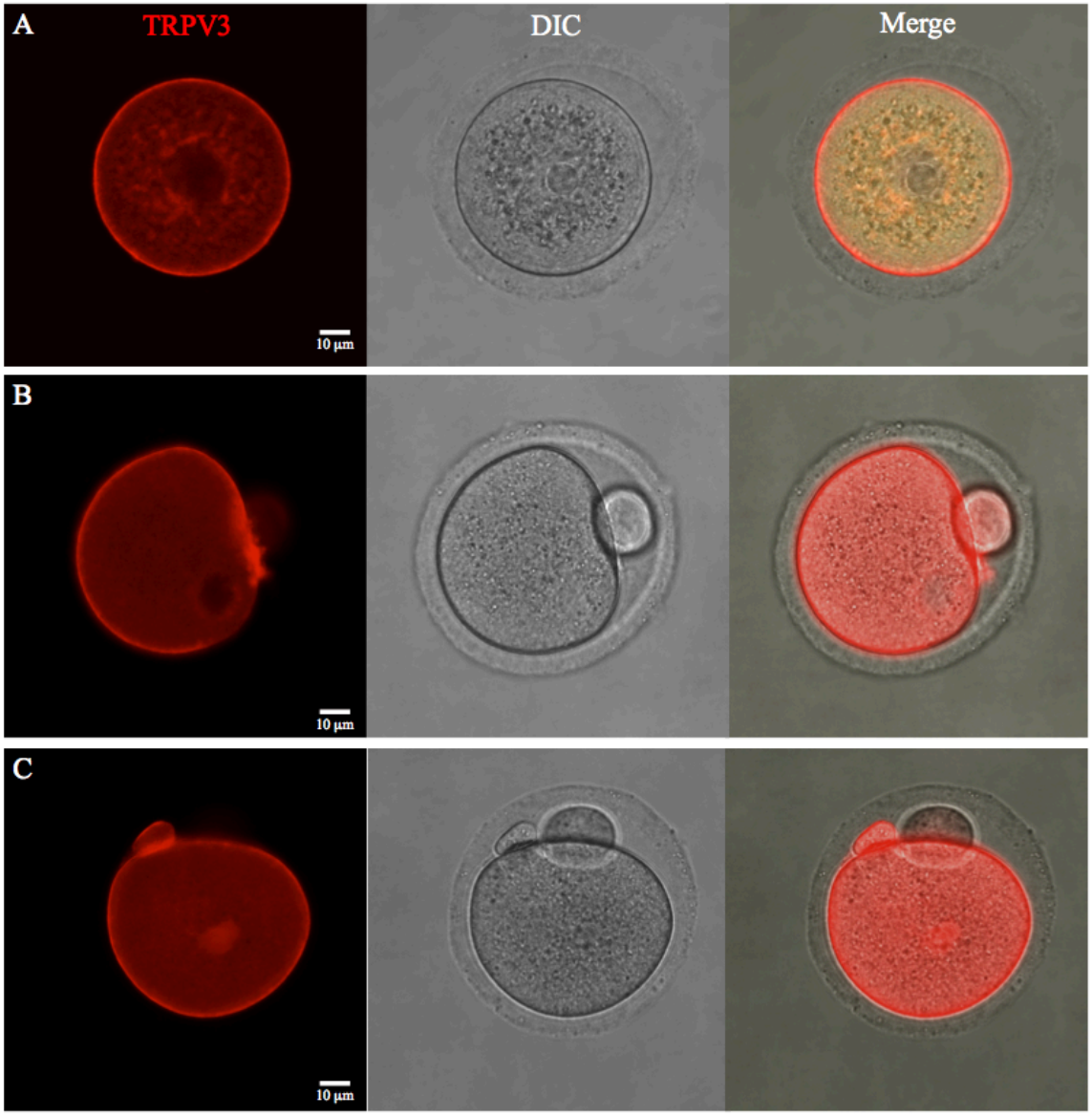

Figure 2-8. Over-expressed RFP-TRPV3 channels localize to the plasma membrane of mouse oocytes, eggs and zygotes. GV oocytes were injected with mRNA encoding Rfp-mTrpV3 and incubated for 8 hr to assure protein synthesis prior to being released to resume maturation. GV oocytes were maintained in IBMX (100 µM) (*upper panel)* or matured 12-14 hr *in-vitro* to the MII stage (*middle panel).* 10-15% of matured eggs showed spontaneous PN progression (*lower panel*). Minor staining was observed in the cytoplasm, especially after cells had resumed meiosis.

FIGURE 2-9

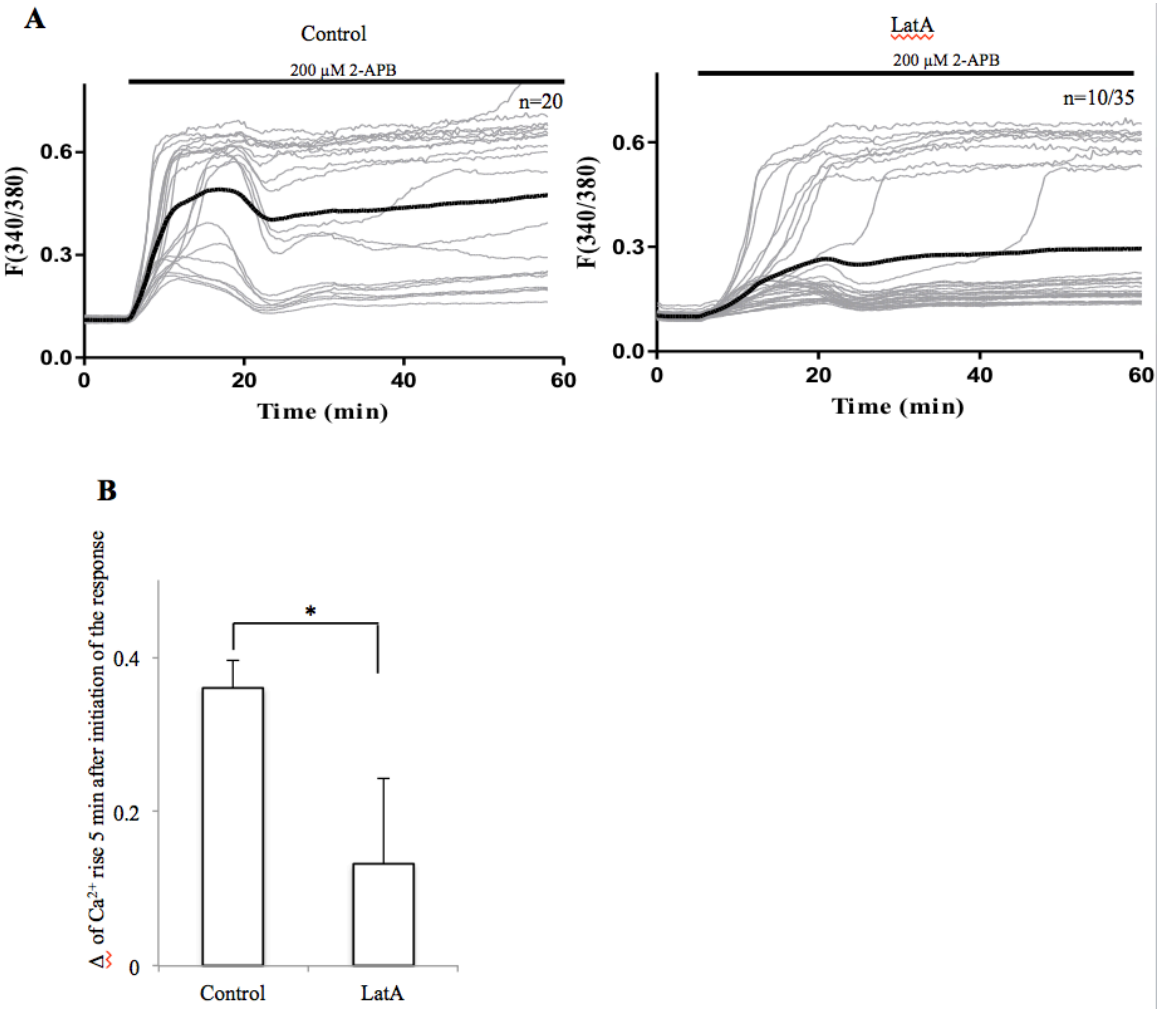

Figure 2-9. LatA impairs TRPV3 function in eggs. (A) Changes in $[Ca^{2+}]_i$ responses to 200 µM 2-APB were evaluated in control eggs (*left panel*) and in eggs incubated with LatA (LatA 5 µM, 30 min; *right panel*). (B) Quantification of $[Ca^{2+}]_i$ responses 5 min after initiation of response in A. are shown in a bar graph. Note a significant difference (*, $P < 0.05$). (C) Changes in oscillations induced by Sr^{2+} (10 mM $SrCl_2$) were evaluated in control eggs (*left panel,* DMSO 0,1%) and in eggs incubated with LatA (LatA 2,5 µM, *right panel*; Numbers of eggs are indicated in each graph. DMSO and LatA were added as indicated by the shaded horizontal bars over the oscillation traces.

FIGURE 2-10

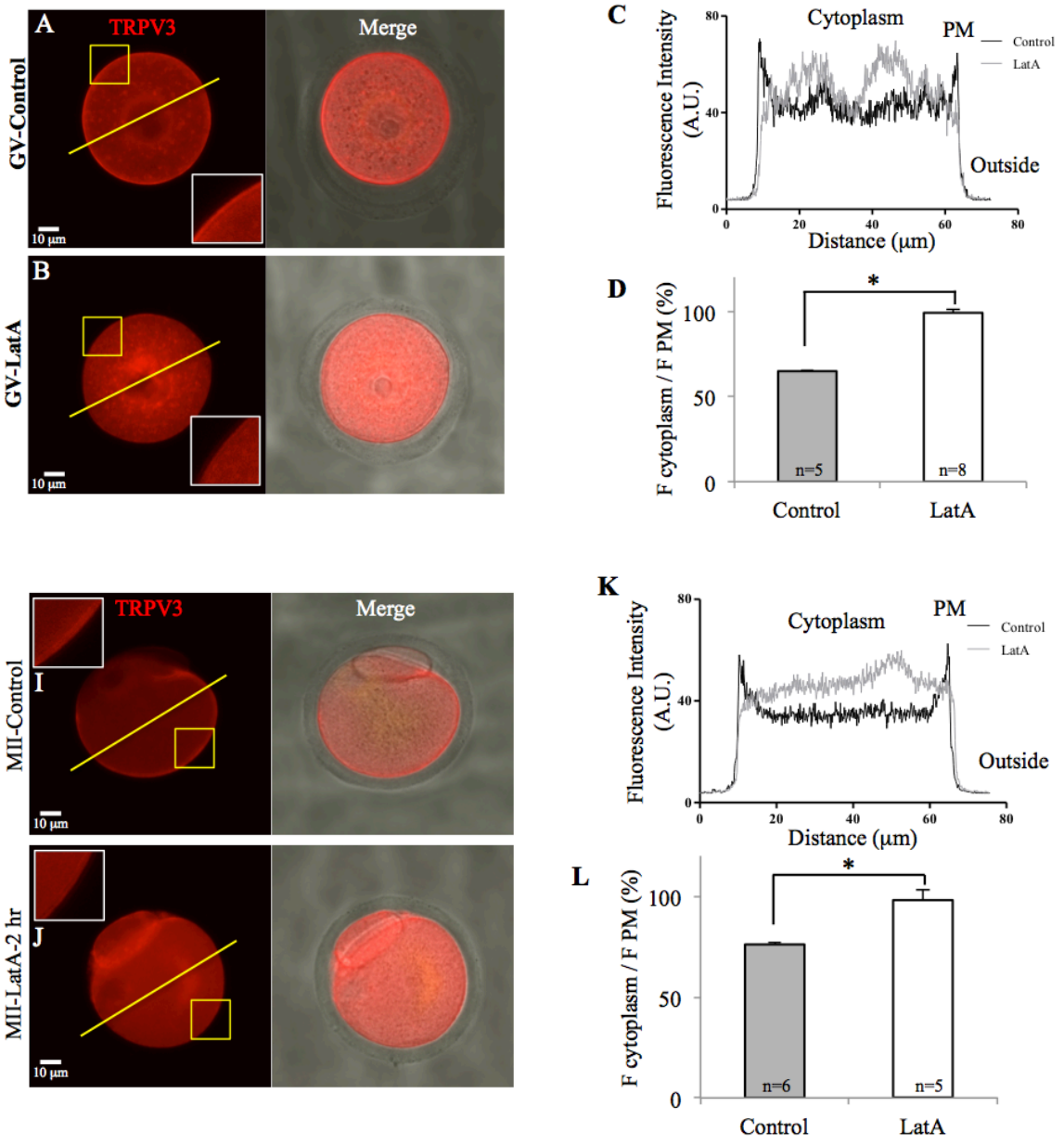

Figure 2-10. LatA treatment changes the distribution of TRPV3 in oocytes and eggs. The localization of TRPV3 was analyzed by confocal microscopy in oocytes and eggs expressing RFP-TRPV3 cultured in absence (Control) or presence of LatA (5 µM). (A-C) GV oocytes overexpressing TRPV3 ± LatA for3 hr. (A) Control GV oocytes. (B) Oocytes incubated with LatA. (C) Fluorescence intensity on a line crossing the entire cell from PM to PM (yellow line, Figure 2-10 A. B., *left panel*). (D) Ratio of intensity of fluorescence in cytoplasm vs. PM (*, $P < 0.05$). Insets show a zoomed area of the PM and surrounding areas (yellow square). (E-H) MII eggs overexpressing TRPV3 ± 2 hr with LatA. (E) Control MII eggs. (F) MII eggs treated with LatA. (G) Fluorescence intensity on a line crossing the entire cell from PM to PM (yellow line, Figure 2-10 E. F., *left panel*). H. Ratio of intensity of fluorescence in cytoplasm vs. PM (*, $P < 0.05$). Insets

show a zoomed area of the PM and surrounding areas (yellow square). Number of oocytes/eggs analyzed is indicated inside the bars.

FIGURE 2-11

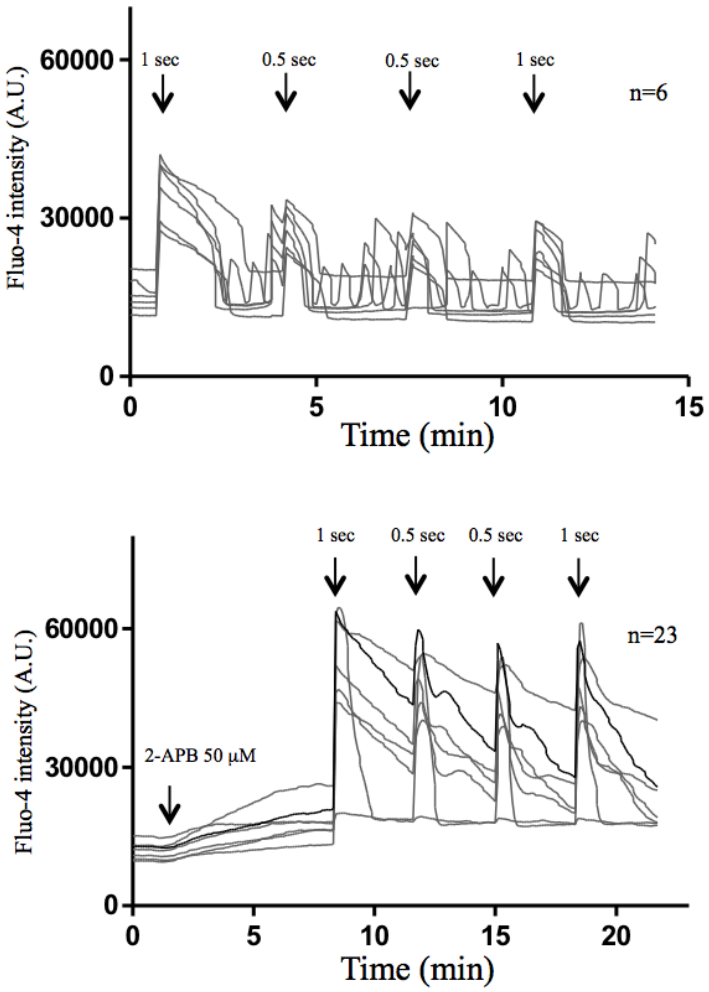

Figure 2-11. The function of IP_3R1 in mouse eggs is not affected by 2-APB. IP_3-induced Ca^{2+} release obtained after photolysis of cIP_3 by a flash of UV light. Changes in $[Ca^{2+}]_i$ induced by UV-flashes of increasing duration, which are indicated in the graphs, in control mouse eggs (*upper panel*) and oocytes and eggs pre-treated with 50 µM 2-APB (arrow; *lower panel*). Numbers of eggs evaluated are indicated in each graph.

FIGURE 3-1

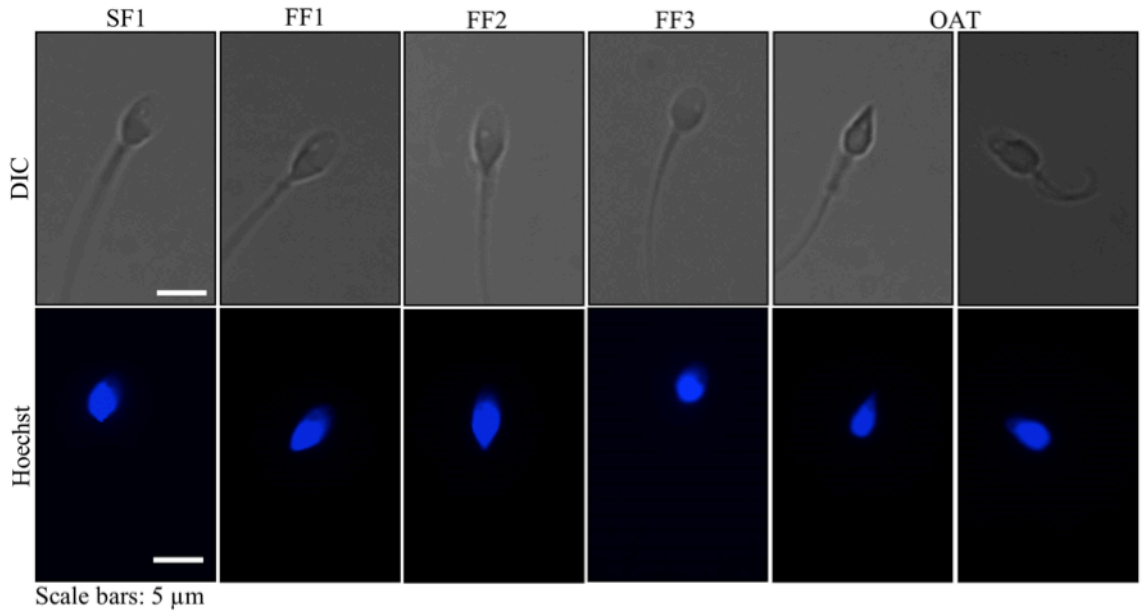

Figure 3-1. DIC and DNA staining images of sperm from successful, SF1, and unsuccessful, FF1-3 and OAT, fertilization ICSI cases. DIC images, top panels, and same samples stained with Hoechst to assess nuclear DNA, lower panels, of sperm from FF1-3 and OAT patients, which failed ICSI, and from a control, SF1, patient whose sperm successfully activated eggs during ICSI.

FIGURE 3-2

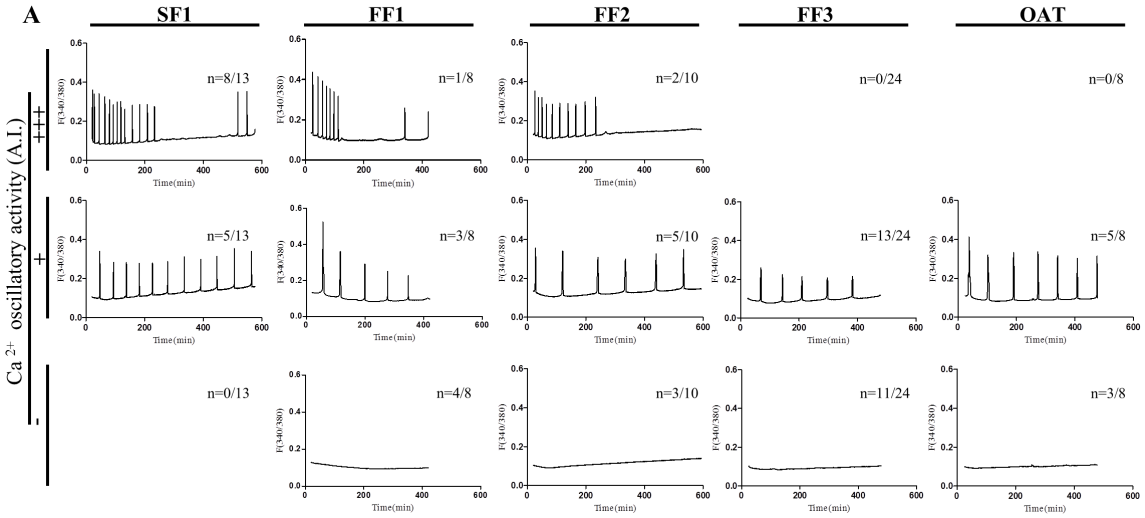

Figure 3-2. $[Ca^{2+}]_i$ response-inducing ability of sperm from patients with successful (SF1) and unsuccessful, FF1-3 and OAT, ICSI. (A) Ca^{2+} oscillations in mouse eggs injected with sperm of control the control patient SF1, or with sperm from patients that failed ICSI, FF1, FF2, FF3 and OAT. *n*, numerator indicates the number of eggs that displayed the $[Ca^{2+}]_i$ profile shown in each panel, whereas the denominator denotes the total number of eggs tested.

FIGURE 3-3

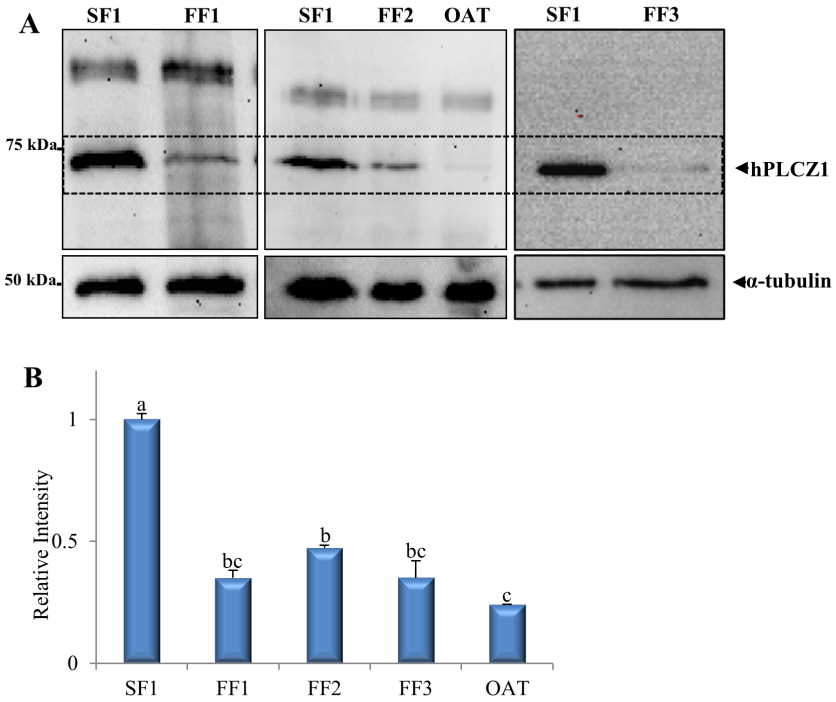

Figure 3-3. PLCZ1 expression in sperm of control, SF1, and failed fertilization, FF1-3 and OAT, ICSI patients. (A) Western blot displaying PLCZ1 IB expression in sperm of a control, SF1, patient and in the sperm of patients that failed ICSI, FF1, FF2, FF3 and OAT. The MW of human PLCZ1 is ~ 70 kDa and is denoted by an arrowhead on the right side of the panel. α-tubulin was used as a loading control, and immunoblots against it show ~equal loading (lower panels) (B) Bar graph displaying the relative intensity of the PLCZ1 band in the upper panel. Bars with different superscript are significantly different ($P < 0.05$). Please note that western blots were run on different dates, as samples became available. The SF1 sample was prepared once and used for all Immunoblots.

FIGURE 3-4

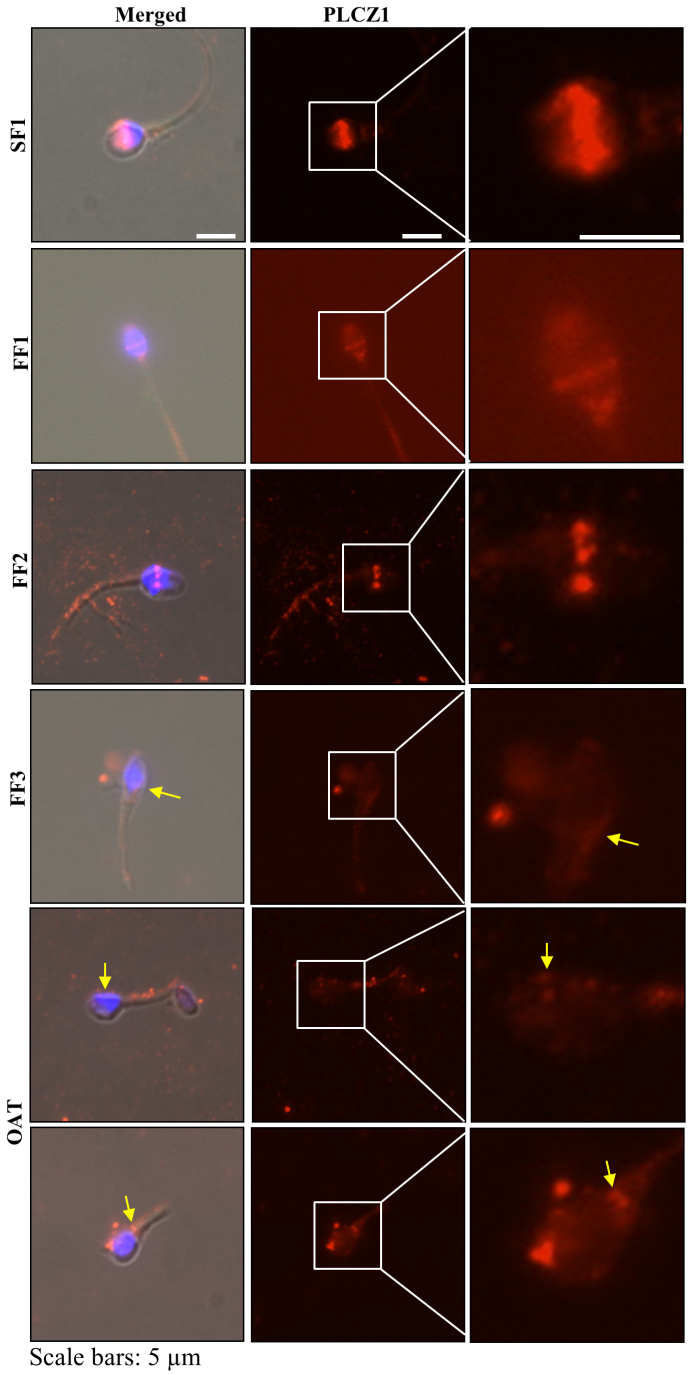

Figure 3-4. PLCZ1 localization in SF1, FF1, FF2, and FF3. Using, immunofluorescence (IF), PLCZ1 is shown to adopt the expected equatorial localization, whereas in FF1-FF3 sperm, the intensity of PLCZ1 reactivity is highly decreased or mis-localized, or both. Images on the left panels are a combination of bright field, DNA staining and fluorescence; whereas middle panel show IF images, and the right panels show higher

magnifications of the IF images. In the lower three panels, yellow arrows denote the abnormal localization and weak presence of PLCZ1.

FIGURE 3-5

A

Semen parameters	P1	P2
Semen Volume (ml)	3	5.8
Sperm concentration (10^6/ml)	150	101
Motility (A+B+C) 1 h (%)	50	40
Vitality (%)	63	70
Normal spermatozoa (%)	20	7
Anomalies of the flagella (%)	10	20
Abnormal acrosome (%)	50	78
Other anomalies of the head (%)	10	20
Multiple anomalies index	1.3	1.4

B

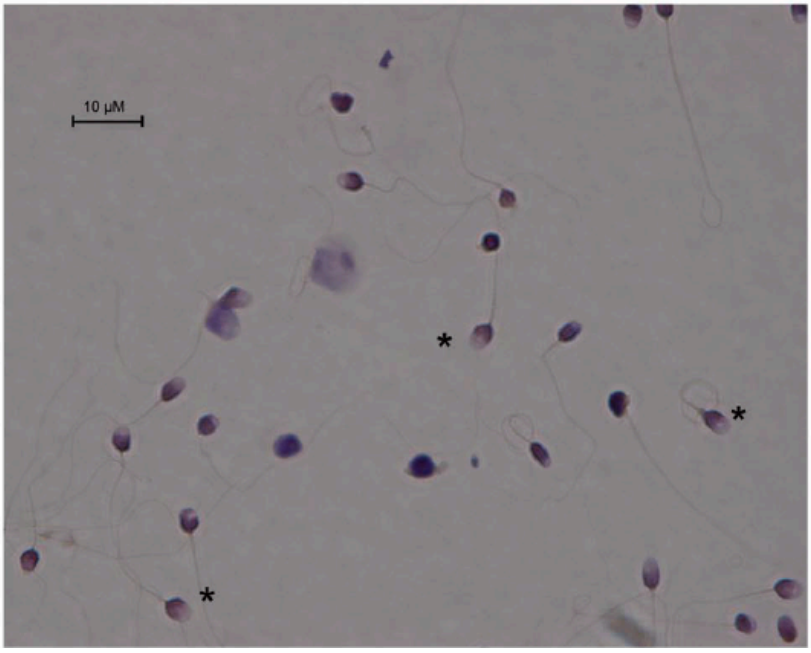

Figure 3-5. Spermatocytogram of patients exhibiting oocyte activation failure (OAF)
(A) Table showing semen parameters and spermatocytogram of both patients. Sperm samples were spread over a slide and dried at RT, fixed in Ether/Ethanol 1:1 for Harris-Schorr staining. Sperm were then scored according to WHO's laboratory manual for examination and processing of human semen (FIFTH edition). Values are the average of two separate analyses. (B) Examples of sperm morphology in samples. * Indicates fully normal spermatozoa.

FIGURE 3-6

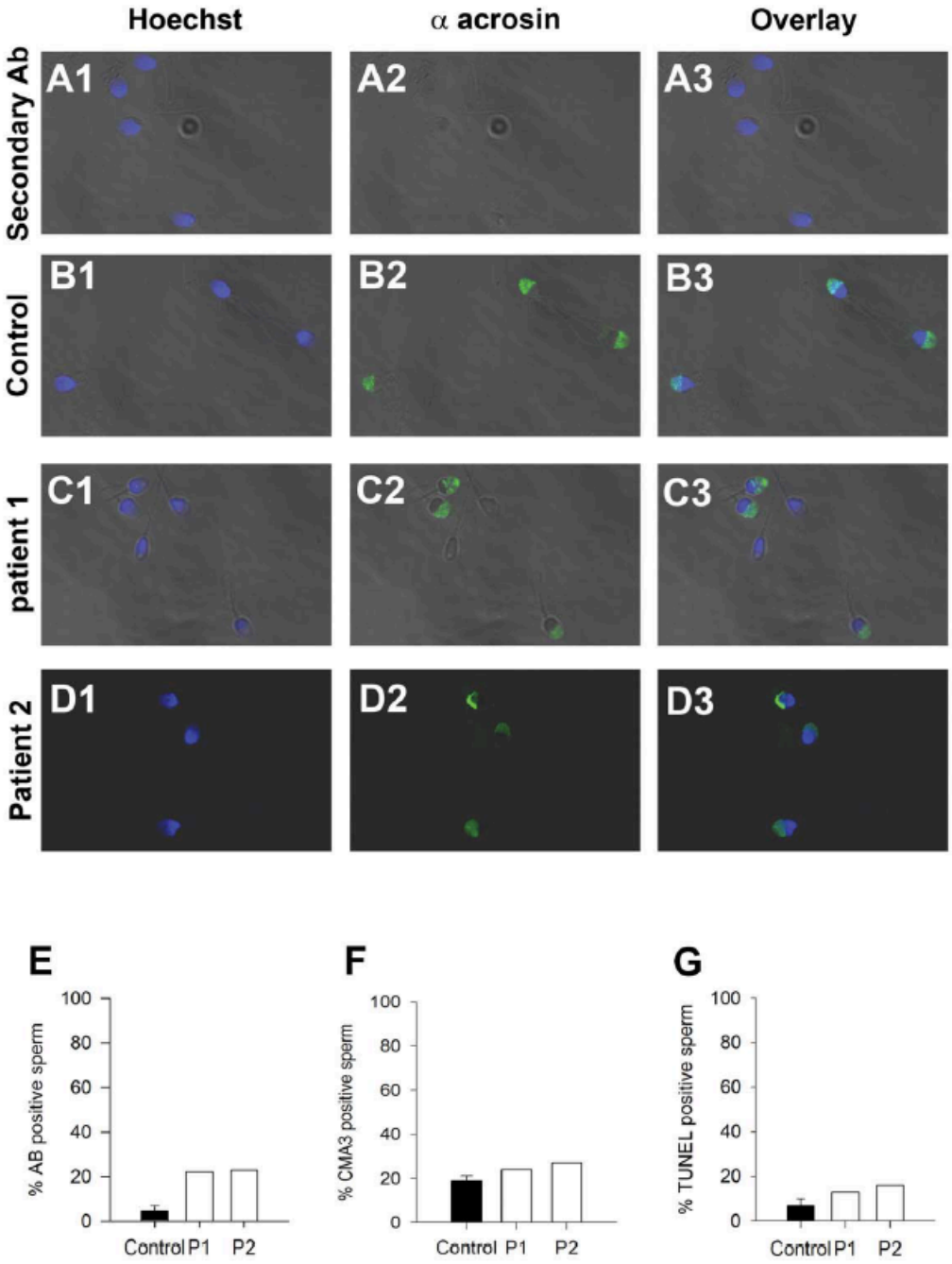

Figure 3-6. Morphology of acrosome stained with anti-acrosin antibody and assessment of nucleus compaction and DNA breaks of sperm from OAF patients (A) Negative control experiment with addition of secondary antibody without primary antibody. (B-D) Acrosin staining (green staining, B2-D2) of sperm from subjects with normal fertility (B) and from OAF patients (C, D) counterstained with Hoechst (blue, B1-D1) to evidence the nucleus/acrosome ratio. The third column corresponds to overlay (B3-D3). (E) Histones content of sperm was assessed using the aniline blue (AB) test. The histogram shows %

of stained sperm in samples from control (n=5 ± SD) and patients (n=1). (F) Protamination of sperm was evaluated using the chromomycin A3 test, and results are displayed in the histogram, which shows % of stained sperm in control (n=5 ± SD) and patients' (n=1) samples. (G) Histogram of DNA fragmentation analysis with TUNEL assay showing level of TUNEL positive sperm in control (n=5 ± SD) and patients' (n=1) samples.

FIGURE 3-7

A

Gene	Variant coordinates	Transcript	cDNA Variation	Amino acid variation	Prediction
PLCZ1	chr12:18841149, T>A	ENST00000266505	c.1465A>T	p.Ile489Phe	Damaging
EPS8	chr12:15776164, A>C	ENTS00000281172	c.2283A>C	p.Asp761Glu	Benign
RP11-1021N1.1	chr16:15528278, T>C	ENST00000568222	c.286T>C	p.Tyr96His	Benign
LKAAEAR1	chr20:62715318, T>G	ENST00000308906	c.255T>G	p.Glu85Asp	Benign

B

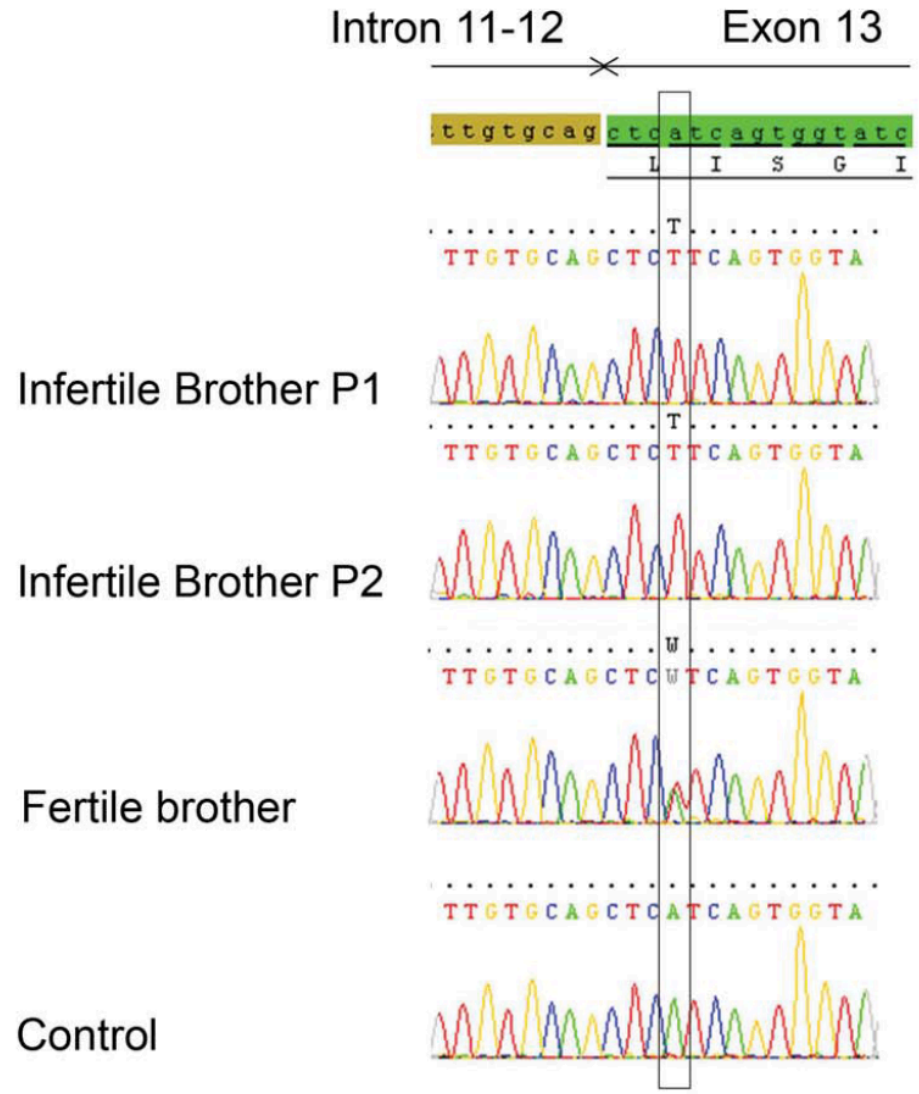

Figure 3-7. Novel point mutation in PLCZ1. (A). List of common homozygous variants present in P1 and P2. Coordinates of all variations are based on the UCSC GRCh37/hg19 assembly. (B) The presence of the identified variation was verified by Sanger sequencing of PLCZ1 exon 13. Electropherogram of PLCZ1 exon 13 showing the mutated sequence and sequence obtained from a control individual. The two infertile brothers carried a homozygous missense mutation (p.Ile489Phe) in PLCZ1 exon 13 whereas the fertile brother harbors the mutation in a heterozygous state. Primers were as followed: PLCZ1_14F: TCAATGTTTGTGGGAGCTGA and PLCZ1_14R: GGACATAATGGAAAACCCTTG. Thirty-five cycles of PCR amplification were carried out at 60°C. Sequencing reactions were carried out with BigDye Terminator v3.1 (Applied Biosystems) and sequence analysis with ABI 3130XL (Applied Biosystems).

FIGURE 3-8

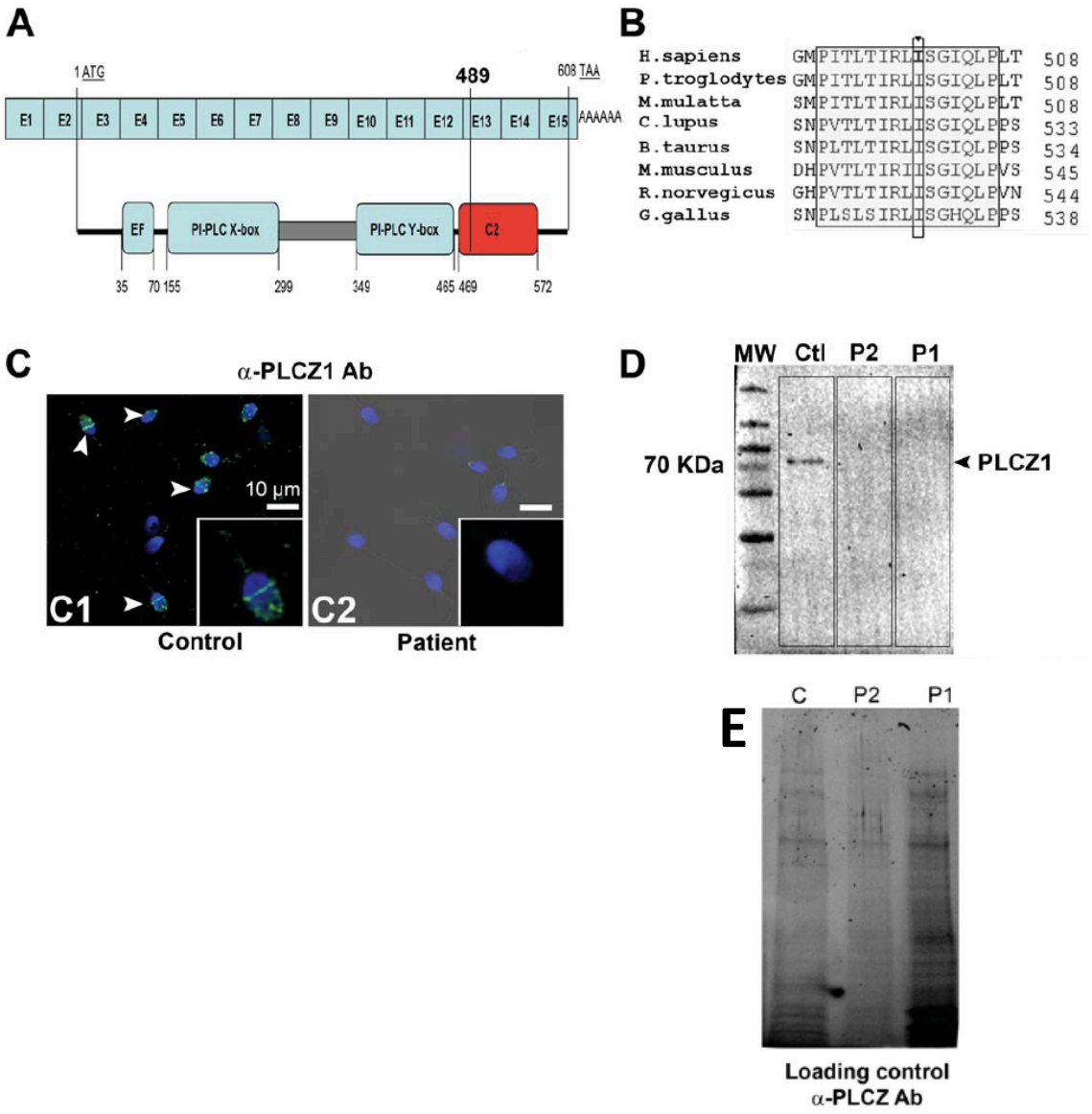

Figure 3-8. The Ile489Phe mutation is located in the C2 domain of PLCZ1. (A) Schematic representation of the exomic structure of human PLCZ1 cDNA sequence and corresponding functional domains of PLCZ1 (http://www.uniprot.org/uniprot/Q86YW0). The first coding exon is exon 2 (exon sizes are not to scale). The mutation is located in exon 13 and changes Isoleucine 489 located in the C2 domain into a Phenylalanine. (B) The mutation is located in a cluster of 15 highly conserved amino acids. (C, D) PLCZ1 expression is undetectable by IF and WB in sperm of patients exhibiting oocyte activation failure (OAF) after ICSI. (C1) Overlay of Hoechst staining (blue) and PLCZ1 staining (green) of sperm from a fertile control patient showing strong immunoreactivity in the post acrosomal area (white arrow heads and inset) and to a lesser extent in the acrosome. (C2) Representative staining of sperm from patients with OAF showing absence of PLCZ1 staining in the post acrosomal area and very faint staining over the

acrosome. (D) WB using protein extracts of sperm from a fertile control (Ctl), or patient 1 (P1) and patient 2 (P2) and an anti-PLCZ1 antibody that fails to detect reactivity in the patients' lanes. (E) Protein gel representing loading control for Figure 3-8D showing that all lanes were similarly loaded. Protein loads were controlled with TGX stain free™ precast gels.

FIGURE 3-9

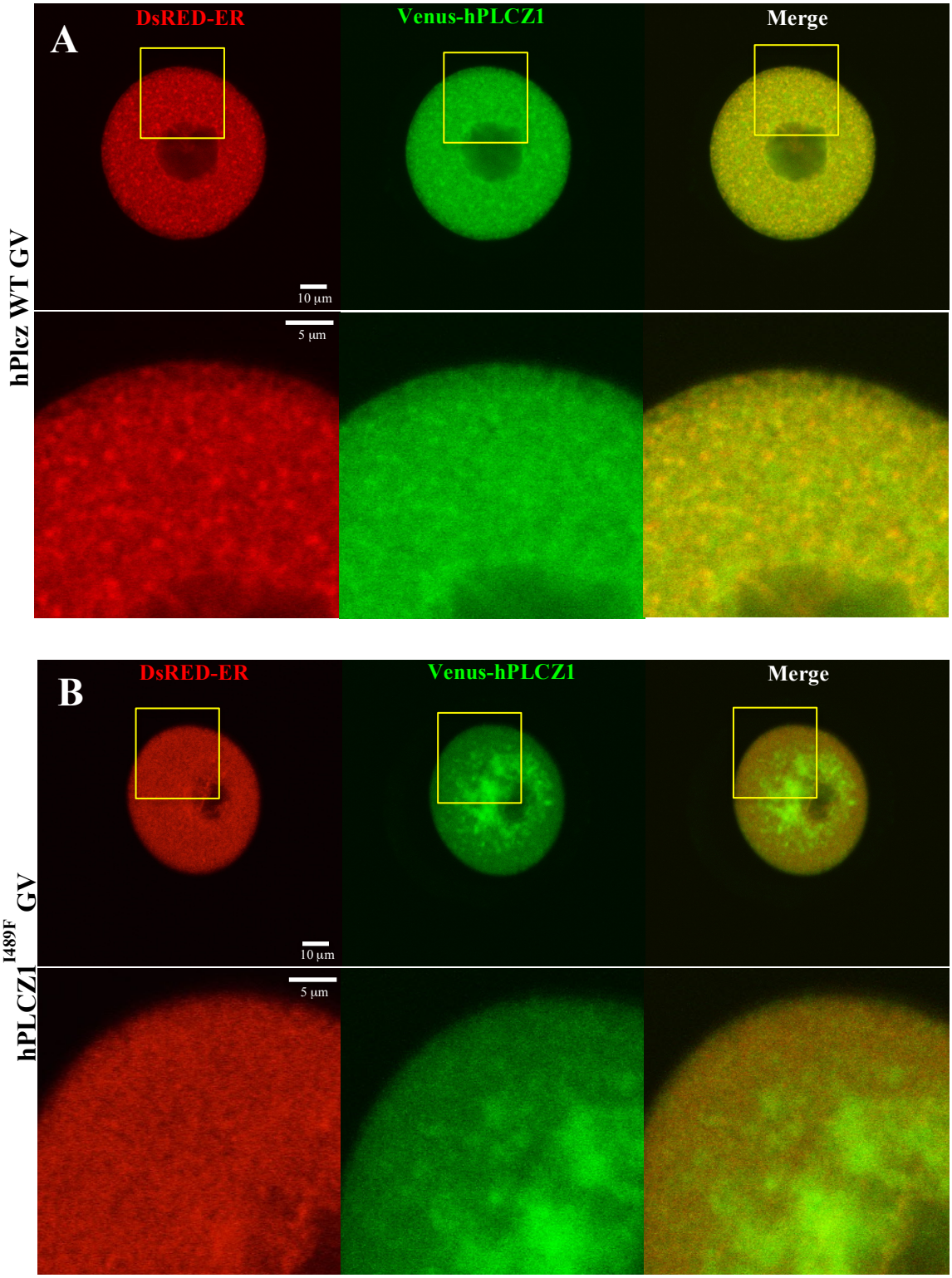
A
DsRED-ER
Venus-hPLCZ1
Merge
hPlez WT GV
10 µm
5 µm
B
DsRED-ER
Venus-hPLCZ1
Merge
hPLCZ1 I489F GV
10 µm
5 µm

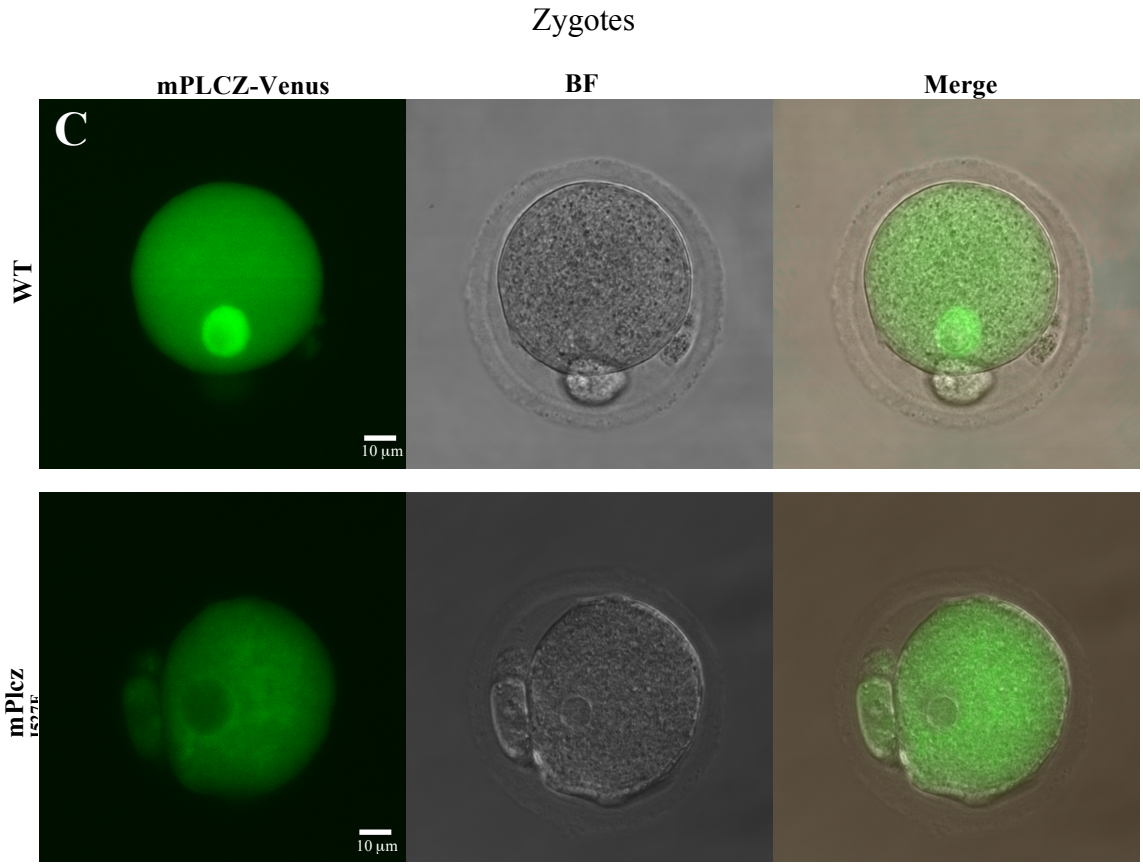

Figure 3-9. Mislocalization of PLCZ1 following expression in GV and MII oocytes. (A) Venus tagged human PLCZ1 cRNA (green) was co-injected in mouse GV stage oocytes with ER-DsRed cRNA as a marker of the endoplasmic reticulum (red). Both PLCZ1 and ER-DsRed exhibited a widespread punctiform staining throughout the cytoplasm and the overlay shows mostly overlapping distribution of the signals. (B) Co-injection of Ile489Phe PLCZ1 and ER-DsRed resulted in different distribution, with most of the PLCZ1 staining (green) concentrated around the nucleus (GV); whereas ER-DsRed remained uniformly distributed in the cytoplasm; there was minimal overlap of the signals at the oocyte periphery. (C) cRNAs encoding for WT mPlcz1 and the equivalent mutant in mice, Ile527Phe, were injected in MII oocytes and their ability to translocate into the PN compared. Where WT Plcz1 (left images) concentrated on the PN, Ile527Phe Plcz1 did not (right images).

FIGURE 3-10

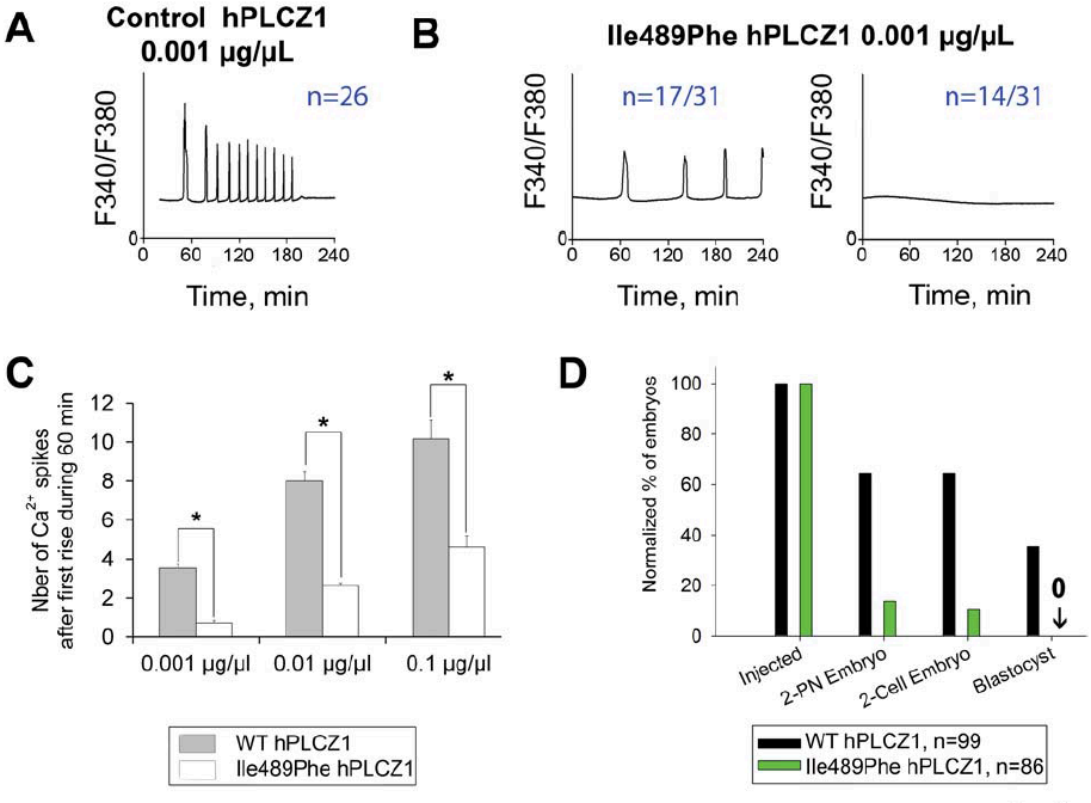

Figure 3-10. Ile489Phe PLCZ1 induces fewer Ca^{2+} oscillations compromising embryo development. (A) Injection of hPLCZ1 cRNA (0.001 µg/µl) in MII mouse oocytes triggered high frequency Ca^{2+} oscillations, 6 and 10 rises per hour that end by 120 - 180 min after injection. (B) In contrast, injection of cRNA of Ile489Phe hPLCZ1 (0.001 µg/µl) triggered oscillations that are either delayed and with low frequency (17/31) or failed to initiate them (14/31). (C) Histogram showing means + SD of the frequency of Ca^{2+} rises in function of control or Ile489Phe cRNA PLCZ1 concentrations injected into oocytes; Asterisks indicate significant differences determined by t-test, $p<0.01$ (D) Rates of 2PN, 2-cell embryos and blastocysts obtained after injection of WT or Ile489Phe cRNA PLCZ1 (0.01 µg/µl) in mouse MII oocytes; n corresponds to the number of injected oocytes.

FIGURE 3-11

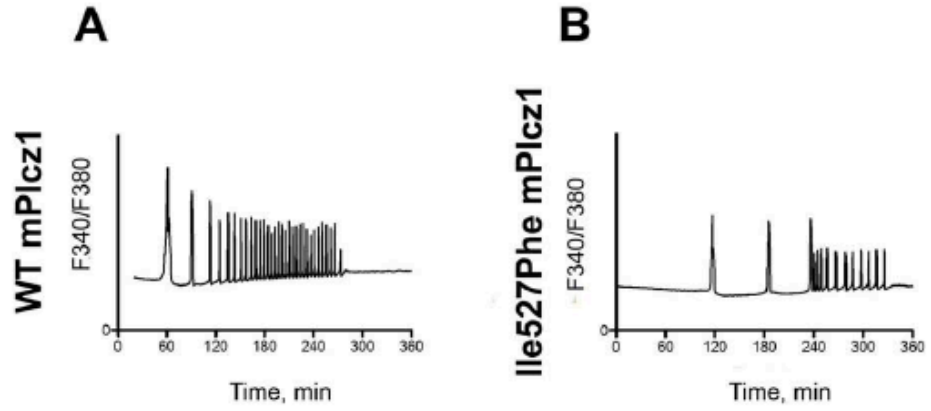

C

	mPlcz 0.01 µg/µl		mPlcz 0.05 µg/µl	
	PN (6 hr)	PN (10 hr)	PN (6 hr)	PN (10 hr)
WT Plcz1	5/5 100%	5/5 100%	16/16 100%	16/16 100%
Ile527Phe mPlcz1	2/10 20%	6/10 60%	7/30 23%	23/30 76%

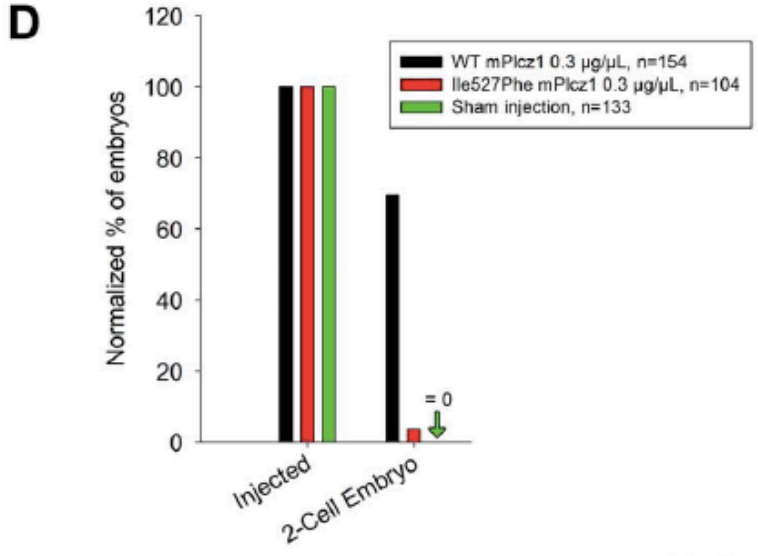

Figure 3-11. Ca^{2+} responses induced by Ile527Phe mPlcz1 are altered and lead to defective embryo development. (A) Profile of Ca^{2+} responses induced by injection of WT mPlcz1 cRNA (0.01 µg/µL) into mouse oocytes. (B) Ca^{2+} profiles recorded after injection

of Ile527Phe mPlcz1 cRNA (the mouse equivalent of Ile489Phe hPLCZ1), show delayed and reduced response. (C) 2PN formation rates are reduced and delayed when both 0.01 and 0.05 μg Ile527Phe mPlcz1 cRNA cRNA/μl concentrations are used (D) injections of Ile527Phe mPlcz1 cRNAs do not support embryo development, as the rate of 2-cell embryos formation was strongly reduced or abolished; n corresponds to the number of injected MII oocytes.

FIGURE 3-12

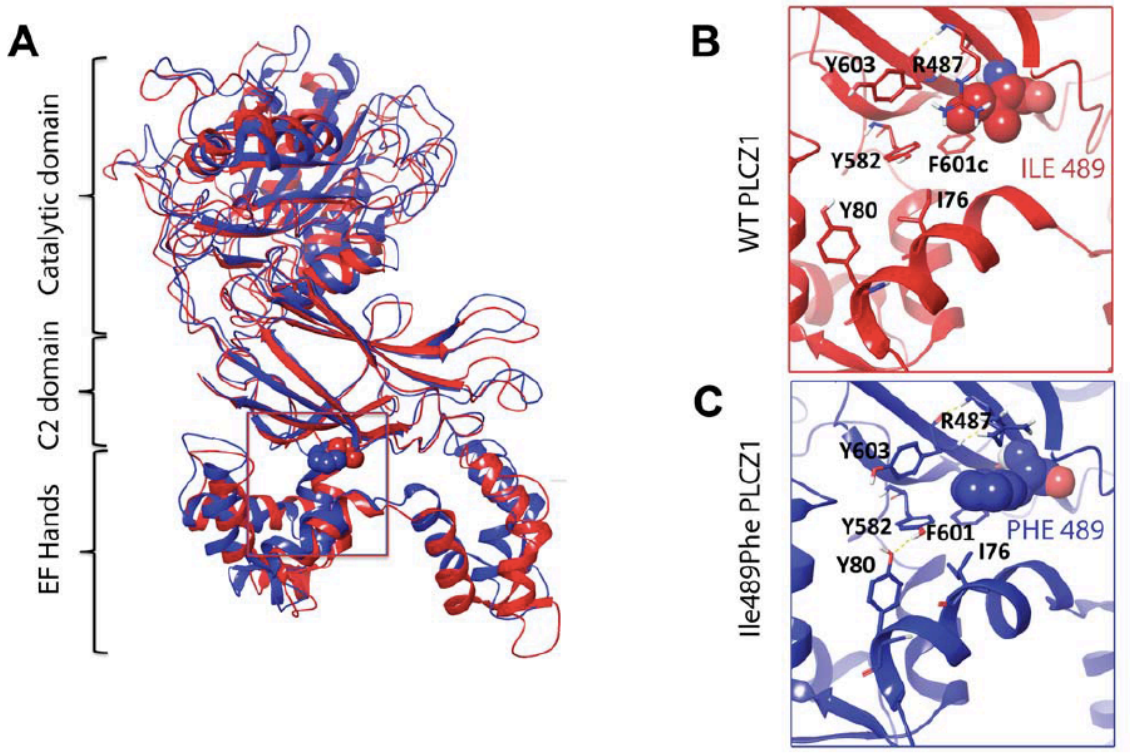

Figure 3-12. (A) The site of the Ile489Phe mutation is located at the interface of C2 and EF-hand domains of PLCZ1 (red box) (B, C) Enlargement of the red box for WT and mutant PLCZ1. As suggested by molecule dynamics simulation, the mutation results in a displacement of the surrounding C2 residues (Y582, F601, Y603, and R487) by the larger side chain of Phe. This reorganization, in turn, leads to novel contacts between C2 and EF2 hand via persistent hydrophobic (Phe489–Ile76) and H-bonding (Tyr582–Tyr80) side chain interactions, which shift the entire EF-hand domain toward C2 by approximately 1.5 Å by the end of the 1.2- ns simulation.

FIGURE 3-13

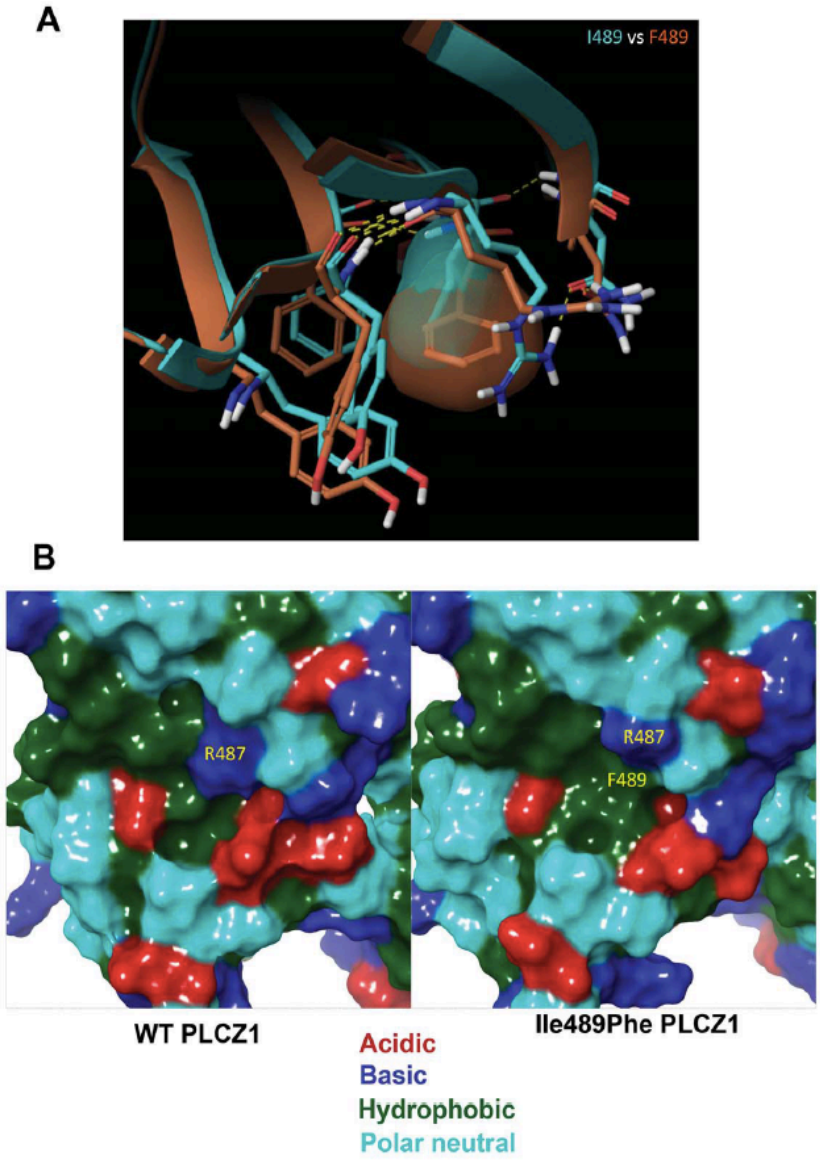

Figure 3-13. Prediction of Intra C2 domain effect induced by Ile489Phe mutation
(A) Backbone superimposition of the WT (light blue) and Ile489Phe (rustcoloured) PLCZ1 regions proximal to the mutagenesis site and optimized by molecular dynamics. Briefly, the homology models of the WT and mutant PLCZ1 were generated with the Prime homology modeling workflow (version 3.8, Schrödinger, LLC), using the structure of rPlcz1 (pdb code: 1DJX) as the template. Upon minimization of the models using Prime's OPLS2005 force field, the models were further optimized via 1.2-ns molecular dynamics simulations (NPT ensemble, 300K, 1 atm, SPC solvent model, 150 mM NaCl) within Desmond (version4.0, D. E. Shaw Research & Schrödinger, LLC). The side chain of the 489 residues is shown as transparent molecular surfaces of the respective colors. In

the mutant PLCZ1, adjacent aromatic residues (Y582, F601, Y603) move to accommodate the larger Phe ring, and R487 no longer can or needs to shield Ile489 from the solvent due to lower hydrophobicity of the aromatic Phe. Taken together, these changes are predicted to result in the formation of an aromatic-rich binding sub-site, capable of associating with lipophilic molecules. (B) The molecular surfaces of WT and mutant PLCZ1 in the vicinity of the 489 residues, demonstrating the formation of a novel hydrophobic sub-site at the C2/EF hand junction. The basic, acidic hydrophobic and polar neutral residues shown in blue, red, green and cyan, respectively.

FIGURE 3-14

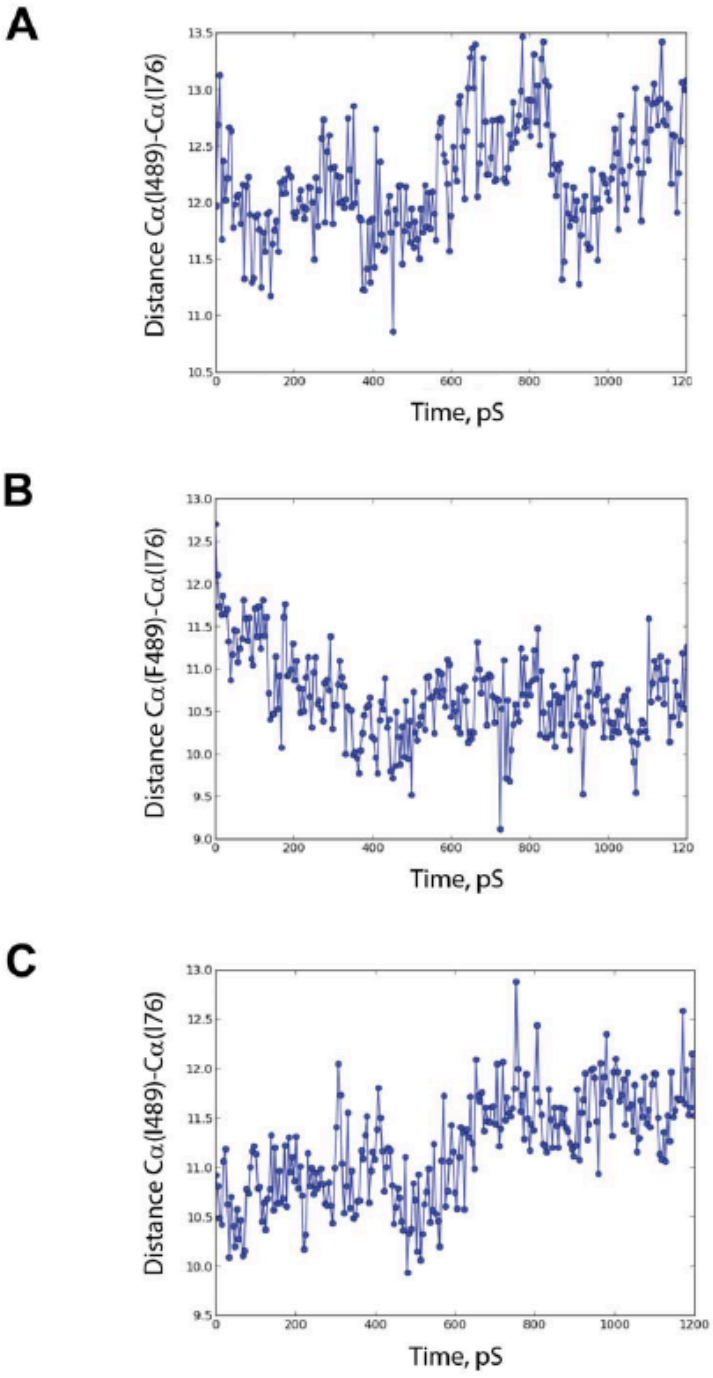

Figure 3-14. Molecular dynamics simulations of the WT and Ile489Phe PLCZ1 detect a shift of the EF2 hand helix proximal to the mutation site. Topological changes were detected using Simulated Event Analysis program by monitoring the CαI76–CαI489 and CαI76–CαF489 distances and root mean square fluctuations (RMSF) as a function of

simulation time. The mutant structure from the final frame was modified back to contain Ile489, and a simulation under the identical conditions was conducted to ascertain the persistence of the mutant's conformation. (A) The distance between the Cα-Ile76 and Cα-Ile489 atoms of the WT PLCZ1 model is in the 11.0–13.5 Å range (mean: 12.2 Å). (B) The distance between the Cα-Ile76 and Cα-Phe489 atoms in the mutant model is reduced to the 9.5–11.5 Å range in the second half of the simulation (mean: 10.7 Å). (C) Finally, a WT model, with Ile489 incorporated into the final frame structure of the mutant simulation; returning back to the 11.0–13.0 Å range (Cα-Ile76–Cα-Ile489) by the second half of the simulation.

FIGURE 3-15

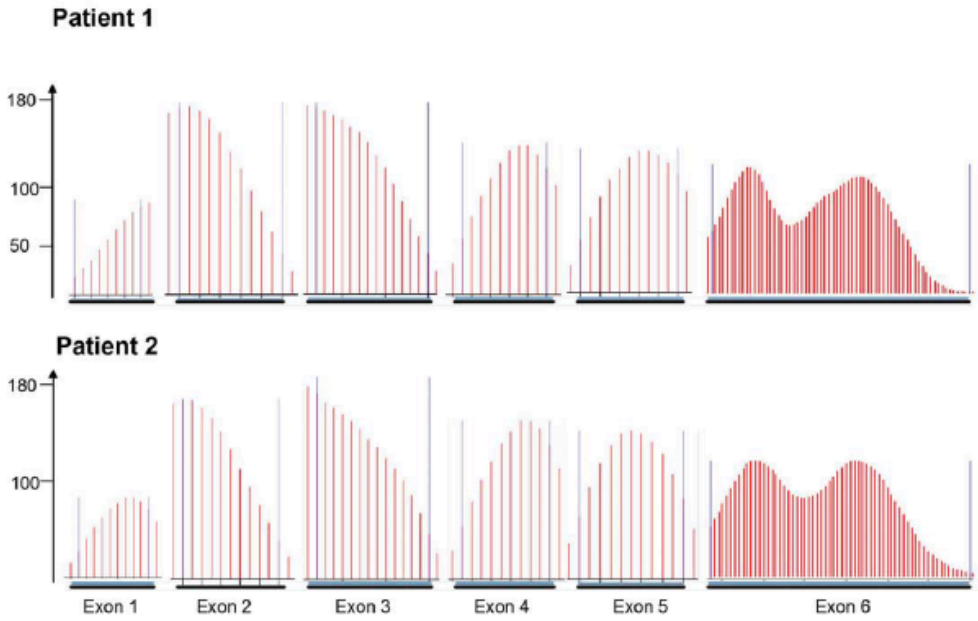

Figure 3-15. NGS coverage of WBP2NL exonic sequence for patients 1 and 2. The read depth for each patient is indicated in ordinate. For each patient, the minimal coverage for the whole coding sequence is 40X. Note that regions of lesser coverage (beginning of exon 1 and end of exon 6) are the 5' and 3' untranslated regions, respectively.

FIGURE 3-16

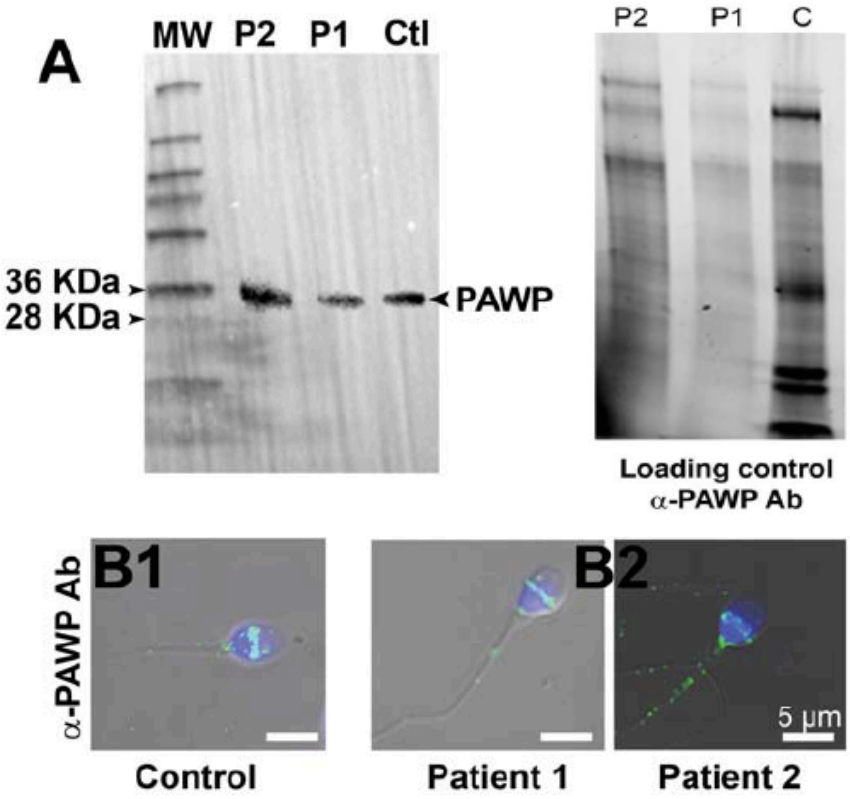

Figure 3-16. Normal expression and localization of PAWP in patients with OAF. (A) WB using protein extracts from sperm of a fertile control (Ctl), patient 1 (P1) and patient 2 (P2) and an anti-PAWP antibody. Immunoreactivity is observed in the lanes of control and patients' sperm extracts. (B1) Sperm from a fertile control were stained with anti-PAWP antibody and counterstained with Hoechst. Overlay shows that the antibody stains strongly the postacrosomal area. (B2) Similar staining of sperm from patients 1 and 2, show the same reactivity to that of the control fertile sperm. (C) Protein gel representing loading control for Figure 3-16A showing that all lanes were similarly loaded. Protein loads were controlled with TGX stain free™ precast gels.

FIGURE 3-17

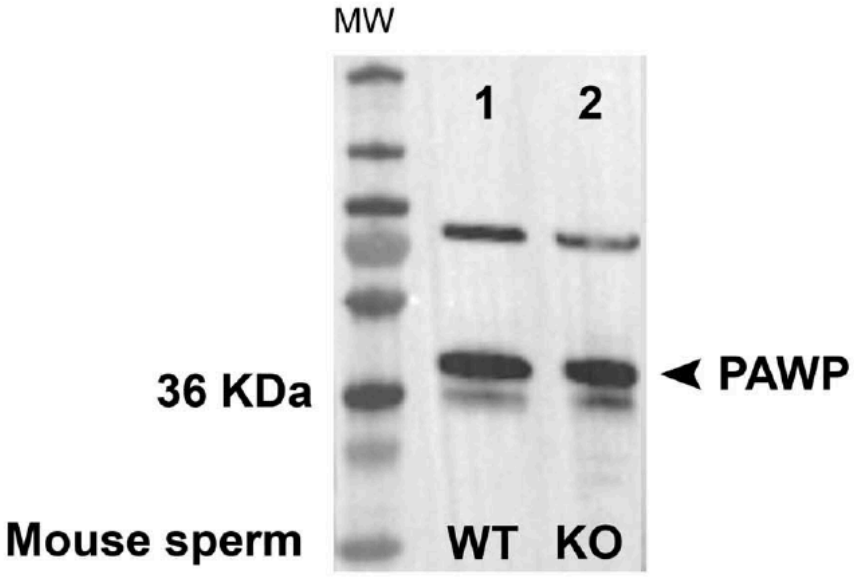

Figure 3-17. PAWP is expressed normally in globozoospermic sperm from Dpy19l2 KO males WB of protein extracts from sperm of WT (lane 1) and Dpy19l2 KO mice (lane 2) using an anti-PAWP antibody. Immmunoreactivity is observed in the form of a strong band just above 36 kDa, which is near the 37.4 kDa, the expected MW of mouse PAWP.

BIBLIOGRAPHY

1. Berridge MJ, Lipp P, Bootman MD. The versatility and universality of calcium signalling. Nature reviews Molecular cell biology. 2000;1(1):11-21. doi: 10.1038/35036035.
2. Jones KT, Carroll J, Merriman JA, Whittingham DG, Kono T. Repetitive sperm-induced Ca2+ transients in mouse oocytes are cell cycle dependent. Development (Cambridge, England). 1995;121(10):3259-66.
3. Ducibella T, Schultz RM, Ozil J-PP. Role of calcium signals in early development. Seminars in cell & developmental biology. 2006;17(2):324-32. doi: 10.1016/j.semcdb.2006.02.010.
4. Miyazaki S, Hashimoto N, Yoshimoto Y, Kishimoto T, Igusa Y, Hiramoto Y. Temporal and spatial dynamics of the periodic increase in intracellular free calcium at fertilization of golden hamster eggs. Developmental biology. 1986;118(1):259-67. Epub 1986/11/01. PubMed PMID: 3770302.
5. Krauchunas AR, Wolfner MF. Molecular changes during egg activation. Current topics in developmental biology. 2013;102:267-92. doi: 10.1016/B978-0-12-416024-8.00010-6. PubMed PMID: 23287037; PMCID: 3931425.
6. Kashir J, Deguchi R, Jones C, Coward K, Stricker SA. Comparative biology of sperm factors and fertilization-induced calcium signals across the animal kingdom. Molecular reproduction and development. 2013;80(10):787-815. doi: 10.1002/mrd.22222.

7. Kline D, Kline JT. Thapsigargin activates a calcium influx pathway in the unfertilized mouse egg and suppresses repetitive calcium transients in the fertilized egg. The Journal of biological chemistry. 1992;267(25):17624-30.
8. Miao Y-LL, Stein P, Jefferson WN, Padilla-Banks E, Williams CJ. Calcium influx-mediated signaling is required for complete mouse egg activation. Proceedings of the National Academy of Sciences of the United States of America. 2012;109(11):4169-74. doi: 10.1073/pnas.1112333109.
9. McGuinness OM, Moreton RB, Johnson MH, Berridge MJ. A direct measurement of increased divalent cation influx in fertilised mouse oocytes. Development (Cambridge, England). 1996;122(7):2199-206.
10. Stricker SA. Comparative biology of calcium signaling during fertilization and egg activation in animals. Developmental biology. 1999;211(2):157-76. doi: 10.1006/dbio.1999.9340.
11. Miyazaki S, Ito M. Calcium signals for egg activation in mammals. Journal of pharmacological sciences. 2006;100(5):545-52.
12. Giusti AF, Carroll DJ, Abassi YA, Terasaki M, Foltz KR, Jaffe LA. Requirement of a Src family kinase for initiating calcium release at fertilization in starfish eggs. The Journal of biological chemistry. 1999;274(41):29318-22.
13. Sato K, Tokmakov AA, Iwasaki T, Fukami Y. Tyrosine kinase-dependent activation of phospholipase Cgamma is required for calcium transient in Xenopus egg fertilization. Developmental biology. 2000;224(2):453-69. doi: 10.1006/dbio.2000.9782.

14. Wakai T, Fissore RA. Ca(2+) homeostasis and regulation of ER Ca(2+) in mammalian oocytes/eggs. Cell calcium. 2013;53(1):63-7. doi: 10.1016/j.ceca.2012.11.010.
15. Swann K. A cytosolic sperm factor stimulates repetitive calcium increases and mimics fertilization in hamster eggs. Development (Cambridge, England). 1990;110(4):1295-302.
16. Wu H, He CL, Fissore RA. Injection of a porcine sperm factor triggers calcium oscillations in mouse oocytes and bovine eggs. Molecular reproduction and development. 1997;46(2):176-89. doi: 10.1002/(SICI)1098-2795(199702)46:2<176::AID-MRD8>3.0.CO;2-N.
17. Kyozuka K, Deguchi R, Mohri T, Miyazaki S. Injection of sperm extract mimics spatiotemporal dynamics of Ca2+ responses and progression of meiosis at fertilization of ascidian oocytes. Development (Cambridge, England). 1998;125(20):4099-105.
18. Harada Y, Matsumoto T, Hirahara S, Nakashima A, Ueno S, Oda S, Miyazaki S, Iwao Y. Characterization of a sperm factor for egg activation at fertilization of the newt Cynops pyrrhogaster. Developmental biology. 2007;306(2):797-808. doi: 10.1016/j.ydbio.2007.04.019.
19. Saunders C, Larman M, Parrington J, Cox L, Royse J, Blayney L, Swann K, Lai F. PLC zeta: a sperm-specific trigger of Ca^{2+} oscillations in eggs and embryo development. Development. 2002;129(15):3533-44.
20. Peres A. The calcium current of mouse egg measured in physiological calcium and temperature conditions. The Journal of physiology. 1987;391:573-88.

21. Kang D, Hur C-GG, Park J-YY, Han J, Hong S-GG. Acetylcholine increases Ca2+ influx by activation of CaMKII in mouse oocytes. Biochemical and biophysical research communications. 2007;360(2):476-82. doi: 10.1016/j.bbrc.2007.06.083.

22. Chen C-CC, Lamping KG, Nuno DW, Barresi R, Prouty SJ, Lavoie JL, Cribbs LL, England SK, Sigmund CD, Weiss RM, Williamson RA, Hill JA, Campbell KP. Abnormal coronary function in mice deficient in alpha1H T-type Ca2+ channels. Science (New York, NY). 2003;302(5649):1416-8. doi: 10.1126/science.1089268.

23. Igusa Y, Miyazaki S, Yamashita N. Periodic hyperpolarizing responses in hamster and mouse eggs fertilized with mouse sperm. The Journal of physiology. 1983;340:633-47.

24. Cosens DJ, Manning A. Abnormal electroretinogram from a Drosophila mutant. Nature. 1969;224(5216):285-7. Epub 1969/10/18. PubMed PMID: 5344615.

25. Montell C, Jones K, Hafen E, Rubin G. Rescue of the Drosophila phototransduction mutation trp by germline transformation. Science (New York, NY). 1985;230(4729):1040-3. doi: 10.1126/science.3933112.

26. Montell C, Rubin GM. Molecular characterization of the Drosophila trp locus: a putative integral membrane protein required for phototransduction. Neuron. 1989;2(4):1313-23. Epub 1989/04/01. PubMed PMID: 2516726.

27. Nilius B, Bíró T. TRPV3: a 'more than skinny' channel. Experimental dermatology. 2013;22(7):447-52. doi: 10.1111/exd.12163.

28. Nilius B, Owsianik G. Transient receptor potential channelopathies. Pflugers Archiv : European journal of physiology. 2010;460(2):437-50. Epub 2010/02/04. doi: 10.1007/s00424-010-0788-2. PubMed PMID: 20127491.

29. Clapham DE. TRP channels as cellular sensors. Nature. 2003;426(6966):517-24. Epub 2003/12/05. doi: 10.1038/nature02196. PubMed PMID: 14654832.

30. Hardie RC, Minke B. The trp gene is essential for a light-activated Ca 2+ channel in Drosophila photoreceptors. Neuron. 1992;8(4):643-51. doi: 10.1016/0896-6273(92)90086-S.

31. Xue T, Do MT, Riccio A, Jiang Z, Hsieh J, Wang HC, Merbs SL, Welsbie DS, Yoshioka T, Weissgerber P, Stolz S, Flockerzi V, Freichel M, Simon MI, Clapham DE, Yau KW. Melanopsin signalling in mammalian iris and retina. Nature. 2011;479(7371):67-73. Epub 2011/11/05. doi: 10.1038/nature10567. PubMed PMID: 22051675; PMCID: Pmc3270891.

32. Colbert HA, Bargmann CI. Odorant-specific adaptation pathways generate olfactory plasticity in C. elegans. Neuron. 1995.

33. Kwon Y, Kim SH, Ronderos DS, Lee Y, Akitake B. Drosophila TRPA1 channel is required to avoid the naturally occurring insect repellent citronellal. Current Biology. 2010.

34. Zhang Y, Hoon MA, Chandrashekar J, Mueller KL. Coding of sweet, bitter, and umami tastes: different receptor cells sharing similar signaling pathways. Cell. 2003.

35. Kim SH, Lee Y, Akitake B. Drosophila TRPA1 channel mediates chemical avoidance in gustatory receptor neurons. Proceedings of the …. 2010. doi: 10.1073/pnas.1001425107.

36. Yu Y, Ulbrich MH, Li M, Dobbins S, Zhang WK. Molecular mechanism of the assembly of an acid-sensing receptor ion channel complex. Nature …. 2012.

37. Jordt SE, Tominaga M, Julius D. Acid potentiation of the capsaicin receptor determined by a key extracellular site. Proceedings of the …. 2000. doi: 10.1073/pnas.100129497.
38. Caterina MJ, Schumacher MA, Tominaga M, Rosen TA. The capsaicin receptor: a heat-activated ion channel in the pain pathway. Nature. 1997. doi: 10.1038/39807.
39. McKemy DD, Neuhausser WM, Julius D. Identification of a cold receptor reveals a general role for TRP channels in thermosensation. Nature. 2002.
40. Sun Y, Liu L, Ben-Shahar Y. TRPA channels distinguish gravity sensing from hearing in Johnston's organ. Proceedings of the …. 2009. doi: 10.1073/pnas.0906377106.
41. Sidi S, Friedrich RW, Nicolson T. NompC TRP channel required for vertebrate sensory hair cell mechanotransduction. Science (New York, NY). 2003.
42. Kamikouchi A, Inagaki HK, Effertz T, Hendrich O. The neural basis of Drosophila gravity-sensing and hearing. Nature. 2009. doi: 10.1038/nature07810.
43. Yan Z, Zhang W, He Y, Gorczyca D, Xiang Y, Cheng LE. Drosophila NOMPC is a mechanotransduction channel subunit for gentle-touch sensation. Nature. 2013. doi: 10.1038/nature11685.
44. Li W, Kang L, Piggott BJ, Feng Z, Xu XZS. The neural circuits and sensory channels mediating harsh touch sensation in Caenorhabditis elegans. Nature communications. 2011.
45. Walker RG, Willingham AT, Zuker CS. A Drosophila mechanosensory transduction channel. Science (New York, NY). 2000.

46. Liu C, Yue B, Yuan C, Zhao S, Fang C, Yu Y, Yan D. Elevated expression of Thoc1 is associated with aggressive phenotype and poor prognosis in colorectal cancer. Biochemical and biophysical research communications. 2015. Epub 2015/11/08. doi: 10.1016/j.bbrc.2015.10.166. PubMed PMID: 26545775.

47. Rohacs T, Nilius B. Regulation of transient receptor potential (TRP) channels by phosphoinositides. Pflugers Archiv : European journal of physiology. 2007;455(1):157-68. doi: 10.1007/s00424-007-0275-6.

48. Carvacho I, Lee HC, Fissore RA, Clapham DE. TRPV3 channels mediate strontium-induced mouse-egg activation. Cell reports. 2013;5(5):1375-86. doi: 10.1016/j.celrep.2013.11.007.

49. Peier AM, Reeve AJ, Andersson DA, Moqrich A, Earley TJ, Hergarden AC, Story GM, Colley S, Hogenesch JB, McIntyre P, Bevan S, Patapoutian A. A heat-sensitive TRP channel expressed in keratinocytes. Science (New York, NY). 2002;296(5575):2046-9. Epub 2002/05/23. doi: 10.1126/science.1073140. PubMed PMID: 12016205.

50. Smith GD, Gunthorpe MJ, Kelsell RE, Hayes PD, Reilly P, Facer P, Wright JE, Jerman JC, Walhin JP, Ooi L, Egerton J, Charles KJ, Smart D, Randall AD, Anand P, Davis JB. TRPV3 is a temperature-sensitive vanilloid receptor-like protein. Nature. 2002;418(6894):186-90. Epub 2002/06/22. doi: 10.1038/nature00894. PubMed PMID: 12077606.

51. Yang P, Zhu MX. TRPV3. Handbook of experimental pharmacology. 2014;222:273-91. Epub 2014/04/24. doi: 10.1007/978-3-642-54215-2_11. PubMed PMID: 24756710.

52. Xu H, Ramsey IS, Kotecha SA, Moran MM, Chong JA, Lawson D, Ge P, Lilly J, Silos-Santiago I, Xie Y, DiStefano PS, Curtis R, Clapham DE. TRPV3 is a calcium-permeable temperature-sensitive cation channel. Nature. 2002;418(6894):181-6. doi: 10.1038/nature00882.
53. Moqrich A, Hwang SW, Earley TJ, Petrus MJ, Murray AN, Spencer KS, Andahazy M, Story GM, Patapoutian A. Impaired thermosensation in mice lacking TRPV3, a heat and camphor sensor in the skin. Science (New York, NY). 2005;307(5714):1468-72. doi: 10.1126/science.1108609.
54. Cheng X, Jin J, Hu L, Shen D, Dong X, Samie MA. TRP channel regulates EGFR signaling in hair morphogenesis and skin barrier formation. Cell. 2010. doi: 10.1016/j.cell.2010.03.013.
55. Borbíró I, Lisztes E, Tóth BI, Czifra G, Oláh A, Szöll, odblac, si AG, Szentandrássy N, Nánási PP, Péter Z, Paus R, Kovács L, Bíró T. Activation of Transient Receptor Potential Vanilloid-3 Inhibits Human Hair Growth. Journal of Investigative Dermatology. 2011;131(8). doi: 10.1038/jid.2011.122.
56. Chung M-KK, Lee H, Mizuno A, Suzuki M, Caterina MJ. 2-aminoethoxydiphenyl borate activates and sensitizes the heat-gated ion channel TRPV3. The Journal of neuroscience : the official journal of the Society for Neuroscience. 2004;24(22):5177-82. doi: 10.1523/JNEUROSCI.0934-04.2004.
57. Fujiwara T, Nakada K, Shirakawa H, Miyazaki S. Development of inositol trisphosphate-induced calcium release mechanism during maturation of hamster oocytes. Developmental biology. 1993;156(1):69-79. doi: 10.1006/dbio.1993.1059.

58. Xu Z, Kopf GS, Schultz RM. Involvement of inositol 1,4,5-trisphosphate-mediated Ca2+ release in early and late events of mouse egg activation. Development. 1994;120(7):1851-9. Epub 1994/07/01. PubMed PMID: 7924992.

59. Ozil JP, Banrezes B, Toth S, Pan H, Schultz RM. Ca2+ oscillatory pattern in fertilized mouse eggs affects gene expression and development to term. Developmental biology. 2006;300(2):534-44. Epub 2006/09/26. doi: 10.1016/j.ydbio.2006.08.041. PubMed PMID: 16996050.

60. Miyazaki S, Yuzaki M, Nakada K, Shirakawa H, Nakanishi S, Nakade S, Mikoshiba K. Block of Ca2+ wave and Ca2+ oscillation by antibody to the inositol 1,4,5-trisphosphate receptor in fertilized hamster eggs. Science (New York, NY). 1992;257(5067):251-5.

61. Runft LL, Jaffe LA, Mehlmann LM. Egg activation at fertilization: where it all begins. Developmental biology. 2002;245(2):237-54. doi: 10.1006/dbio.2002.0600.

62. Kurokawa M, Sato K-i, Fissore R. Mammalian fertilization: from sperm factor to phospholipase Czeta. Biology of the cell / under the auspices of the European Cell Biology Organization. 2004;96(1):37-45. doi: 10.1016/j.biolcel.2003.11.003.

63. Swann K, Saunders CM, Rogers NT, Lai FA. PLCzeta(zeta): a sperm protein that triggers Ca2+ oscillations and egg activation in mammals. Seminars in cell & developmental biology. 2006;17(2):264-73. doi: 10.1016/j.semcdb.2006.03.009.

64. Swann K, Parrington J. Mechanism of Ca2+ release at fertilization in mammals. The Journal of experimental zoology. 1999;285(3):267-75. Epub 1999/09/25. PubMed PMID: 10497326.

65. Dale B, DeFelice LJ, Ehrenstein G. Injection of a soluble sperm fraction into sea-urchin eggs triggers the cortical reaction. Experientia. 1985;41(8):1068-70. Epub 1985/08/15. PubMed PMID: 4018233.

66. McDougall A, Levasseur M, O'Sullivan AJ, Jones KT. Cell cycle-dependent repetitive Ca(2+)waves induced by a cytosolic sperm extract in mature ascidian eggs mimic those observed at fertilization. Journal of cell science. 2000;113 Pt 19:3453-62. Epub 2000/09/14. PubMed PMID: 10984436.

67. Kim ST, Gye MC. Activation of mouse oocytes following intracytoplasmic injection of chicken sperm extract. Reproduction in domestic animals = Zuchthygiene. 2003;38(5):401-4. Epub 2003/09/03. PubMed PMID: 12950693.

68. Swann K. A cytosolic sperm factor stimulates repetitive calcium increases and mimics fertilization in hamster eggs. Development. 1990;110(4):1295-302. Epub 1990/12/01. PubMed PMID: 2100264.

69. Parrington J, Swann K, Shevchenko VI, Sesay AK, Lai FA. Calcium oscillations in mammalian eggs triggered by a soluble sperm protein. Nature. 1996;379(6563):364-8. Epub 1996/01/25. doi: 10.1038/379364a0. PubMed PMID: 8552195.

70. Ito M, Shikano T, Oda S, Horiguchi T, Tanimoto S, Awaji T, Mitani H, Miyazaki S. Difference in Ca2+ oscillation-inducing activity and nuclear translocation ability of PLCZ1, an egg-activating sperm factor candidate, between mouse, rat, human, and medaka fish. Biology of reproduction. 2008;78(6):1081-90. doi: 10.1095/biolreprod.108.067801.

71. Machaty Z, Bonk AJ, Kuhholzer B, Prather RS. Porcine oocyte activation induced by a cytosolic sperm factor. Mol Reprod Dev. 2000;57(3):290-5. Epub 2000/10/03.

doi: 10.1002/1098-2795(200011)57:3<290::aid-mrd11>3.0.co;2-#. PubMed PMID: 11013437.

72. Wilding M, Kyozuka K, Russo GL, Tosti E, Dale B. A soluble extract from human spermatozoa activates ascidian oocytes. Development, growth & differentiation. 1997;39(3):329-36. Epub 1997/06/01. PubMed PMID: 9227899.

73. Stice SL, Robl JM. Activation of mammalian oocytes by a factor obtained from rabbit sperm. Mol Reprod Dev. 1990;25(3):272-80. Epub 1990/03/01. doi: 10.1002/mrd.1080250309. PubMed PMID: 2331376.

74. Kouchi Z, Fukami K, Shikano T, Oda S, Nakamura Y, Takenawa T, Miyazaki S. Recombinant phospholipase Czeta has high Ca2+ sensitivity and induces Ca2+ oscillations in mouse eggs. J Biol Chem. 2004;279(11):10408-12. Epub 2004/01/01. doi: 10.1074/jbc.M313801200. PubMed PMID: 14701816.

75. Knott JG, Kurokawa M, Fissore RA, Schultz RM, Williams CJ. Transgenic RNA interference reveals role for mouse sperm phospholipase Czeta in triggering Ca2+ oscillations during fertilization. Biology of reproduction. 2005;72(4):992-6. Epub 2004/12/17. doi: 10.1095/biolreprod.104.036244. PubMed PMID: 15601914.

76. Cox LJ, Larman MG, Saunders CM, Hashimoto K, Swann K, Lai FA. Sperm phospholipase Czeta from humans and cynomolgus monkeys triggers Ca2+ oscillations, activation and development of mouse oocytes. Reproduction (Cambridge, England). 2002;124(5):611-23.

77. Suh HN, Huong HT, Song CH, Lee JH, Han HJ. Linoleic acid stimulates gluconeogenesis via Ca2+/PLC, cPLA2, and PPAR pathways through GPR40 in primary cultured chicken hepatocytes. American journal of physiology Cell

physiology. 2008;295(6):C1518-27. Epub 2008/10/10. doi: 10.1152/ajpcell.00368.2008. PubMed PMID: 18842827.

78. Kadamur G, Ross EM. Mammalian phospholipase C. Annual review of physiology. 2013;75:127-54. Epub 2012/11/13. doi: 10.1146/annurev-physiol-030212-183750. PubMed PMID: 23140367.
79. Fukami K, Inanobe S, Kanemaru K, Nakamura Y. Phospholipase C is a key enzyme regulating intracellular calcium and modulating the phosphoinositide balance. Progress in lipid research. 2010;49(4):429-37. Epub 2010/06/18. doi: 10.1016/j.plipres.2010.06.001. PubMed PMID: 20553968.
80. Rebecchi MJ, Pentyala SN. Structure, function, and control of phosphoinositide-specific phospholipase C. Physiological reviews. 2000;80(4):1291-335. Epub 2000/10/04. PubMed PMID: 11015615.
81. Katan M. Families of phosphoinositide-specific phospholipase C: structure and function. Biochimica et biophysica acta. 1998;1436(1-2):5-17. Epub 1998/12/05. PubMed PMID: 9838022.
82. Nomikos M, Blayney LM, Larman MG, Campbell K, Rossbach A, Saunders CM, Swann K, Lai FA. Role of phospholipase C-zeta domains in Ca2+-dependent phosphatidylinositol 4,5-bisphosphate hydrolysis and cytoplasmic Ca2+ oscillations. J Biol Chem. 2005;280(35):31011-8. Epub 2005/07/08. doi: 10.1074/jbc.M500629200. PubMed PMID: 16000311.
83. Kouchi Z, Shikano T, Nakamura Y, Shirakawa H, Fukami K, Miyazaki S. The role of EF-hand domains and C2 domain in regulation of enzymatic activity of

phospholipase Czeta. J Biol Chem. 2005;280(22):21015-21. Epub 2005/03/26. doi: 10.1074/jbc.M412123200. PubMed PMID: 15790568.

84. Medkova M, Cho W. Interplay of C1 and C2 domains of protein kinase C-alpha in its membrane binding and activation. J Biol Chem. 1999;274(28):19852-61. Epub 1999/07/03. PubMed PMID: 10391930.

85. Bittova L, Sumandea M, Cho W. A structure-function study of the C2 domain of cytosolic phospholipase A2. Identification of essential calcium ligands and hydrophobic membrane binding residues. J Biol Chem. 1999;274(14):9665-72. Epub 1999/03/27. PubMed PMID: 10092653.

86. Lomasney JW, Cheng HF, Roffler SR, King K. Activation of phospholipase C delta1 through C2 domain by a Ca(2+)-enzyme-phosphatidylserine ternary complex. J Biol Chem. 1999;274(31):21995-2001. Epub 1999/07/27. PubMed PMID: 10419523.

87. Nomikos M, Elgmati K, Theodoridou M, Calver BL, Nounesis G, Swann K, Lai FA. Phospholipase Czeta binding to PtdIns(4,5)P2 requires the XY-linker region. Journal of cell science. 2011;124(Pt 15):2582-90. Epub 2011/07/07. doi: 10.1242/jcs.083485. PubMed PMID: 21730019; PMCID: Pmc3138701.

88. Kuroda K, Ito M, Shikano T, Awaji T, Yoda A, Takeuchi H, Kinoshita K, Miyazaki S. The role of X/Y linker region and N-terminal EF-hand domain in nuclear translocation and Ca2+ oscillation-inducing activities of phospholipase Czeta, a mammalian egg-activating factor. J Biol Chem. 2006;281(38):27794-805. Epub 2006/07/21. doi: 10.1074/jbc.M603473200. PubMed PMID: 16854985.

89. Nakanishi T, Ishibashi N, Kubota H, Inoue K, Ogonuki N, Ogura A, Kashiwabara S, Baba T. Birth of normal offspring from mouse eggs activated by a phospholipase

Czeta protein lacking three EF-hand domains. The Journal of reproduction and development. 2008;54(4):244-9. Epub 2008/05/21. PubMed PMID: 18490860.

90. Yoda A, Oda S, Shikano T, Kouchi Z, Awaji T, Shirakawa H, Kinoshita K, Miyazaki S. Ca2+ oscillation-inducing phospholipase C zeta expressed in mouse eggs is accumulated to the pronucleus during egg activation. Developmental biology. 2004;268(2):245-57. Epub 2004/04/06. doi: 10.1016/j.ydbio.2003.12.028. PubMed PMID: 15063165.
91. Larman MG, Saunders CM, Carroll J, Lai FA, Swann K. Cell cycle-dependent Ca2+ oscillations in mouse embryos are regulated by nuclear targeting of PLCzeta. Journal of cell science. 2004;117(Pt 12):2513-21. Epub 2004/05/26. doi: 10.1242/jcs.01109. PubMed PMID: 15159452.
92. Halet G, Marangos P, Fitzharris G, Carroll J. Ca2+ oscillations at fertilization in mammals. Biochemical Society transactions. 2003;31(Pt 5):907-11. Epub 2003/09/25. doi: 10.1042/. PubMed PMID: 14505446.
93. Sato K, Wakai T, Seita Y, Takizawa A, Fissore RA, Ito J, Kashiwazaki N. Molecular characteristics of horse phospholipase C zeta (PLCzeta). Animal science journal = Nihon chikusan Gakkaiho. 2013;84(4):359-68. Epub 2013/04/18. doi: 10.1111/asj.12044. PubMed PMID: 23590511.
94. Cooney MA, Malcuit C, Cheon B, Holland MK, Fissore RA, D'Cruz NT. Species-specific differences in the activity and nuclear localization of murine and bovine phospholipase C zeta 1. Biology of reproduction. 2010;83(1):92-101. Epub 2010/04/02. doi: 10.1095/biolreprod.109.079814. PubMed PMID: 20357268; PMCID: Pmc2888965.

95. Yoon SY, Fissore RA. Release of phospholipase C zetaand [Ca2+]i oscillation-inducing activity during mammalian fertilization. Reproduction (Cambridge, England). 2007;134(5):695-704. Epub 2007/10/30. doi: 10.1530/rep-07-0259. PubMed PMID: 17965260.

96. Young C, Grasa P, Coward K, Davis LC, Parrington J. Phospholipase C zeta undergoes dynamic changes in its pattern of localization in sperm during capacitation and the acrosome reaction. Fertility and sterility. 2009;91(5 Suppl):2230-42. Epub 2008/08/20. doi: 10.1016/j.fertnstert.2008.05.021. PubMed PMID: 18710717.

97. Seita Y, Ito J, Kashiwazaki N. Removal of acrosomal membrane from sperm head improves development of rat zygotes derived from intracytoplasmic sperm injection. The Journal of reproduction and development. 2009;55(5):475-9. Epub 2009/05/16. PubMed PMID: 19444004.

98. Yoon SY, Jellerette T, Salicioni AM, Lee HC, Yoo MS, Coward K, Parrington J, Grow D, Cibelli JB, Visconti PE, Mager J, Fissore RA. Human sperm devoid of PLC, zeta 1 fail to induce Ca(2+) release and are unable to initiate the first step of embryo development. The Journal of clinical investigation. 2008;118(11):3671-81. Epub 2008/10/18. doi: 10.1172/jci36942. PubMed PMID: 18924610; PMCID: Pmc2567839.

99. Heytens E, Parrington J, Coward K, Young C, Lambrecht S, Yoon SY, Fissore RA, Hamer R, Deane CM, Ruas M, Grasa P, Soleimani R, Cuvelier CA, Gerris J, Dhont M, Deforce D, Leybaert L, De Sutter P. Reduced amounts and abnormal forms of phospholipase C zeta (PLCzeta) in spermatozoa from infertile men. Human

reproduction (Oxford, England). 2009;24(10):2417-28. Epub 2009/07/09. doi: 10.1093/humrep/dep207. PubMed PMID: 19584136.

100. Bedford-Guaus SJ, McPartlin LA, Xie J, Westmiller SL, Buffone MG, Roberson MS. Molecular cloning and characterization of phospholipase C zeta in equine sperm and testis reveals species-specific differences in expression of catalytically active protein. Biology of reproduction. 2011;85(1):78-88. Epub 2011/03/11. doi: 10.1095/biolreprod.110.089466. PubMed PMID: 21389344.

101. Nakai M, Ito J, Sato K, Noguchi J, Kaneko H, Kashiwazaki N, Kikuchi K. Pre-treatment of sperm reduces success of ICSI in the pig. Reproduction (Cambridge, England). 2011;142(2):285-93. Epub 2011/05/26. doi: 10.1530/rep-11-0073. PubMed PMID: 21610169.

102. Grasa P, Coward K, Young C, Parrington J. The pattern of localization of the putative oocyte activation factor, phospholipase Czeta, in uncapacitated, capacitated, and ionophore-treated human spermatozoa. Human reproduction (Oxford, England). 2008;23(11):2513-22. Epub 2008/07/26. doi: 10.1093/humrep/den280. PubMed PMID: 18653671.

103. Wu AT, Sutovsky P, Manandhar G, Xu W, Katayama M, Day BN, Park K-WW, Yi Y-JJ, Xi YW, Prather RS, Oko R. PAWP, a sperm-specific WW domain-binding protein, promotes meiotic resumption and pronuclear development during fertilization. The Journal of biological chemistry. 2007;282(16):12164-75. doi: 10.1074/jbc.M609132200.

104. Wu AT, Sutovsky P, Xu W, van der Spoel AC, Platt FM, Oko R. The postacrosomal assembly of sperm head protein, PAWP, is independent of acrosome formation and

dependent on microtubular manchette transport. Developmental biology. 2007;312(2):471-83. Epub 2007/11/09. doi: 10.1016/j.ydbio.2007.08.051. PubMed PMID: 17988661.

105. Aarabi M, Balakier H, Bashar S, Moskovtsev SI, Sutovsky P, Librach CL, Oko R. Sperm content of postacrosomal WW binding protein is related to fertilization outcomes in patients undergoing assisted reproductive technology. Fertility and sterility. 2014;102(2):440-7. Epub 2014/06/09. doi: 10.1016/j.fertnstert.2014.05.003. PubMed PMID: 24907910.

106. Aarabi M, Qin Z, Xu W, Mewburn J, Oko R. Sperm-borne protein, PAWP, initiates zygotic development in Xenopus laevis by eliciting intracellular calcium release. Mol Reprod Dev. 2010;77(3):249-56. Epub 2009/12/18. doi: 10.1002/mrd.21140. PubMed PMID: 20017143.

107. Aarabi M, Balakier H, Bashar S, Moskovtsev SI, Sutovsky P, Librach CL, Oko R. Sperm-derived WW domain-binding protein, PAWP, elicits calcium oscillations and oocyte activation in humans and mice. FASEB journal : official publication of the Federation of American Societies for Experimental Biology. 2014;28(10):4434-40. Epub 2014/06/28. doi: 10.1096/fj.14-256495. PubMed PMID: 24970390.

108. Nomikos M, Sanders JR, Theodoridou M, Kashir J, Matthews E, Nounesis G, Lai FA, Swann K. Sperm-specific post-acrosomal WW-domain binding protein (PAWP) does not cause Ca2+ release in mouse oocytes. Molecular human reproduction. 2014;20(10):938-47. Epub 2014/07/25. doi: 10.1093/molehr/gau056. PubMed PMID: 25057041; PMCID: Pmc4172172.

109. Nomikos M, Sanders JR, Kashir J, Sanusi R, Buntwal L, Love D, Ashley P, Sanders D, Knaggs P, Bunkheila A, Swann K, Lai FA. Functional disparity between human PAWP and PLCzeta in the generation of Ca2+ oscillations for oocyte activation. Molecular human reproduction. 2015;21(9):702-10. Epub 2015/06/28. doi: 10.1093/molehr/gav034. PubMed PMID: 26116451.

110. Satouh Y, Nozawa K, Ikawa M. Sperm Postacrosomal WW Domain-Binding Protein Is Not Required for Mouse Egg Activation. Biology of reproduction. 2015;93(4):94. Epub 2015/09/18. doi: 10.1095/biolreprod.115.131441. PubMed PMID: 26377222.

111. Brawand D, Soumillon M, Necsulea A, Julien P, Csardi G, Harrigan P, Weier M, Liechti A, Aximu-Petri A, Kircher M, Albert FW, Zeller U, Khaitovich P, Grutzner F, Bergmann S, Nielsen R, Paabo S, Kaessmann H. The evolution of gene expression levels in mammalian organs. Nature. 2011;478(7369):343-8. Epub 2011/10/21. doi: 10.1038/nature10532. PubMed PMID: 22012392.

112. Maruyama T, Kanaji T, Nakade S, Kanno T, Mikoshiba K. 2APB, 2-aminoethoxydiphenyl borate, a membrane-penetrable modulator of Ins(1,4,5)P3-induced Ca2+ release. Journal of biochemistry. 1997;122(3):498-505. Epub 1997/11/05. PubMed PMID: 9348075.

113. Bilmen JG, Wootton LL, Godfrey RE, Smart OS, Michelangeli F. Inhibition of SERCA Ca2+ pumps by 2-aminoethoxydiphenyl borate (2-APB). 2-APB reduces both Ca2+ binding and phosphoryl transfer from ATP, by interfering with the pathway leading to the Ca2+-binding sites. European journal of biochemistry / FEBS. 2002;269(15):3678-87. Epub 2002/08/03. PubMed PMID: 12153564.

114. Bogeski I, Kummerow C, Al-Ansary D, Schwarz EC, Koehler R, Kozai D, Takahashi N, Peinelt C, Griesemer D, Bozem M, Mori Y, Hoth M, Niemeyer BA. Differential redox regulation of ORAI ion channels: a mechanism to tune cellular calcium signaling. Science signaling. 2010;3(115):ra24. Epub 2010/04/01. doi: 10.1126/scisignal.2000672. PubMed PMID: 20354224.

115. Clapham DE, Runnels LW, Strubing C. The TRP ion channel family. Nature reviews Neuroscience. 2001;2(6):387-96. Epub 2001/06/05. doi: 10.1038/35077544. PubMed PMID: 11389472.

116. Hu HZ, Gu Q, Wang C, Colton CK, Tang J, Kinoshita-Kawada M, Lee LY, Wood JD, Zhu MX. 2-aminoethoxydiphenyl borate is a common activator of TRPV1, TRPV2, and TRPV3. J Biol Chem. 2004;279(34):35741-8. Epub 2004/06/15. doi: 10.1074/jbc.M404164200. PubMed PMID: 15194687.

117. Shuttleworth TJ. Orai3--the 'exceptional' Orai? The Journal of physiology. 2012;590(Pt 2):241-57. Epub 2011/11/02. doi: 10.1113/jphysiol.2011.220574. PubMed PMID: 22041188; PMCID: Pmc3285062.

118. Lee B, Palermo G, Machaca K. Downregulation of store-operated Ca2+ entry during mammalian meiosis is required for the egg-to-embryo transition. Journal of cell science. 2013;126(Pt 7):1672-81. Epub 2013/02/21. doi: 10.1242/jcs.121335. PubMed PMID: 23424198.

119. Cheon B, Lee H-CC, Wakai T, Fissore RA. Ca2+ influx and the store-operated Ca2+ entry pathway undergo regulation during mouse oocyte maturation. Molecular biology of the cell. 2013;24(9):1396-410. doi: 10.1091/mbc.E13-01-0065.

120. Sasaki S, Yui N, Noda Y. Actin directly interacts with different membrane channel proteins and influences channel activities: AQP2 as a model. Biochimica et biophysica acta. 2014;1838(2):514-20. Epub 2013/06/19. doi: 10.1016/j.bbamem.2013.06.004. PubMed PMID: 23770358.

121. Singh H, Cousin MA, Ashley RH. Functional reconstitution of mammalian 'chloride intracellular channels' CLIC1, CLIC4 and CLIC5 reveals differential regulation by cytoskeletal actin. The FEBS journal. 2007;274(24):6306-16. Epub 2007/11/22. doi: 10.1111/j.1742-4658.2007.06145.x. PubMed PMID: 18028448.

122. Field CM, Lenart P. Bulk cytoplasmic actin and its functions in meiosis and mitosis. Current biology : CB. 2011;21(19):R825-30. Epub 2011/10/15. doi: 10.1016/j.cub.2011.07.043. PubMed PMID: 21996509.

123. Clift D, Schuh M. Restarting life: fertilization and the transition from meiosis to mitosis. Nature reviews Molecular cell biology. 2013;14(9):549-62. Epub 2013/08/15. doi: 10.1038/nrm3643. PubMed PMID: 23942453; PMCID: Pmc4021448.

124. Yi K, Unruh JR, Deng M, Slaughter BD, Rubinstein B, Li R. Dynamic maintenance of asymmetric meiotic spindle position through Arp2/3-complex-driven cytoplasmic streaming in mouse oocytes. Nature cell biology. 2011;13(10):1252-8. Epub 2011/08/30. doi: 10.1038/ncb2320. PubMed PMID: 21874009; PMCID: Pmc3523671.

125. Liu L, Trimarchi JR, Keefe DL. Haploidy but not parthenogenetic activation leads to increased incidence of apoptosis in mouse embryos. Biology of reproduction. 2002;66(1):204-10.

126. Wakayama T, Perry AC, Zuccotti M, Johnson KR, Yanagimachi R. Full-term development of mice from enucleated oocytes injected with cumulus cell nuclei. Nature. 1998;394(6691):369-74. doi: 10.1038/28615.

127. Homa ST. Calcium and meiotic maturation of the mammalian oocyte. Mol Reprod Dev. 1995;40(1):122-34. Epub 1995/01/01. doi: 10.1002/mrd.1080400116. PubMed PMID: 7702866.

128. Hille B. Ion channels of excitable membranes: Sinauer Sunderland, MA; 2001.

129. Swann K, Lai FA. PLCzeta and the initiation of Ca(2+) oscillations in fertilizing mammalian eggs. Cell Calcium. 2013;53(1):55-62. Epub 2012/12/12. doi: 10.1016/j.ceca.2012.11.001. PubMed PMID: 23218672.

130. Kono T, Jones KT, Bos-Mikich A, Whittingham DG, Carroll J. A cell cycle-associated change in Ca2+ releasing activity leads to the generation of Ca2+ transients in mouse embryos during the first mitotic division. The Journal of cell biology. 1996;132(5):915-23. Epub 1996/03/01. PubMed PMID: 8603922; PMCID: Pmc2120737.

131. Tomashov-Matar R, Tchetchik D, Eldar A, Kaplan-Kraicer R, Oron Y, Shalgi R. Strontium-induced rat egg activation. Reproduction (Cambridge, England). 2005;130(4):467-74. Epub 2005/09/27. doi: 10.1530/rep.1.00746. PubMed PMID: 16183864.

132. Nixon VL, Levasseur M, McDougall A, Jones KT. Ca(2+) oscillations promote APC/C-dependent cyclin B1 degradation during metaphase arrest and completion of meiosis in fertilizing mouse eggs. Current biology : CB. 2002;12(9):746-50. Epub 2002/05/15. PubMed PMID: 12007419.

133. Becker D, Bereiter-Hahn J, Jendrach M. Functional interaction of the cation channel transient receptor potential vanilloid 4 (TRPV4) and actin in volume regulation. European journal of cell biology. 2009;88(3):141-52. Epub 2008/11/26. doi: 10.1016/j.ejcb.2008.10.002. PubMed PMID: 19027987.

134. Kuipers AJ, Middelbeek J, van Leeuwen FN. Mechanoregulation of cytoskeletal dynamics by TRP channels. European journal of cell biology. 2012;91(11-12):834-46. Epub 2012/06/26. doi: 10.1016/j.ejcb.2012.05.006. PubMed PMID: 22727433.

135. Schatten G, Schatten H, Spector I, Cline C, Paweletz N, Simerly C, Petzelt C. Latrunculin inhibits the microfilament-mediated processes during fertilization, cleavage and early development in sea urchins and mice. Experimental cell research. 1986;166(1):191-208. Epub 1986/09/01. PubMed PMID: 3743654.

136. Whittingham DG, Siracusa G. The involvement of calcium in the activation of mammalian oocytes. Experimental cell research. 1978;113(2):311-7. Epub 1978/05/01. PubMed PMID: 299649.

137. Fraser LR. Strontium supports capacitation and the acrosome reaction in mouse sperm and rapidly activates mouse eggs. Gamete research. 1987;18(4):363-74. Epub 1987/12/01. doi: 10.1002/mrd.1120180410. PubMed PMID: 3507382.

138. Spector I, Shochet NR, Blasberger D, Kashman Y. Latrunculins--novel marine macrolides that disrupt microfilament organization and affect cell growth: I. Comparison with cytochalasin D. Cell motility and the cytoskeleton. 1989;13(3):127-44. Epub 1989/01/01. doi: 10.1002/cm.970130302. PubMed PMID: 2776221.

139. Wakai T, Vanderheyden V, Yoon S-Y, Cheon B, Zhang N, Parys J, Fissore R. Regulation of inositol 1,4,5-trisphosphate receptor function during mouse oocyte maturation. Journal of cellular physiology. 2012;227(2):705-17. doi: 10.1002/jcp.22778.

140. Ducibella T, Huneau D, Angelichio E, Xu Z, Schultz R, Kopf G, Fissore R, Madoux S, Ozil J-P. Egg-to-embryo transition is driven by differential responses to Ca^{2+} oscillation number. Developmental biology. 2002;250(2):280-91. doi: 10.1006/dbio.2002.0788.

141. Okamoto H, Takahashi K, Yamashita N. Ionic currents through the membrane of the mammalian oocyte and their comparison with those in the tunicate and sea urchin. The Journal of physiology. 1977;267(2):465-95. Epub 1977/05/01. PubMed PMID: 559759; PMCID: Pmc1283624.

142. Whitaker M. Calcium at fertilization and in early development. Physiological reviews. 2006;86(1):25-88. Epub 2005/12/24. doi: 10.1152/physrev.00023.2005. PubMed PMID: 16371595; PMCID: Pmc3299562.

143. Tombes RM, Simerly C, Borisy GG, Schatten G. Meiosis, egg activation, and nuclear envelope breakdown are differentially reliant on Ca2+, whereas germinal vesicle breakdown is Ca2+ independent in the mouse oocyte. The Journal of cell biology. 1992;117(4):799-811. Epub 1992/05/01. PubMed PMID: 1577859; PMCID: Pmc2289470.

144. Carroll J, Swann K. Spontaneous cytosolic calcium oscillations driven by inositol trisphosphate occur during in vitro maturation of mouse oocytes. J Biol Chem. 1992;267(16):11196-201. Epub 1992/06/05. PubMed PMID: 1597455.

145. Asakawa M, Yoshioka T, Matsutani T, Hikita I, Suzuki M, Oshima I, Tsukahara K, Arimura A, Horikawa T, Hirasawa T, Sakata T. Association of a mutation in TRPV3 with defective hair growth in rodents. The Journal of investigative dermatology. 2006;126(12):2664-72. Epub 2006/07/22. doi: 10.1038/sj.jid.5700468. PubMed PMID: 16858425.

146. Yoshioka T, Imura K, Asakawa M, Suzuki M, Oshima I, Hirasawa T, Sakata T, Horikawa T, Arimura A. Impact of the Gly573Ser substitution in TRPV3 on the development of allergic and pruritic dermatitis in mice. The Journal of investigative dermatology. 2009;129(3):714-22. Epub 2008/08/30. doi: 10.1038/jid.2008.245. PubMed PMID: 18754035.

147. Swain JE, Pool TB. ART failure: oocyte contributions to unsuccessful fertilization. Human reproduction update. 2008;14(5):431-46. Epub 2008/07/08. doi: 10.1093/humupd/dmn025. PubMed PMID: 18603645.

148. Heindryckx B, Van der Elst J, De Sutter P, Dhont M. Treatment option for sperm- or oocyte-related fertilization failure: assisted oocyte activation following diagnostic heterologous ICSI. Human reproduction (Oxford, England). 2005;20(8):2237-41. Epub 2005/04/16. doi: 10.1093/humrep/dei029. PubMed PMID: 15831504.

149. Nasr-Esfahani MH, Deemeh MR, Tavalaee M. Artificial oocyte activation and intracytoplasmic sperm injection. Fertility and sterility. 2010;94(2):520-6. Epub 2009/04/28. doi: 10.1016/j.fertnstert.2009.03.061. PubMed PMID: 19393997.

150. Jellerette T, He CL, Wu H, Parys JB, Fissore RA. Down-regulation of the inositol 1,4,5-trisphosphate receptor in mouse eggs following fertilization or parthenogenetic

activation. Developmental biology. 2000;223(2):238-50. Epub 2000/07/07. doi: 10.1006/dbio.2000.9675. PubMed PMID: 10882513.

151. Brind S, Swann K, Carroll J. Inositol 1,4,5-trisphosphate receptors are downregulated in mouse oocytes in response to sperm or adenophostin A but not to increases in intracellular Ca(2+) or egg activation. Developmental biology. 2000;223(2):251-65. Epub 2000/07/07. doi: 10.1006/dbio.2000.9728. PubMed PMID: 10882514.

152. Girard S, Clapham D. Acceleration of intracellular calcium waves in Xenopus oocytes by calcium influx. Science (New York, NY). 1993;260(5105):229-32. Epub 1993/04/09. PubMed PMID: 8385801.

153. Marshall IC, Taylor CW. Two calcium-binding sites mediate the interconversion of liver inositol 1,4,5-trisphosphate receptors between three conformational states. The Biochemical journal. 1994;301 (Pt 2):591-8. Epub 1994/07/15. PubMed PMID: 8043006; PMCID: Pmc1137122.

154. Backs J, Stein P, Backs T, Duncan FE, Grueter CE, McAnally J, Qi X, Schultz RM, Olson EN. The gamma isoform of CaM kinase II controls mouse egg activation by regulating cell cycle resumption. Proceedings of the National Academy of Sciences of the United States of America. 2010;107(1):81-6. Epub 2009/12/08. doi: 10.1073/pnas.0912658106. PubMed PMID: 19966304; PMCID: Pmc2806780.

155. Hirano Y, Fozzard HA, January CT. Characteristics of L- and T-type Ca2+ currents in canine cardiac Purkinje cells. The American journal of physiology. 1989;256(5 Pt 2):H1478-92. Epub 1989/05/01. PubMed PMID: 2470265.

156. Igarashi H, Knott JG, Schultz RM, Williams CJ. Alterations of PLCbeta1 in mouse eggs change calcium oscillatory behavior following fertilization. Developmental biology. 2007;312(1):321-30. Epub 2007/10/27. doi: 10.1016/j.ydbio.2007.09.028. PubMed PMID: 17961538; PMCID: Pmc2170533.

157. Clapham DE. Calcium signaling. Cell. 2007;131(6):1047-58. Epub 2007/12/18. doi: 10.1016/j.cell.2007.11.028. PubMed PMID: 18083096.

158. Eusebi F, Mangia F, Alfei L. Acetylcholine-elicited responses in primary and secondary mammalian oocytes disappear after fertilisation. Nature. 1979;277(5698):651-3. Epub 1979/02/22. PubMed PMID: 423964.

159. Swann K. Different triggers for calcium oscillations in mouse eggs involve a ryanodine-sensitive calcium store. The Biochemical journal. 1992;287 (Pt 1):79-84. Epub 1992/10/01. PubMed PMID: 1417794; PMCID: Pmc1133126.

160. Halet G, Tunwell R, Parkinson SJ, Carroll J. Conventional PKCs regulate the temporal pattern of Ca2+ oscillations at fertilization in mouse eggs. The Journal of cell biology. 2004;164(7):1033-44. Epub 2004/03/31. doi: 10.1083/jcb.200311023. PubMed PMID: 15051735; PMCID: Pmc2172066.

161. Xu H, Delling M, Jun JC, Clapham DE. Oregano, thyme and clove-derived flavors and skin sensitizers activate specific TRP channels. Nature neuroscience. 2006;9(5):628-35. Epub 2006/04/18. doi: 10.1038/nn1692. PubMed PMID: 16617338.

162. Doerner JF, Hatt H, Ramsey IS. Voltage- and temperature-dependent activation of TRPV3 channels is potentiated by receptor-mediated PI(4,5)P2 hydrolysis. The

Journal of general physiology. 2011;137(3):271-88. Epub 2011/02/16. doi: 10.1085/jgp.200910388. PubMed PMID: 21321070; PMCID: Pmc3047606.

163. Markoulaki S, Matson S, Abbott AL, Ducibella T. Oscillatory CaMKII activity in mouse egg activation. Developmental biology. 2003;258(2):464-74. Epub 2003/06/12. PubMed PMID: 12798302.

164. Ducibella T, Fissore R. The roles of Ca2+, downstream protein kinases, and oscillatory signaling in regulating fertilization and the activation of development. Developmental biology. 2008;315(2):257-79. Epub 2008/02/08. doi: 10.1016/j.ydbio.2007.12.012. PubMed PMID: 18255053; PMCID: Pmc4276041.

165. Xiao R, Tang J, Wang C, Colton CK, Tian J, Zhu MX. Calcium plays a central role in the sensitization of TRPV3 channel to repetitive stimulations. J Biol Chem. 2008;283(10):6162-74. Epub 2008/01/08. doi: 10.1074/jbc.M706535200. PubMed PMID: 18178557; PMCID: Pmc2287377.

166. Su LT, Agapito MA, Li M, Simonson WT, Huttenlocher A, Habas R, Yue L, Runnels LW. TRPM7 regulates cell adhesion by controlling the calcium-dependent protease calpain. J Biol Chem. 2006;281(16):11260-70. Epub 2006/01/27. doi: 10.1074/jbc.M512885200. PubMed PMID: 16436382; PMCID: Pmc3225339.

167. Cheng X, Jin J, Hu L, Shen D, Dong XP, Samie MA, Knoff J, Eisinger B, Liu ML, Huang SM, Caterina MJ, Dempsey P, Michael LE, Dlugosz AA, Andrews NC, Clapham DE, Xu H. TRP channel regulates EGFR signaling in hair morphogenesis and skin barrier formation. Cell. 2010;141(2):331-43. Epub 2010/04/21. doi: 10.1016/j.cell.2010.03.013. PubMed PMID: 20403327; PMCID: Pmc2858065.

168. Lim D, Lange K, Santella L. Activation of oocytes by latrunculin A. FASEB journal : official publication of the Federation of American Societies for Experimental Biology. 2002;16(9):1050-6. Epub 2002/06/28. doi: 10.1096/fj.02-0021com. PubMed PMID: 12087066.

169. Wollman R, Meyer T. Coordinated oscillations in cortical actin and Ca2+ correlate with cycles of vesicle secretion. Nature cell biology. 2012;14(12):1261-9. Epub 2012/11/13. doi: 10.1038/ncb2614. PubMed PMID: 23143397; PMCID: Pmc3777337.

170. Patterson RL, van Rossum DB, Gill DL. Store-operated Ca2+ entry: evidence for a secretion-like coupling model. Cell. 1999;98(4):487-99. Epub 1999/09/11. PubMed PMID: 10481913.

171. Versieren K, Heindryckx B, Lierman S, Gerris J, De Sutter P. Developmental competence of parthenogenetic mouse and human embryos after chemical or electrical activation. Reproductive biomedicine online. 2010;21(6):769-75. Epub 2010/11/06. doi: 10.1016/j.rbmo.2010.07.001. PubMed PMID: 21051286.

172. Latorre R, Brauchi S, Orta G, Zaelzer C, Vargas G. ThermoTRP channels as modular proteins with allosteric gating. Cell Calcium. 2007;42(4-5):427-38. Epub 2007/05/15. doi: 10.1016/j.ceca.2007.04.004. PubMed PMID: 17499848.

173. Clemens JC, Worby CA, Simonson-Leff N, Muda M, Maehama T, Hemmings BA, Dixon JE. Use of double-stranded RNA interference in Drosophila cell lines to dissect signal transduction pathways. Proceedings of the National Academy of Sciences of the United States of America. 2000;97(12):6499-503. Epub 2000/05/24. doi: 10.1073/pnas.110149597. PubMed PMID: 10823906; PMCID: Pmc18635.

174. Kurokawa M, Sato K, Wu H, He C, Malcuit C, Black SJ, Fukami K, Fissore RA. Functional, biochemical, and chromatographic characterization of the complete [Ca2+]i oscillation-inducing activity of porcine sperm. Developmental biology. 2005;285(2):376-92. Epub 2005/08/16. doi: 10.1016/j.ydbio.2005.06.029. PubMed PMID: 16098961.

175. Steinhardt RA, Epel D, Carroll EJ, Jr., Yanagimachi R. Is calcium ionophore a universal activator for unfertilised eggs? Nature. 1974;252(5478):41-3. Epub 1974/11/01. PubMed PMID: 4473722.

176. Berridge MJ, Irvine RF. Inositol phosphates and cell signalling. Nature. 1989;341(6239):197-205. Epub 1989/09/21. doi: 10.1038/341197a0. PubMed PMID: 2550825.

177. Berridge MJ. The endoplasmic reticulum: a multifunctional signaling organelle. Cell Calcium. 2002;32(5-6):235-49. Epub 2003/01/25. PubMed PMID: 12543086.

178. Aarabi M, Yu Y, Xu W, Tse MY, Pang SC, Yi YJ, Sutovsky P, Oko R. The testicular and epididymal expression profile of PLCzeta in mouse and human does not support its role as a sperm-borne oocyte activating factor. PloS one. 2012;7(3):e33496. Epub 2012/03/20. doi: 10.1371/journal.pone.0033496. PubMed PMID: 22428063; PMCID: Pmc3299792.

179. Sousa M, Tesarik J. Ultrastructural analysis of fertilization failure after intracytoplasmic sperm injection. Human reproduction (Oxford, England). 1994;9(12):2374-80. Epub 1994/12/01. PubMed PMID: 7714161.

180. Flaherty SP, Payne D, Matthews CD. Fertilization failures and abnormal fertilization after intracytoplasmic sperm injection. Human reproduction (Oxford, England). 1998;13 Suppl 1:155-64. Epub 1998/07/15. PubMed PMID: 9663780.

181. Kashir J, Konstantinidis M, Jones C, Lemmon B, Lee H, Hamer R, Heindryckx B, Deane C, De Sutter P, Fissore R, Parrington J, Wells D, Coward K. A maternally inherited autosomal point mutation in human phospholipase C zeta (PLCζ) leads to male infertility. Human reproduction. 2012;27(1):222-31. doi: 10.1093/humrep/der384.

182. Esfandiari N, Javed MH, Gotlieb L, Casper RF. Complete failed fertilization after intracytoplasmic sperm injection--analysis of 10 years' data. International journal of fertility and women's medicine. 2005;50(4):187-92. Epub 2006/01/13. PubMed PMID: 16405104.

183. Escoffier J, Yassine S, Lee HC, Martinez G, Delaroche J, Coutton C, Karaouzene T, Zouari R, Metzler-Guillemain C, Pernet-Gallay K, Hennebicq S, Ray PF, Fissore R, Arnoult C. Subcellular localization of phospholipase Czeta in human sperm and its absence in DPY19L2-deficient sperm are consistent with its role in oocyte activation. Molecular human reproduction. 2015;21(2):157-68. Epub 2014/10/31. doi: 10.1093/molehr/gau098. PubMed PMID: 25354701; PMCID: Pmc4311148.

184. Yassine S, Escoffier J, Martinez G, Coutton C, Karaouzene T, Zouari R, Ravanat JL, Metzler-Guillemain C, Lee HC, Fissore R, Hennebicq S, Ray PF, Arnoult C. Dpy19l2-deficient globozoospermic sperm display altered genome packaging and DNA damage that compromises the initiation of embryo development. Molecular

human reproduction. 2015;21(2):169-85. Epub 2014/10/31. doi: 10.1093/molehr/gau099. PubMed PMID: 25354700; PMCID: Pmc4311149.

185. Terada Y, Hasegawa H, Takahashi A, Ugajin T, Yaegashi N, Okamura K. Successful pregnancy after oocyte activation by a calcium ionophore for a patient with recurrent intracytoplasmic sperm injection failure, with an assessment of oocyte activation and sperm centrosomal function using bovine eggs. Fertility and sterility. 2009;91(3):935.e11-4. Epub 2008/11/18. doi: 10.1016/j.fertnstert.2008.09.043. PubMed PMID: 19013567.

186. Taylor SL, Yoon SY, Morshedi MS, Lacey DR, Jellerette T, Fissore RA, Oehninger S. Complete globozoospermia associated with PLCzeta deficiency treated with calcium ionophore and ICSI results in pregnancy. Reproductive biomedicine online. 2010;20(4):559-64. Epub 2010/02/06. doi: 10.1016/j.rbmo.2009.12.024. PubMed PMID: 20133201; PMCID: Pmc2847674.

187. Escalier D. Failure of differentiation of the nuclear-perinuclear skeletal complex in the round-headed human spermatozoa. The International journal of developmental biology. 1990;34(2):287-97. Epub 1990/06/01. PubMed PMID: 2201396.

188. Sutovsky P, Oko R, Hewitson L, Schatten G. The removal of the sperm perinuclear theca and its association with the bovine oocyte surface during fertilization. Developmental biology. 1997;188(1):75-84. Epub 1997/08/01. doi: 10.1006/dbio.1997.8618. PubMed PMID: 9245513.

189. Coutton C, Zouari R, Abada F, Ben Khelifa M, Merdassi G, Triki C, Escalier D, Hesters L, Mitchell V, Levy R, Sermondade N, Boitrelle F, Vialard F, Satre V, Hennebicq S, Jouk PS, Arnoult C, Lunardi J, Ray PF. MLPA and sequence analysis

of DPY19L2 reveals point mutations causing globozoospermia. Human reproduction (Oxford, England). 2012;27(8):2549-58. Epub 2012/05/26. doi: 10.1093/humrep/des160. PubMed PMID: 22627659.

190. Pierre V, Martinez G, Coutton C, Delaroche J, Yassine S, Novella C, Pernet-Gallay K, Hennebicq S, Ray PF, Arnoult C. Absence of Dpy19l2, a new inner nuclear membrane protein, causes globozoospermia in mice by preventing the anchoring of the acrosome to the nucleus. Development. 2012;139(16):2955-65. Epub 2012/07/06. doi: 10.1242/dev.077982. PubMed PMID: 22764053.

191. Kashir J, Konstantinidis M, Jones C, Heindryckx B, De Sutter P, Parrington J, Wells D, Coward K. Characterization of two heterozygous mutations of the oocyte activation factor phospholipase C zeta (PLCζ) from an infertile man by use of minisequencing of individual sperm and expression in somatic cells. Fertility and sterility. 2012;98(2):423-31. doi: 10.1016/j.fertnstert.2012.05.002.

192. Setti AS, Paes de Almeida Ferreira Braga D, Iaconelli A, Jr., Aoki T, Borges E, Jr. Twelve years of MSOME and IMSI: a review. Reproductive biomedicine online. 2013;27(4):338-52. Epub 2013/08/21. doi: 10.1016/j.rbmo.2013.06.011. PubMed PMID: 23948449.

193. Coutton C, Escoffier J, Martinez G, Arnoult C, Ray PF. Teratozoospermia: spotlight on the main genetic actors in the human. Human reproduction update. 2015;21(4):455-85. Epub 2015/04/19. doi: 10.1093/humupd/dmv020. PubMed PMID: 25888788.

194. Martianov I, Brancorsini S, Catena R, Gansmuller A, Kotaja N, Parvinen M, Sassone-Corsi P, Davidson I. Polar nuclear localization of H1T2, a histone H1

variant, required for spermatid elongation and DNA condensation during spermiogenesis. Proceedings of the National Academy of Sciences of the United States of America. 2005;102(8):2808-13. Epub 2005/02/16. doi: 10.1073/pnas.0406060102. PubMed PMID: 15710904; PMCID: Pmc549447.

195. Zhao M, Shirley CR, Hayashi S, Marcon L, Mohapatra B, Suganuma R, Behringer RR, Boissonneault G, Yanagimachi R, Meistrich ML. Transition nuclear proteins are required for normal chromatin condensation and functional sperm development. Genesis (New York, NY : 2000). 2004;38(4):200-13. Epub 2004/04/15. doi: 10.1002/gene.20019. PubMed PMID: 15083521.

196. Yu Y, Nomikos M, Theodoridou M, Nounesis G, Lai FA, Swann K. PLCzeta causes Ca(2+) oscillations in mouse eggs by targeting intracellular and not plasma membrane PI(4,5)P(2). Molecular biology of the cell. 2012;23(2):371-80. Epub 2011/11/25. doi: 10.1091/mbc.E11-08-0687. PubMed PMID: 22114355; PMCID: Pmc3258180.

197. Lee HC, Arny M, Grow D, Dumesic D, Fissore RA, Jellerette-Nolan T. Protein phospholipase C Zeta1 expression in patients with failed ICSI but with normal sperm parameters. Journal of assisted reproduction and genetics. 2014;31(6):749-56. Epub 2014/04/24. doi: 10.1007/s10815-014-0229-9. PubMed PMID: 24756570; PMCID: Pmc4048377.

198. Arslan M, Bocca S, Mirkin S, Barroso G, Stadtmauer L, Oehninger S. Controlled ovarian hyperstimulation protocols for in vitro fertilization: two decades of experience after the birth of Elizabeth Carr. Fertility and sterility. 2005;84(3):555-

69. Epub 2005/09/20. doi: 10.1016/j.fertnstert.2005.02.053. PubMed PMID: 16169382.

199. Hsu A, Arny M, Knee AB, Bell C, Cook E, Novak AL, Grow DR. Antral follicle count in clinical practice: analyzing clinical relevance. Fertility and sterility. 2011;95(2):474-9. Epub 2010/05/04. doi: 10.1016/j.fertnstert.2010.03.023. PubMed PMID: 20434151.

200. Gibson DG, Young L, Chuang RY, Venter JC, Hutchison CA, 3rd, Smith HO. Enzymatic assembly of DNA molecules up to several hundred kilobases. Nature methods. 2009;6(5):343-5. Epub 2009/04/14. doi: 10.1038/nmeth.1318. PubMed PMID: 19363495.

201. Kimura Y, Yanagimachi R. Intracytoplasmic sperm injection in the mouse. Biology of reproduction. 1995;52(4):709-20. Epub 1995/04/01. PubMed PMID: 7779992.

202. Kurokawa M, Fissore RA. ICSI-generated mouse zygotes exhibit altered calcium oscillations, inositol 1,4,5-trisphosphate receptor-1 down-regulation, and embryo development. Molecular human reproduction. 2003;9(9):523-33. Epub 2003/08/06. PubMed PMID: 12900511.